DOCTORAL PUBLICATIONS

COMPENDIUM ON "ASSESSMENT OF INTENDED DEFORMATIONS AND KINEMATIC IDENTIFICATION OF PARALLEL MECHANISMS UNDER QUASI-STATIC CONDITIONS"

Doctoral Student

SEBASTIÁN DURANGO IDÁRRAGA

Doctoral Supervisor

PROF. DR. ENG. OSCAR E. RUIZ

DISSERTATION

Submitted in partial fulfillment of the requirements
for the degree of Doctor of Philosophy in Engineering
in the College of Engineering of the
EAFIT University

EAFIT University
College of Engineering
Doctoral Program in Engineering
Medellín
Dec. 16, 2010

Doctoral Committee:

of a dissertation submitted by

Sebastián Durango Idárraga

This dissertation has been read by each member of the following graduate committee and by majority vote has been found to be satisfactory.

Prof. Dr. Eng. Oscar E. Ruiz, Chair
CAD CAM CAE Laboratory at EAFIT University

Prof. Dr. Eng. Gabriel Calle
College of Engineering at Universidad Tecnológica, Pereira, Colombia

Dr. Eng. Rodrigo Marín
Schlumberger Riboud Product Center, Clamart, France

Prof. Dr. Eng. Diego A. Acosta
College of Engineering at EAFIT University

Accepted for the Doctoral Program

Dean Alberto Rodriguez
President of the Board of the Doctoral Program in Engineering

EAFIT University,
Medellín, Dec. 16, 2010

Abstract

This doctoral work contributes in two main aspects: (i) closed form (analytical) force-deformation models for compliant mechanisms, and (ii) assessment of permanent deformations and / or manufacturing errors in mechanisms and manipulators (i.e. kinematic identification).

In aspect (i) above, we augment the current state of the art in the following areas: (1) For planar compliant mechanisms whose elasticity is concentrated in limbs with cantilever geometry a kinematic solution is developed in this work which relies on: (1.a) The mapping of the compliant mechanism to an equivalent one based on kinematic pairs. (1.b) A decomposition of the equivalent mechanism in Assur Groups by using partitions of the equivalent mechanism, which also produces as a bi-product the formation law of the parallel mechanism. (1.c) A calculation of the kinematic solution of the individual Assur-equivalent mechanisms, possible since the compliant zones accept closed solutions. (1.d) An integration of the closed kinematic solutions by using the formation law of the mechanism. (2) For general compliance mechanisms we present a Design of Computer Experiments (DOCE) formulation which is able to produce an invertible closed force-deformation model suitable for real-time control applications.

Regarding aspect (ii) above, we advance the known methodologies for kinematic pair-based parallel planar mechanisms by implementing a Divide-and-Conquer approach for the planning of the mechanism poses that are to be performed in order to apply Kinematic Identification algorithms. For the symmetric subclass, we present an algorithm which exploits the symmetrical dihedral groups present, in order to mirror already calculated pose plannings.

Dedicado a Andrea, Ana María y Valentina,
la luz en mi vida

Acknowledgments

I want to express my sincere gratitude to my Doctoral thesis advisor, Professor Oscar E. Ruiz Salguero for his guidance, encouragement and support in the course of this work.

I thank professors John Restrepo-Giraldo and Sofiane Achiche from Technical University of Denmark, who guided and supported me academically during my research internship at DTU. They gave me valuable advice to develop this thesis. Also Prof. Diego A. Acosta Maya from EAFIT, for his advice and collaboration in the area of Design of Computer Experiments. I owe special recognition to Professor Gabriel Calle Trujillo from Technical University of Pereira, my advisor in the Masters program, for the encouragement, fairness and respect that he always had for me.

It is my pleasure to thank faculty members from Autónoma de Manizales University for their personal interest in my career: Prof. José G. Hoyos Salazar (Head of Mechanical Eng. Department), Prof. Alba P. Arias Orozco (Dean of Eng. School), Prof. Carlos Murillo-Sánchez (former Dean of Eng. School), Dr. Iván Escobar Escobar (Director of Academic Affairs), Ing. Carlos E. Jaramillo Sanint (Director of Financial Affairs), Dr. Cesar Vallejo Mejía (former Rector, now co-director of the Bank of the Colombian Republic), Dr. Gabriel Cadena Gómez (Rector), and Prof. Fabio M. Peña Bustos.

Deep thanks to my partners at the CAD CAM CAE laboratory at EAFIT (Jorge Correa Panesso, David Restrepo arango and Mauricio Aristizábal Cano) and friends (David Uribe Gallo, John E. Congote Calle, Alejandro Hoyos, Ricardo Serrano Salazar) because we shared our technical knowledge and friendship.

I owe a great debt to my wife Andrea, and my daughters Ana María and Valentina, for their love, sacrifice and patience during these years. I am also grateful for the love and encouragement I received from my parents Gustavo and María Elena, grand mothers Hylduara and Isabel, grand father Alberto, and my sisters Elisa and Laura.

Financial support for this work was provided by Colombian Administrative Department of Science, Technology and Innovation (COLCIENCIAS), and Colombian National Service of Learning (SENA), grant 1216-479-22001, EAFIT University (COL) and Autónoma de Manizales University (COL). I gratefully acknowledge this support.

Table of Contents

List of Figures . . . . . **xi**

List of Tables . . . . . **xv**

Introduction **1**

List of Publications **5**

Chapter 1 Force-Displacement Model of Compliant Mechanisms based on Assur-Groups Decomposition and Force Analysis of Assur Groups **7**

1.1 Force-Displacement Model of Compliant Mechanisms using Assur Sub-Chains . . 8

1.1.1 Introduction 9

1.1.2 Literature Review 10

1.1.3 Background 12

1.1.4 Force-Displacement Model of Compliant Mechanisms using Assur Sub-Chains 13

1.1.5 Results 24

1.1.6 Conclusions 32

1.2 Analytical Method for the Kinetostatic Analysis of the Second-Class RRR Assur Group Allowing for Friction in the Kinematic Pairs 33

1.2.1 Introduction 34

1.2.2 Literature Review 35

1.2.3 Methodology . . . 37

1.2.4 Results . . . 45

1.2.5 Conclusions and Prospective . . . 51

1.3 "Erratum to A Novel Technique for Position Analysis of Planar Compliant Mechanisms" . . . 53

Chapter 2 Force-Displacement Model of Compliant Mechanisms by Design of Computer Experiments . . . 54

2.1 Design of Computer Experiments Applied to Modeling Compliant Mechanisms . . 55

2.1.1 Introduction . . . 56

2.1.2 Literature Review. Modeling of Compliant Mechanisms . . . 58

2.1.3 Pseudo Rigid Body Modeling . . . 59

2.1.4 Methodology for Meta-modeling of Compliant Mechanisms. . . . 63

2.1.5 Case Study. Force-displacement Meta-modeling of the HexFlex Mechanism 66

2.1.6 Conclusions . . . 77

Chapter 3 Kinematic Identification of Parallel Mechanisms . . . 80

3.1 A Divide-and-Conquer Protocol for Kinematic Identification of Parallel Mechanisms Using Symmetric Groups . . . 81

3.1.1 Introduction . . . 83

3.1.2 Literature Review . . . 85

3.1.3 Divide-and-Conquer Kinematic Identification Protocol for Symmetrical Parallel Mechanisms . . . 87

3.1.4 Results . . . 97

3.1.5 Conclusions . . . 105

3.2 Symmetrical Observability of Kinematic Parameters in Parallel Mechanisms . . . 108

3.2.1 Introduction . . . 110

3.2.2 Literature Review . . . 111
3.2.3 Fundamentals of Symmetry Groups . . . 113
3.2.4 Symmetrical Active-joint Workspace of Symmetrical Parallel Mechanisms 114
3.2.5 Symmetrical Observability of Kinematic Parameters . . . 117
3.2.6 Results . . . 124
3.2.7 Conclusions . . . 131

Chapter 4 General Conclusion . . . 135

General Conclusion . . . 135

4.1 Recommendations for Future Research . . . 137

References . . . 147

Vita . . . 148

List of Figures

1 Impact of error sources according to size and frequency 2

1.1 3-DOF flexure-based parallel mechanism and its rigid-equivalent mechanism . . . 12

1.2 3*R*RR mechanism generation principle 15

1.3 Equivalent Assur group convention 16

1.4 Equivalent Assur groups and driving mechanism convention 17

1.5 Flexure hinge deflection analysis 17

1.6 Flexure effective rotation 19

1.7 Kinematic analysis of a rigid-body mechanism 20

1.8 Static analysis of a rigid-body mechanism 21

1.9 Compliant mechanism case study 24

1.10 Compliant mechanism and rigid equivalent 25

1.11 Compliant mechanism at deflected configuration 29

1.12 Joint and end-effector workspaces with maximal axial bending stress (colormap) . 31

1.13 Joint and end-effector workspaces with end-effector absolute position error compared to FEA (colormap) 31

1.14 Joint and end-effector workspaces with end-effector absolute orientation error compared to FEA (colormap) 31

1.15 First-class (driving) mechanisms 37

1.16 Second-class structural groups 37

1.17 Kinematics and kinetostatic analysis of mechanisms with a modular approach . . . 38

1.18 Kinetostatic modeling of structural groups allowing friction in the kinematic pairs . 39

1.19 Second-class first-type Assur group, dynamic equilibrium diagram 41

1.20 Second-class first-type Assur group, dynamic equilibrium diagrams with friction moments 42

1.21 Kinetostatic model of a second-class first-type Assur group allowing friction in the kinematic pairs 44

1.22 Rotational primary mechanism: dynamic equilibrium diagram allowing friction in the rotational pair 45

1.23 Kinematic modular analysis of a four-bar mechanism using a graphic user interface (GUI). Structural sequence: $I^{R}_{0,1} \rightarrow I^{RRR}_{2,3}$ 46

1.24 Four-bar mechanism 47

1.25 Kinetostatic analysis of a four-bar mechanism with a modular approach 48

1.26 Kinetostatic analysis of a four-bar mechanism. Required driving torque 49

1.27 Kinetostatic analysis of a four-bar mechanism. Required power to overcome pair friction 49

1.28 Kinetostatic analysis of a four-bar mechanism. Pair *D* reaction 50

2.1 ANSYS© as a FEA server controlled from MATLAB© 64

2.2 Methodology for force-displacement meta-modeling of compliant mechanisms . . 65

2.3 Six DOFs compliant mechanism 67

2.4 Six DOFs complaint mechanism in deflection 68

2.5 HexFlex actuators direction 69

2.6 FEA model of the HexFlex Mechanism 70

2.7 Half Normal Probability Plots. Placket-Burman DOE for 12 runs and 6 factors for HexFlex quasi-static conditions 72

2.8 Pareto Charts. Placket-Burman DOE for 12 runs and 6 factors for HexFlex quasi-static conditions 73

2.9 Deflected shape of the HexFlex mechanism for one meta-model validation experiment . . . 77

3.1 Position of fixed point A_κ . . . 92

3.2 Divide-and-conquer kinematic identification of symmetrical parallel mechanisms protocol . . . 94

3.3 Symmetrical pose selection procedure . . . 96

3.4 3*RRR* symmetrical parallel mechanism. Kinematic parameters and constraint loop . 97

3.5 3*RRR* symmetrical parallel mechanism. Active-joint workspace obtained by symmetrical operations . . . 100

3.6 3*RRR* symmetrical parallel mechanism. Optimal postures for kinematic identification 102

3.7 3*RRR* symmetrical parallel mechanism. Active robot calibration algorithm performance . . . 102

3.8 3*RRR* symmetrical parallel mechanism. Observability of kinematic parameters corresponding to symmetrical optimal sets of identification poses . . . 103

3.9 3*RRR* calibrated symmetrical parallel mechanism. End-effector position error estimated for constant orientation $\phi = 0.4$ rad . . . 104

3.10 3*RRR* symmetrical parallel mechanism. Estimated Root Mean Square Error of the end-effector position for a singularity-free workspace . . . 105

3.11 3*RRR* symmetrical parallel mechanism. Estimated Root Mean Square Error of the end-effector orientation for a singularity-free workspace . . . 105

3.12 Reflection lines of an equilateral triangle . . . 114

3.13 Position of fixed point A_κ . . . 118

3.14 Symmetrical pose selection for kinematic identification . . . 121

3.15 Divide-and-conquer kinematic identification of parallel mechanisms protocol with symmetrical pose selection . . . 123

3.16 3*RRR* symmetrical parallel mechanism. Symmetrical configuration and kinematic parameters . . . 124

3.17 3*RRR* symmetrical parallel mechanism. Constraint loop . . . 124

3.18 *3RRR* symmetrical parallel mechanism. Active-joint workspace obtained by symmetrical operations 127

3.19 3*RRR* symmetrical parallel mechanism. Selected poses for kinematic identification 129

3.20 3*RRR* symmetrical parallel mechanism. Observability of kinematic parameters . . 129

3.21 3*RRR* symmetrical parallel mechanism. Estimated end-effector pose root-mean-square error for a singularity-free workspace 131

3.22 3*RRR* symmetrical parallel mechanism. Estimated end-effector position error on constant orientation workspaces 132

4.1 Two step identification protocol 138

List of Tables

1 Summary of publications 6

1.1 Case study dimensions 24

1.2 Four-bar mechanism: geometric and inertial parameters 47

2.1 Studied Factors. Forces in Tabs of the HexFlex 70

2.2 Plackett-Burman DOE Matrix for Six factors and 12 runs 71

2.3 Lenth's analysis of Six DOF HexFlex Mechanism 74

2.4 Uniform DOE and results of the Experiments 75

2.5 Error between meta-model estimations and Ansys© simulations for 1000 random experiments with uniform distribution 77

3.1 Computational and measurement cost of kinematic identification 106

Introduction

Compliant and parallel mechanisms are two types of mechanical devices aimed at performing high-precision tasks, having their accuracy related to their closed-loop kinematic structure. The design, analysis, and operation of compliant and parallel mechanisms requires the development of accurate kinematic models.

Compliant Mechanisms (CMs) comprise the mechanisms that derive their mobility from the deflection of flexible elements rather than from kinematic pairs [1]. The term force-displacement analysis is used for CMs since the kinematic analysis cannot be isolated from the force analysis as it is done on rigid-body mechanisms. Two main techniques are currently available in the literature for the force-displacement model of CMs: techniques using an equivalent rigid-body mechanism and FEA-based techniques.

Two novel analysis alternatives are herein proposed:

1. Force-displacement model of compliant mechanisms using Assur sub-chains (chapter 1).
2. Force-displacement model of compliant mechanisms by Design of Computer Experiments (DOCE) (chapter 2).

The first alternative models flexure-based CMs by assigning an equivalent rigid-body mechanism that is divided into statically determinated kinematic chains (Assur groups) whose kinematics and force models are well known. An iterative scheme is implemented to assess the large deflection behavior. The second alternative presents a DOCE methodology in which a force-displacement (Input / Output) function is obtained. The function is a polynomial suitable for real-time control application.

Furthermore, article 1.2 develops a contribution to the force analysis of Assur groups in which friction on kinematic pairs is considered [2].

The kinematic analysis of parallel mechanisms addresses the challenge of assessing the kinematic parameters that improve their end-effector accuracy. End-effector pose errors are related to several aspects of the mechanism structure. Such errors are caused by:

1. Manufacturing tolerances and assembly errors of the machine elements.
2. Weight of the links.
3. Elastic deformations due to inertial and workload forces and thermal sources.
4. Natural oscillations of the kinematics due to the operation of the machine.

Source errors varying slowly in time (quasi-static) are recognized to be a main error source [3] (see Fig. 1), and can be modeled as geometric parameters associated to the structure of the machine since they are closely related to it. These parameters are formally denoted as kinematic parameters, and their calibration is mandatory in order to improve the accuracy of the end-effector [4].

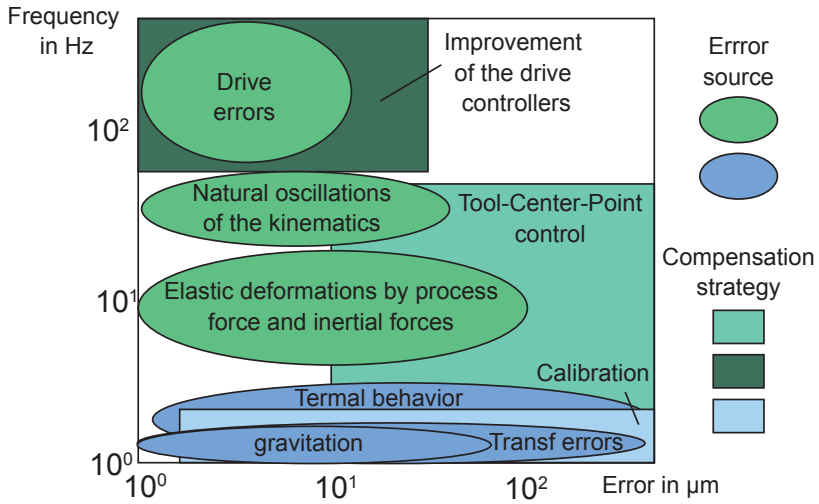

Figure 1: Impact of error sources according to size and frequency [5]

The process of estimating the kinematic parameters and updating the kinematic model is formally known as kinematic identification or kinematic calibration [6]. The kinematic calibration of parallel mechanisms is traditionally carried out through four different strategies [7]:

1. Constrained calibration, where mechanical systems are used to restrict the motion of the legs. The calibration efficiency decreases because the constraints limit the available workspace, leading to a possible non-optimal selection of calibration poses.

2. Self calibration, it relies on the use of redundant metrology (instrumentation of some passive joints) in order to replace the information provided by external measurement devices.

3. Forward kinematics calibration, adapted from the calibration methods of serial mechanisms. It requires the evaluation of the forward kinematics, resulting in a major drawback related to the instability associated with the numerical evaluation of the forward kinematics of parallel mechanisms.

4. Inverse kinematics method, accepted as the natural and most numerically efficient among the identification algorithms for parallel mechanisms. The kinematic parameters are estimated by minimizing the difference between measured and computed active-joint variables, calculated through the inverse kinematics of the end-effector pose measurements.

The contribution of this dissertation to this matter is a new Divide-and-Conquer (DC) protocol for the kinematic identification of parallel mechanisms (chapter 3). This protocol is based on the inverse calibration method, and unlike available kinematic identification methods, it exploits the usual structural symmetries of parallel mechanisms in order to set a symmetrically independent identification for each leg.

This dissertation is a compendium of six articles divided into three chapters. Two additional published articles are not included because their contents are included in one or more of the presented articles (see Summary of Publications on page 5). Each article is self-contained (introduction, literature review, methodology, results, and conclusions. Some figures and tables are repeated for the sake of clarity. The layout of the compendium is as follows:

Chapter 1 is devoted to the *Force-Displacement Model of Compliant Mechanisms based on Assur-Groups Decomposition* and the *Force Analysis of Assur Groups*. It includes three articles: two published ones, and an accepted one (see items 1, 2 and 3 on Table 1).

Chapter 2 presents the *Force-Displacement Model of Compliant Mechanisms by Design of Computer Experiments*. It contains two articles: a published one and asubmitted one (see items 3 and 4 on Table 1). Only one of them is included in the present work (article 4 in Table 1), corresponding to an invitation to rework the paper [8] for republication in the Special Issue of the Journal of Engineering with Computers (Elsevier) on "Engineering Analysis and Simulations Based on Virtual Prototypes".

Chapter 3 develops the *Kinematic Identification of Parallel Mechanisms by a Divide-and-Conquer Strategy*. It consists of three articles: a published one, an accepted one, and a submitted

one (see items 6, 7 and 8 on Table 1).

General concluding remarks are presented in chapter 4.

List of Publications

This Table presents the list of publications related to this doctoral research. In general, a conference article might be extended and published in a Journal or in a book of selected Articles of the Conference. In this document only the most advanced version of a material is presented for the sake of avoiding repetition and to respect the reader. In this table, however, all the related publications are mentioned.

	Title	State	Authors	Journal / Conference	Chapter
1.	Analytical Method for the Kinetostatic Analysis of the Second-class RRR Assur Group Allowing for Friction in the Kinematic Pairs	Published	S. Durango, G. Calle and O. Ruiz	Journal of the Brazilian Society of Mechanical Sciences and Engineering 32 (3), 2010, pp.200–207. ISSN: 1678-5878. See [2].	1
2.	Erratum to "A Novel Technique for Position Analysis of Planar Compliant Mechanisms" [Mechanism and Machine Theory 40, 2005, pp. 1224–1239]	Published	J. Correa, S. Durango and O. Ruiz (Erratum authors). S. Venanzi, P. Giesen, V. Parenti-Castelli	Mechanism and Machine Theory (IFToMM Journal) 45 (5), 2010, p. 811, ISSN 0094-114X. See [9].	1
3.	Force-Displacement Model of Compliant Mechanisms using Assur Sub-Chains	Accepted	S. Durango, J. Correa, O. Ruiz, M. Aristizabal, J. Restrepo-Giraldo, and S. Achiche	The 13th World Congress in Mechanism and Machine Science (IFToMM conference). Guanajuato, México. June 19–25, 2011.	1
4.	Design of Computer Experiments Applied to Modeling Compliant Mechanisms	Submitted (second round revision)	D. Restrepo, D. A. Acosta, S. Durango and O. Ruiz	Journal of Engineering with Computers (Springer), ISSN:0177-0667.	2, a
5.	Design of Computer Experiments Applied to Modeling Compliant Mechanisms	Published	D. Restrepo, D. A. Acosta, S. Durango and O. Ruiz	8th International Symposium on Tools and Methods of Competitive Engineering. Ancona, Italy. 2010. Vol. 2, pp. 775–788, ISBN 978-90-5155-060-3. See [8].	2, b
6.	A Divide-and-Conquer Protocol for Kinematic Identification of Parallel Mechanisms Using Symmetric Groups	Accepted	S. Durango, D. Restrepo, O. Ruiz, J. Restrepo-Giraldo, and S. Achiche	Journal of Mechanisms and Robotics (ASME), ISSN: 1942-4302.	3
7.	Symmetrical Observability of Kinematic Parameters in Parallel Mechanisms	Submitted	S. Durango, D. Restrepo, O. Ruiz, J. Restrepo-Giraldo, and S. Achiche	Journal of Control Engineering Practice (Elsevier), ISSN: 0967-0661.	3
8.	Kinematic Identification of Parallel Mechanisms by a Divide-and-Conquer Strategy	Published	S. Durango, D. Restrepo, O. Ruiz, J. Restrepo-Giraldo and S. Achiche	7th International Conference on Informatics in Control, Automation and Robotics. Funchal-Madeira, Portugal. 2010. Vol. 2, pp. 167–173, ISBN 978-989-8425-01-0. See [10].	3, c

a. This paper corresponds to an invitation for republication of article 5 (see [8]) in the Special Issue on Engineering Analysis and Simulations Based on Virtual Prototypes of the Journal of Engineering with Computers (Springer).

b. This article is not included in this compendium, but its content is included in article 4.

c. This article is not included in this compendium, but its content is included in articles 6 and 7.

Table 1: Summary of publications

Chapter 1

Force-Displacement Model of Compliant Mechanisms based on Assur-Groups Decomposition and Force Analysis of Assur Groups

This chapter presents a contribution to the *force-displacement model of flexure-based compliant mechanisms*. The contribution is presented in article 1.1 and relies on a novel force-displacement model in which the kinematics and force analysis are carried out onto an equivalent rigid-body mechanism that is divided into statically determinated kinematic chains (Assur groups) whose kinematics and force models are well known. An iterative scheme is implemented to assess the large deflection behavior.

Complementary to this contribution, a new analytical method for the force analysis of Assur groups that allows for friction on their kinematic pairs [2] is presented in article 1.2. The method was developed as an intermediate research step related to the kinematics and force models of the Assur groups.

Finally, an erratum article [9] of position analysis of planar compliant mechanisms is developed in article 1.3. It presents two corrections to [11], which is a seminal paper in force-displacement of flexure-based compliant mechanisms.

1.1 Force-Displacement Model of Compliant Mechanisms using Assur Sub-Chains

Sebastián Durango, Jorge Correa, Oscar Ruiz, Mauricio Aristizabal
{sdurang1, jcorre20, oruiz, maristi7}@eafit.edu.co
CAD CAM CAE Laboratory
EAFIT University
Medellín, Colombia

John Restrepo-Giraldo, Sofiane Achiche
{jdrg, soac}@man.dtu.dk
Engineering Design and Product Development
Technical University of Denmark
Lyngby, Denmark

This article was accepted to the 13th World Congress in Mechanism and Machine Science, June 19–25 (2011), Guanajuato, México (IFToMM conference).

Abstract

This article develops a modular procedure to perform force-displacement modeling of planar flexure-based Compliant Mechanisms (CMs). The procedure is mostly suitable for planar lumped CMs. To achieve the position analysis of CMs requires: (i) to implement the kinematic analysis as in the case of ordinary mechanisms, (ii) to solve the equilibrium problem by means of a static analysis and (iii) to model the flexures behavior through a deflection analysis. The novel contribution of this article relies on the fact that a division strategy of the CM into Assur sub-chains is implemented, so that any CM subjected to such disaggregation can be accurately modeled. For this purpose a mathematical model for the leaf-spring flexure type is presented and used through this paper. However, any other flexure model can be used instead. To support the technique, a three Degree-Of-Freedom (3-DOF) flexure-based parallel mechanism is used as case study. Results are compared with a Finite Element Analysis (FEA).

keywords: Force-displacement Model, Compliant Mechanism, Large-deflection Analysis, Pseudo-Rigid-Body Model, Assur Group.

Glossary

^{A}	Assur group
^{D}	Driving mechanism
E	Young module
F	Force
I	Cross section area moment of inertia
L	Rigid segment length
M	Moment
OXY	Global coordinate system
P	Set of external loads and its application points
R	Set of position vectors
l	Flexure length
oxy	Flexure local coordinate system
$\mathbf{q}$	Set of joint input angles
$\mathbf{r}$	Position vector
s	linear coordinate along a beam
u, v	Flexure free-end local coordinates
Θ	Flexure effective rotation
$^{\Omega}$	Number of Assur groups
α, β	Rigid segment orientation
γ	Number of flexures
φ	Set of geometric parameters and material properties
$\boldsymbol{\tau}$	Set of driving torques
$^{\omega}$	Number of driving mechanisms

1.1.1 Introduction

Compliant Mechanisms (CMs) concern those mechanisms which derive their mobility from the deflection of flexible elements rather than from kinematic pairs [1].

Flexure-based CMs are instances of CMs in which the flexibility is located in slender regions that provide a rotation between rigid parts. The narrow flexible regions are denoted as *flexure hinges* or simply *flexures*. The relative rotation between two paired rigid links is obtained through the bending of its connecting flexure. In this sense the flexure has the same function as the rota-

tional joint connecting two rigid links.

Some of the main aspects that encompass the analysis and design of CMs include the force-displacement behavior, topology optimization and fatigue analysis. The displacement analysis of flexure-based CMs cannot be isolated from the deflection analysis of its flexures. The most common methods used for force-displacement model of flexure-based CMs are the Pseudo-Rigid-Body Modeling (PRBM) and the finite element analysis (FEA). In PRBM the deflection of flexible elements is modeled by rigid-body systems that have equivalent force-displacement characteristics [12], and the force-displacement behavior of the CM is accomplished using classical rigid mechanism theory. FEA advantages include a wide choice of analysis type (static, dynamic, modal, thermal, etc.) and analysis of geometries with complex shapes [13].

An alternative force-displacement method where an iterative scheme is used to perform non-linear position analysis of planar CMs is presented by Venanzi et al [11]. The technique considers large deflections and allows for different mathematical models for the compliant kinematic pairs, thereby producing a modular approach.

The novel contribution of this article is a new force-displacement model procedure that merges the technique proposed in [11] with a divide-and-conquer strategy, in which a number of flexure-based compliant chains (modules) are assembled to yield almost any practical planar CM, leading to an improved modularity. Two basic compliant chain families are conceived for this purpose:

1. Equivalent driving mechanisms.
2. Equivalent Assur groups.

1.1.2 Literature Review

The analysis of flexure-based mechanisms can be classified into two main categories.

1. Strategies in which an equivalent rigid-body mechanism is used to perform kinematic and force analyses [1]. In this strategy, the deflection of the flexures is assessed in two ways.

   PRBM. In this model the flexures are replaced with rigid bodies connected by kinematic pairs that attempt to assess their force displacement characteristics. For this purpose, springs are added to the model to account for the flexure stiffness. In [14], a flexure-based five-bar

mechanism is designed and analyzed through an established kinematic model. No force analysis model is implemented on the formulation. However, validations are carried out by FEA. In [15], a PRBM with a lumped mass-spring model is implemented in the solution of the dynamics of a three Degree-Of-Freedom (3-DOF) flexure-based parallel mechanism. The kinetostatic model of a 3-*RRR* compliant micromotion stage is derived in [16]. The model has a closed form solution and different sets of flexure hinge compliant equations are used and compared with the FEA. It should be noted that the aforementioned references ([14–16]) use particular kinematic and dynamic solutions for their models.

Euler-Bernoulli flexure models. In this technique the deflected shape of the flexures is calculated directly by solving the Euler-Bernoulli equation for long-beam like members. This differential equation can be solved either by using a numerical method [11, 17], e.g. finite differences, or by the implementation of elliptic integrals [18, 19], e.g. solved by numerical integration or series expansion. An input/output model of an XY micromanipulator is presented in [17] in which a full kinematic model that considers the elasticity of the whole CM is proposed allowing to establish the kinematic relationships between output motion and input variables. An iterative technique in which the equivalent rigid-body mechanism dimensions are updated by a large deflection analysis is proposed in [11]. Several types of flexures models can be included into the formulation. The technique can be used to achieve the mechanism pose and required driving loads when subject to a set of input conditions (external load and input links prescribed rotations).

2. Strategies in which FEA is used to solve the force-displacement problem. In [20] a compliant parallel-guiding mechanism is designed and both its force-displacement model and guiding accuracy are obtained through FEA. Reference [21] presents a study of the mobility of different types of flexure hinges. A Roberts-Chebyshev straight-line mechanism is analyzed to validate the study. The design of a compliant robotic wrist able to perform spherical motions is discussed in [22]. The inverse and direct kinematics and the design of its flexures are computed by FEA.

Contribution. Compared to the PRBM, the procedure proposed in this article represents both a more accurate model and a more general approach in which a wide variety of flexure-based CMs can be assessed without the use of closed-form kinematic solutions. Instead, a chain-based analysis technique supported in the Assur group concept is designed and implemented.

Results reported in this work present a good match when compared to FEA. In addition, the alternative here presented allows for the use of analysis and synthesis tools coming from the rigid-

body mechanism theory.

The article is organized as follows: section 1.1.3 summarizes the the force-displacement iterative technique adopted in this work, section 1.1.4 presents the new algorithm for the force-displacement model of CMs in which kinematics and force analysis are based on a division of the mechanism into Assur groups, in section 1.1.5 the algorithm is tested with a 3-DOF flexure-based mechanism, finally, section 1.1.6 develops concluding remarks.

1.1.3 Background

The iterative technique to perform the force-displacement analysis of flexure-based CMs introduced in [11] is suitable for modeling those CMs that take the form of ordinary mechanisms whose kinematic pairs have been replaced by flexure hinges (Fig. 1.1). Unlike other methods, such as non-linear FEA or PRBM, the flexures are considered as whole parts that undergo large deflections and are not divided into smaller elements, this allows for a modular approach where the large displacement analysis of different kinds of flexures is developed so that a great variety of mechanisms with such flexure hinges can be designed and analyzed.

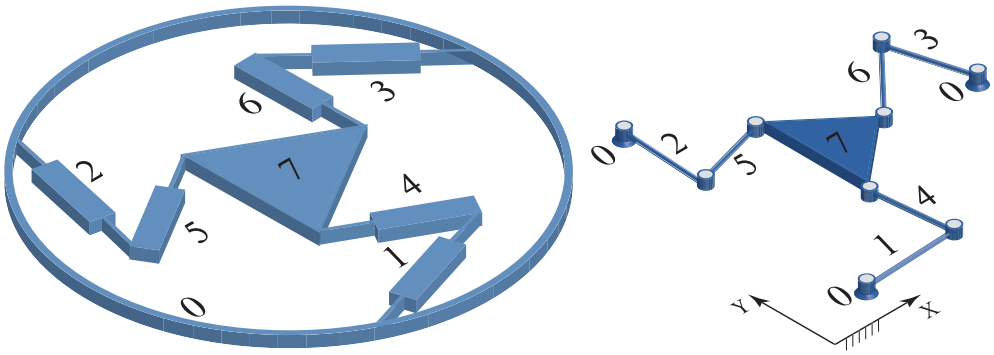

(a) 3-DOF flexure-based mechanism

(b) Rigid-equivalent mechanism of Fig. 1.1(a)

Figure 1.1: 3-DOF flexure-based parallel mechanism and its rigid-equivalent mechanism

To achieve the position analysis of CMs requires not only to implement the kinematic relations used for ordinary mechanisms but also to include static (equilibrium) and elasticity equations that rule the flexure behavior into the formulation of the model. In order to implement the kinematic equations, conventional rotational pairs must be introduced between one of the extremities of each flexure and its adjacent rigid segment (see section 1.1.4.2), therefore allowing at the cur-

rent point the relative rotation between the flexure and its rigid segment. Once the input variables are established (input rigid links orientations), the kinematic analysis is solved as for ordinary rigid-equivalent mechanism.

After the kinematic analysis solution is reached, the equilibrium problem is solved by means of a static analysis to the rigid-equivalent mechanism on its new configuration. The static analysis returns the internal forces acting in each joint together with the moments to be applied on the input links in order to achieve their prescribed orientations and equilibrate the external loads acting on the mechanism.

Finally, the flexure elastic behavior is modeled by means of a deflection analysis where each flexure present in the CM is modeled as an independent part. A differential equation modelling large deflections of the flexure hinge is used to relate the deflected shape of each flexure with the load applied upon it, which results in the computation of a new rigid-equivalent mechanism geometry. In this manner new results of kinematic and force analysis are obtained that leads to a loop. The loop is iterated until all variables converge.

1.1.4 Force-Displacement Model of Compliant Mechanisms using Assur Sub-Chains

The methodology of this work relies on the division of the CM into rigid-equivalent sub-chains derived from its kinematic structure, so that the kinematic and force analyses can be solved independently (within an iteration step) for the sub-chains instead of formulating a solution for the entire mechanism. After that, a deflection analysis is carried out to each flexure within the mechanism where new equivalent dimensions of the sub-chains are estimated. The procedure is mostly suitable for planar-flexure-based compliant mechanisms since this type can be mapped into planar-rigid-body mechanisms by replacing the flexure hinges with traditional kinematic pairs. Furthermore, it is well known that the rigid-body mechanism kinematics and kinetostatics can be solved if a disaggregation of the mechanism into Assur groups is implemented. In this case, particular kinematic and kinetostatic solutions for the groups are used instead of formulating a fully analytical solution for the entire mechanism. The procedure is presented in algorithm 1, and stated through this section in three steps. Prior to that, the topology and geometry of the rigid-equivalent mechanism must be determined together with its disaggregation into driving mechanisms and Assur groups, as pointed out in sections 1.1.4.1 and 1.1.4.2.

Algorithm 1 Force-Displacement Model of Compliant Mechanism.

Require:
- (T, G_0) — Mechanisms with topology T and relaxed geometry G_0
- $\mathbf{q} = \begin{bmatrix} q_1 & q_2 & \dots q_\omega \end{bmatrix}^T$ — Required orientations of driving mechanisms
- φ_i — Flexures geometry and material properties
- P — External loads and application points

Ensure:
- G_f — Deflected mechanism geometry
- $\boldsymbol{\tau} = \begin{bmatrix} \tau_1 & \tau_2 & \dots \tau_\omega \end{bmatrix}^T$ — Driving torques to archive the prescribed orientations $\mathbf{q}$ given the external loads P

1: $G = G_0$ (*G is a reference mechanism geometry*)
2: $M_i = 0$ (*M_i is the ith-flexure internal moment*)
3: $error = tol$
4: **while** $error \geq tol$ **do**
5: (*_Step 1. Modular kinematic analysis_*)
6: $\{G_f, \Theta_i\}$ = **Modular_kinematics**$(T, G, \mathbf{q})$ (*Θ_i is the ith-flexure effective rotation*)
7: (*_Step 2. Modular static analysis_*)
8: $\{Fx_i, Fy_i, \boldsymbol{\tau}\}$ = **Modular_statics**(T, G_f, P, M_i) (*Fx_i, Fy_i are the internal forces acting on the ith-rotational joint*)
9: (*_Step 3. large deflection analysis_*)
10: $\{G, M_i\}$ = **Large_deflection**$(T, G_f, Fx_i, Fy_i, \varphi_i, \Theta_i)$
11: $error = |G_f - G|$
12: **end while**
13: $G_f = G$ (*Mechanism final geometry (deflected configuration)*)

1.1.4.1 Structural analysis of rigid-equivalent mechanism

To perform a structural analysis of the CM, a rigid-equivalent mechanism must be determined. This task can be accomplished by replacing each flexure hinge of the CM with a rotational joint. At this point we are only concerned with the topological characteristics of the rigid-equivalent mechanism. Geometrical characteristics will be determined after the disaggregation into Assur groups of the rigid-equivalent mechanism and its generation principle(generation of a mechanism by the successive joining of Assur groups) are established (section 1.1.4.2).

Figure 1.1 presents a 3 DOF flexure-based parallel mechanism (Fig. 1.1(a)) and its rigid-equivalent mechanism (Fig. 1.1(b)). If the rigid-equivalent mechanism is simple enough, its disaggregation into Assur groups and the determination of its kinematic structure can be accomplished by inspection. However, if the mechanism possesses a complex kinematic structure, there exist available computational methods that allow the separation of planar mechanisms into Assur

groups (e.g. [23]). For the sake of brevity, it is assumed along this work that the disaggregation into Assur groups and the generation principle are established. Two basic groups families are considered:

1. One degree of movability kinematic chains formed by a driving link, a rotational joint and the fixed link and denoted as driving mechanisms.
2. Zero degrees of movability kinematic chains denoted as Assur groups.

The generation principle of a mechanism can vary depending on the selection of its input links. There exist several types of Assur groups from which a mechanism can be formed. Nevertheless, only CMs whose rigid equivalent mechanism include Assur groups of the second and the third class within their kinematic structure are to be considered through this article. The combination of this groups yields almost any practical planar mechanism [24]. Figure 1.2 illustrates the generation principle of a 3-DOF flexure-based parallel mechanism after its three links connected to the ground have been selected as driving links.

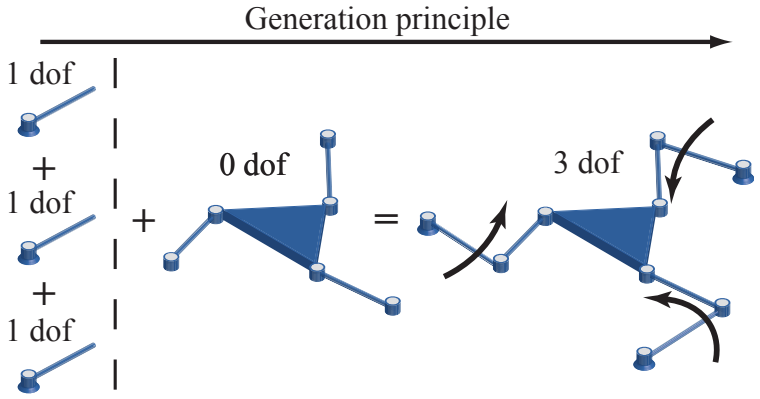

Figure 1.2: 3*RRR* mechanism generation principle

1.1.4.2 Convention for rigid-equivalent mechanism determination

The initial step in the iterative force-displacement modeling of CMs is the calculation of its rigid-equivalent mechanism kinematics. Prior to that, it is necessary to determine the geometry of the rigid-equivalent mechanism. The dimensions of the links are determined by the location of the equivalent rotational joints. Moreover, the location of the joints is determined specifically by each

Assur group type present in the generation principle. Two kinds of joints within the Assur groups are considered:

1. *External* or *free* joints: joints that connect the Assur group to other groups, the fixed link or the driving links.

2. *Internal* joint: joints that connect two Assur group internal links.

The following convention to locate the equivalent rotational joints is adopted:

1. Equivalent *external* joint. The rotational joint is located in any of the two edges between the rigid section and the flexure (Fig. 1.3).

2. Equivalent *internal* joint. The rotational joint is located in any two of the edges between the joined rigid sections and the flexure (Fig. 1.3).

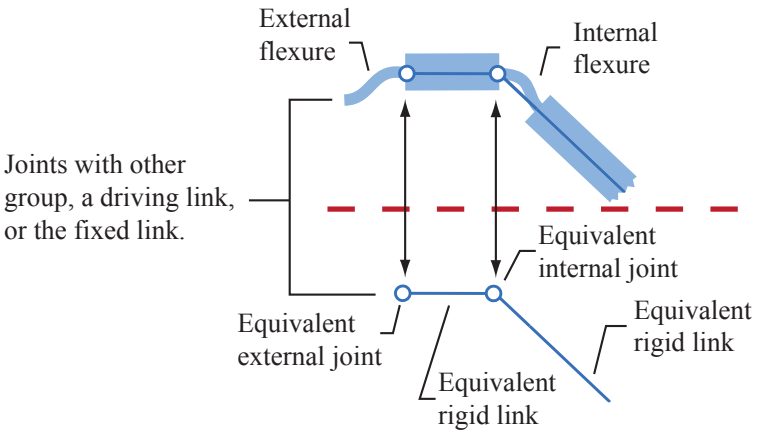

Figure 1.3: Equivalent Assur group convention

According to conventions (1) and (2), the equivalent second and third class Assur groups are defined as illustrated in Fig. 1.4(a) and Fig. 1.4(b) respectively. Similarly, Fig. 1.4(c) shows the convention to assign the rotational joint of an equivalent driving mechanism.

The purpose of locating the rotational joints between one of the extremities of the flexure and one of its adjacent rigid segments is to ensure that the internal forces coming from the static analysis are located such that each flexure can be modeled as a constant cross-section cantilever beam with its free tip under the action of two forces, F_x and F_y, and a moment M (Fig. 1.5).

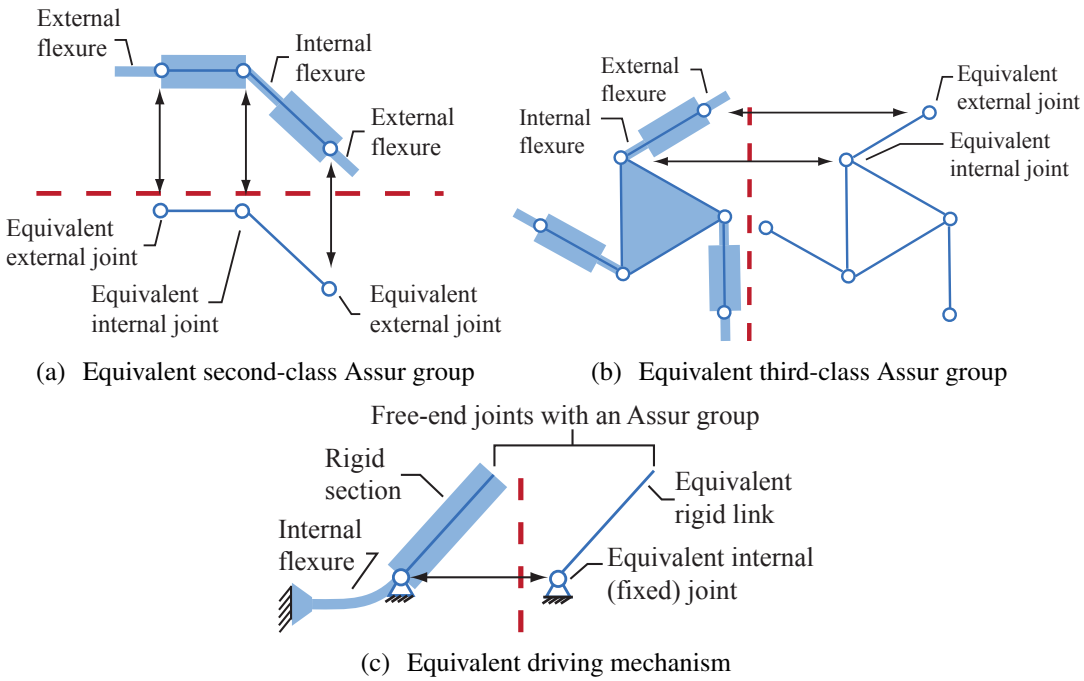

(a) Equivalent second-class Assur group (b) Equivalent third-class Assur group

(c) Equivalent driving mechanism

Figure 1.4: Equivalent Assur groups and driving mechanism convention

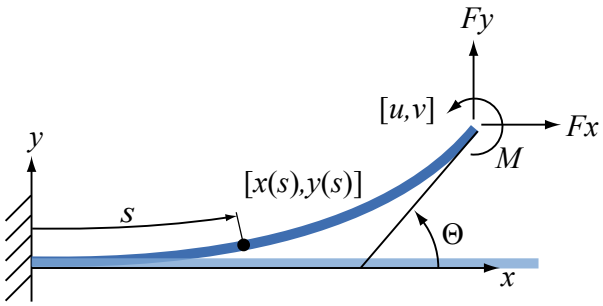

Figure 1.5: Flexure hinge deflection analysis [11]

1.1.4.3 Force-displacement model

The concept of modular kinematics and force analysis is based on a divide-and-conquer approach: the analyses are solved by the disaggregation of the mechanism into simpler kinematic chains that can be analyzed in a hierarchical order rather than analyzing the complete mechanism. The kinematic chains are the so called driving mechanisms and Assur groups. The hierarchy is determined by the order in which the chains must be added to form the mechanism (generation principle) [25]. An Assur group is defined as a determinated kinematic chain that cannot be disaggregated into lower class Assur groups [24, 25]. As a consequence, its kinematic and static models can be stated independently being this property the keystone of the modular approach. Standard solutions for

the kinematics and statics of different classes of groups are available in the literature [24, 25]. The solution of the modular kinematics and force problems requires:

1. To know the generation principle of the mechanism as pointed out in section 1.1.4.1.
2. To have the solution modules of the position and force problems of the driving mechanisms and Assur groups within the generation principle of the mechanism.
3. To have the geometry (dimensions) of the equivalent driving mechanisms and Assur groups withing the generation principle of the mechanism as pointed out in section 1.1.4.2.

Considering requirements (1–3), the force displacement procedure is carried out in the following manner:

Step 1. Modular kinematics

Given:

1. A rigid-equivalent mechanism reference configuration (non-deflected configuration at fist iteration) determined by:
   (a) The position of driving mechanisms joints given by the set $\{\mathbf{r}^{D1}, \ldots, \mathbf{r}^{D\omega}\}$.
   (b) The position of Assur groups joints given by the set $\{R^{A1}, \ldots, R^{A\Omega}\}$.

   Ω and ω are respectively the number of Assur groups and driving mechanisms within the generation principle of the mechanism. $\mathbf{r}^{Di}$ is the position vector of the ith driving mechanism rotational joint and R^{Aj} is the set of position vectors of the jth Assur group rotational joints. Both the $\mathbf{r}^{Di}$ vector and the R^{Aj} set of vectors are referenced to the global coordinate system (OXY).
2. The prescribed orientation of the driving mechanisms,

$$\mathbf{q} = \begin{bmatrix} q_1 & q_2 & \ldots q_\omega \end{bmatrix}^T, \tag{1.1}$$

   where $\mathbf{q}$ is a column vector of input joint angles.

Goal. To find:

1. An updated (deflected) rigid-equivalent mechanism configuration determined by:

   (a) The updated position of the driving mechanisms joints as a function of the input joint angles $\left(\{\mathbf{r}^{D1}, \ldots, \mathbf{r}^{D\omega}\}(\mathbf{q})\right)$.

   (b) The updated position of Assur groups joints $\left(\{R^{A1}, \ldots, R^{A\Omega}\}\right)$.

2. The effective rotation of the flexures $(\Theta_i,\ i = 1, 2, \ldots, \gamma$, where γ is the number of flexures). Θ_i is evaluated after the position $\mathbf{r}^i$ of every equivalent joint (updated rigid-equivalent mechanism configuration) is determined. If the flexure is placed between two rigid segments whose orientations are described by the α and β angles (see Fig. 1.6), then the flexure effective rotation referenced to the local coordinate system oxy is given by

$$\Theta_i = \beta - \beta_0 - \alpha + \alpha_0, \tag{1.2}$$

   Eq. (1.2) reduces to Eq. (1.3) using the angle differences.

$$\Theta_i = \Delta\beta - \Delta\alpha. \tag{1.3}$$

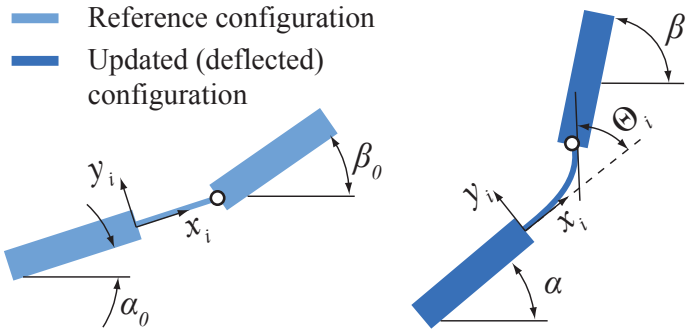

Figure 1.6: Flexure effective rotation

The modular kinematic analysis is carried out as illustrated on Fig 1.7. The mechanism reference configuration is used to calculate the current dimensions of the rigid equivalent mechanism. After that, the position of each rotational joint within the equivalent mechanism is obtained according to the mechanism generation principle. This implies that the driving mechanisms position problem is first solved, which determines the position of any point laying on the driving links

that might connect to the remaining Assur groups. As a result, the positions (constraints) of the free-joints of the first Assur group in the sequence are obtained.

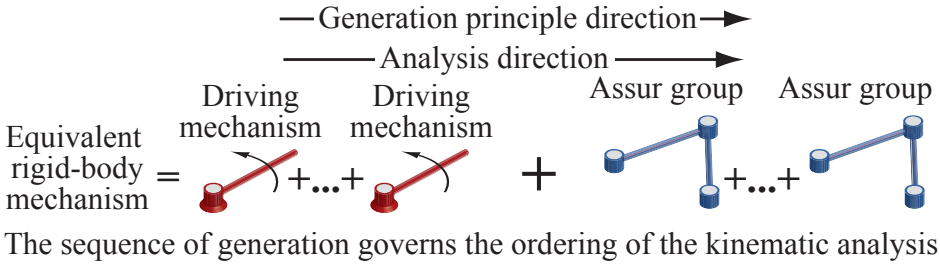

Figure 1.7: Kinematic analysis of a rigid-body mechanism

The solution of the first Assur group position problem provides the free-joint positions of the following Assur groups. The sequence advances in the direction of the generation principle until the position problem of all Assur groups are solved.

Step 2. Modular force analysis

Given:

1. The rigid-equivalent mechanism updated (deflected) configuration is determined by:
   (a) The position of driving mechanisms rotational joints at updated configuration $\left(\{\mathbf{r}^{D1}, \ldots, \mathbf{r}^{D\omega}\}\right)$.
   (b) The position of Assur groups rotational joints at updated configuration $\left(\{R^{A1}, \ldots, R^{A\Omega}\}\right)$.
2. The set of external loads (P) applied to the Assur groups and their application points.
3. The internal moment (M_i, zero at first iteration) that equilibrates the flexure tip loads (F_{X_i}, F_{Y_i}) at the deflected configuration (see Fig. 1.5).

Goal. To find:

1. The internal forces (F_{X_i}, F_{Y_i}) acting on each joint of the rigid-equivalent mechanism referenced to the world coordinate system OXY.

2. The set of driving loads $(\boldsymbol{\tau})$ that has to be applied to the driving links to equilibrate the external loads (P) and achieve the prescribed rotations $(\mathbf{q})$.

$$\boldsymbol{\tau} = \begin{bmatrix} \tau_1 & \tau_2 & \dots & \tau_\omega \end{bmatrix}^T, \tag{1.4}$$

where $\boldsymbol{\tau}$ is a vector of driving loads.

The procedure for the modular static analysis is illustrated in Fig. 1.8. The solution is achieved sequentially in the opposite direction of the generation principle. First the last Assur group static-problem is solved determining a set of joint reactions that are introduced as external loads acting on the previous groups. After that, the previous group is solved and the sequence goes on until all the groups within the mechanism are solved. Finally, the solution of each driving mechanism equilibrium-problem is reached determining the driving loads $(\boldsymbol{\tau})$ and the fixed joint reactions.

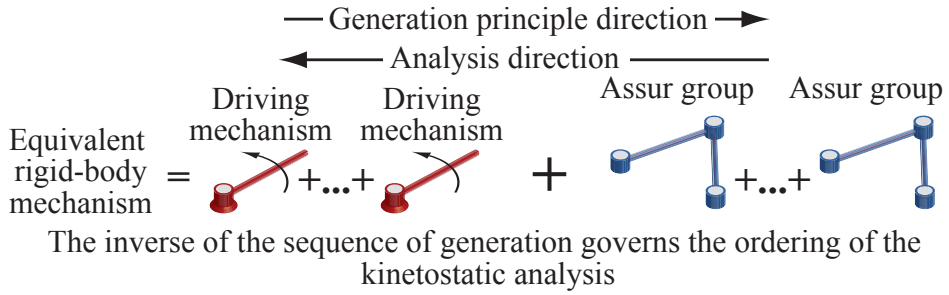

Figure 1.8: Static analysis of a rigid-body mechanism

Step 3. Large deflection analysis

After the kinematic and force analysis problems are solved, the next step is to model the behavior of the flexure hinges through a deflection analysis stated in the following manner:

Given:

1. The flexures effective rotation (Θ_i).

2. The internal forces (F_{X_i}, F_{Y_i}) acting on each rotational joint (flexure hinge free-end) of the rigid-equivalent mechanism.

3. The flexure geometry and material properties (φ_i).

Goal. To find:

1. The flexures free-end position vector ($\mathbf{r}_i$) at deflected configuration. This corresponds to the correction to the position of all joints and therefore, to the new mechanism reference configuration required for the next iteration.
2. The internal moment (M_i) that equilibrates the flexure tip loads (F_{X_i}, F_{Y_i}) at the deflected configuration.

The deflected shape of a flexure is described by its relative free-end position vector (${}^{oxy}\mathbf{r}_i = u_i + v_i$, see Fig. 1.5) and its free-end rotation (Θ_i). The left superscript oxy refers $\mathbf{r}_i$ to the flexure local coordinate system.

Similarly, the load applied to the flexure is described by the forces (Fx_i, Fy_i) and the moment M_i acting on the flexure hinge free-end (Fig. 1.5). It should be noted that the forces (Fx_i, Fy_i) are the axial and shear components of the force acting on the flexure hinge and they correspond to the projection of the global forces (F_{X_i}, F_{Y_i}) to local coordinate system oxy.

The following deflection analysis is adopted from the work by S. Venanzi et al. [11], and it is summarized as follows:

The Euler-Bernoulli equation (for long-beam like members) is used to model each flexure hinge when large deflections are considered by relating both the deflected shape and the forces applied upon it. The non-linear aspect is introduced by combining the bending effects of three end loads (Fx_i ,Fy_i, M_i), as it is well known that linear displacement theory disregards the contribution of the axial force to the bending.

The bending moment acting on a section s is defined as:

$$M(s) = M + Fy(u - x(s)) - Fx(v - y(s)), \tag{1.5}$$

where s is a linear coordinate along the beam, $(x(s), y(s))$ are the local coordinates of the point (s) where the bending moment is evaluated and (u, v) are the local coordinates of the free-end (Fig. 1.5). The Euler-Bernoulli differential equation states

$$\frac{d\theta(s)}{ds} = \frac{M(s)}{EI}, \tag{1.6}$$

where $\theta(s)$ is the beam rotation, E is the material elastic modulus and I is the cross section area moment of inertia. The following identities are valid for a point of the deflected beam:

$$\begin{aligned} \frac{dx(s)}{ds} &= \cos\theta(s), \\ \frac{dy(s)}{ds} &= \sin\theta(s). \end{aligned} \tag{1.7}$$

Combining and reorganizing Eqs. (1.5)–(1.7), the Euler-Bernoulli equation for a deflected beam is formulated as a system of first order differential equations (Eq. (1.8)).

$$\frac{d}{ds}\begin{bmatrix}\theta(s)\\ x(s)\\ y(s)\end{bmatrix} = \begin{bmatrix}\frac{M+Fy(u-x(s))-Fx(v-Y(s))}{EI}\\ \cos\theta(s)\\ \sin\theta(s)\end{bmatrix}, \tag{1.8}$$

subject to the boundary conditions

$$\left.\begin{bmatrix}\theta\\ x\\ y\end{bmatrix}\right|_{s=0} = \begin{bmatrix}0\\ 0\\ 0\end{bmatrix}, \qquad \left.\begin{bmatrix}\theta\\ x\\ y\end{bmatrix}\right|_{s=L} = \begin{bmatrix}\Theta\\ u\\ v\end{bmatrix}. \tag{1.9}$$

The boundary conditions are applied to both bounds of the independent variable s, which varies between 0 and L for the length of the beam. Six parameters are related in Eq. (1.8) and (1.9): M, the moment on the beam free end, F_x and F_y, the components of the load acting on the free-end of the beam (referenced to the local coordinate system oxy), the effective rotation Θ, and the components of the relative free-end position vector of the beam (u, v).

It should be noted that the flexure free-end position vector $\mathbf{r}_i$ (see Sec.1.1.4, step 3, goal 1) corresponds to the projection of the relative free-end position vector ${}^{oxy}\mathbf{r}_i$ to the global coordinate system (OXY)

If the effects of the internal axial force acting on the beam are added to Eq. (1.8), then the accuracy of the solution is reported to be increased [11]. The boundary value problem solution required the parameters Θ, Fx and Fy as known inputs and provides the output parameters M, u and v. A numerical method might be implemented for this purpose [11, 17].

1.1.5 Results

In this section the force-displacement model of a 3-DOF planar CM is performed. The symmetrical mechanism is capable of setting its end-effector pose and consists of an equilateral moving platform connected by three identical compliant legs to an equilateral fixed base (Fig. 1.9). Each compliant leg is formed by an alternating pattern of three flexures connecting two rigid segments. The mechanism is actuated from the rigid elements connected to the base. Dimensions are described on Table 1.1, and aluminum 7075 (E = 70 GPa) is assumed as material.

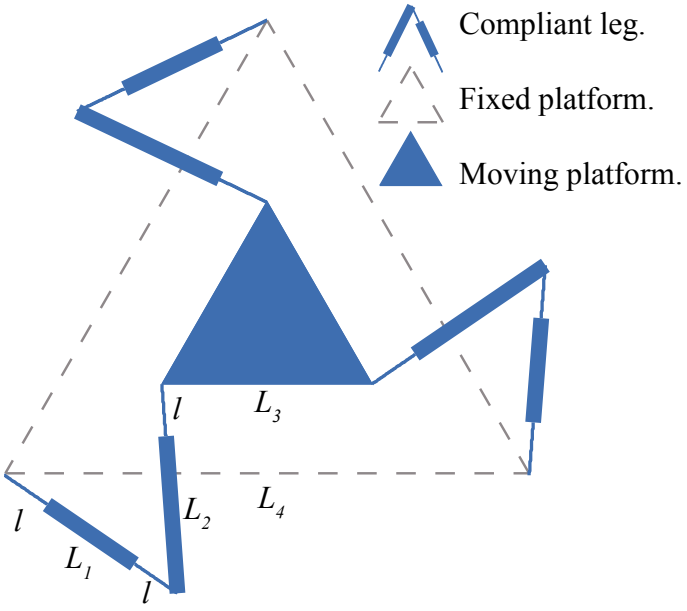

Figure 1.9: Compliant mechanism case study

Parameter	Value
l	10 mm
L_1	20 mm
L_2	30 mm
L_3	40 mm
L_4	100 mm
$Flexure\ width$	5 mm
$Flexure\ thickness$	0.1 mm

Table 1.1: Case study dimensions

1.1.5.1 Generation principle

The topology of the rigid equivalent mechanism is obtained after the flexures are replaced with rotational joints (see Fig. 1.1). If the three links connected to the fixed base are selected as driving links, then the mechanism generation principle is (see Fig. 1.2):

$$I_R \rightarrow I_R \rightarrow I_R \rightarrow III_{RR-RR-RR}, \tag{1.10}$$

where I_R denotes a first-class driving mechanism and $III_{RR-RR-RR}$ denotes a third class Assur group.

1.1.5.2 Rigid-equivalent mechanism

Figure 1.10 shows the assigned rigid-equivalent mechanism at its relaxed position. According to the proposed convention of section 1.1.4.2, the mechanism parameters at relaxed configuration are $\overline{EH} = \overline{FI} = \overline{GJ} = 30.00$ mm, $\overline{HK} = \overline{IL} = \overline{JM} = 40.00$ mm, $\overline{KL} = \overline{LM} = \overline{MK} = 40.00$ mm, $\mathbf{r}_E = (-41.74, -34.51)$ mm, $\mathbf{r}_F = (50.76, -18.90)$ mm, $\mathbf{r}_G = (-9.01, 53.40)$ mm, $\theta_1 = -0.599$ rad, $\theta_2 = 1.495$ rad, and $\theta_3 = -2.694$ rad.

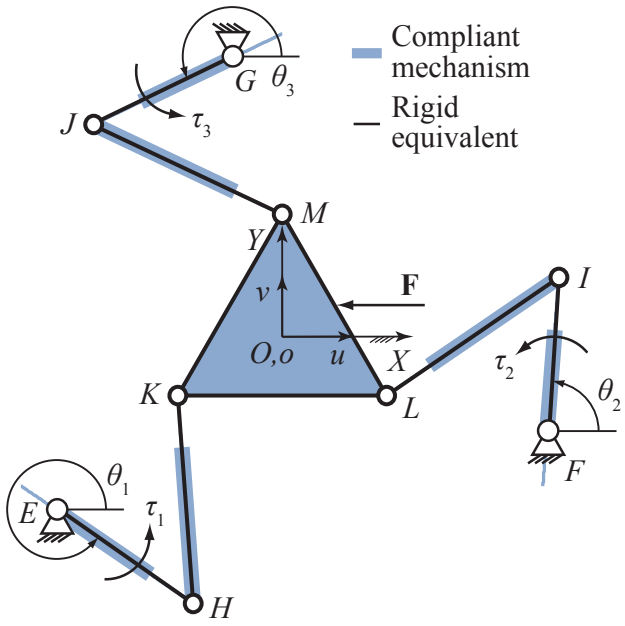

Figure 1.10: Compliant mechanism and rigid equivalent

1.1.5.3 Force-displacement model

At this point, the previous conditions (see requirements 1–3 of Section 1.1.4) to the force-displacement procedure are met:

1. The generation principle of the mechanism is known, expression 1.10.
2. The solution of the position and force problems of the driving mechanisms and the third-class Assur group are known, *e.g.* it is possible to solve the position problem of the third-class Assur group using a numerical strategy such as virtual variable searching. [25].
3. The parameters of the equivalent mechanism at relaxed configuration (see section 1.1.5.2).

The force-displacement model procedure (section 1.1.4), is carried out as follows:

Step 1. Modular kinematics

Given:

1. The rigid equivalent mechanism non-deflected configuration:
   (a) Position of driving mechanisms rotational joints:

$$\begin{aligned} \mathbf{r}^{D1} &= \mathbf{r}_E, \\ \mathbf{r}^{D2} &= \mathbf{r}_F, \\ \mathbf{r}^{D3} &= \mathbf{r}_G. \end{aligned} \tag{1.11}$$

   (b) Position of third-class Assur group rotational joints:

$$R^{A1} = \{\mathbf{r}_H, \mathbf{r}_I, \ldots, \mathbf{r}_M\}. \tag{1.12}$$

2. The prescribed orientation of the driving mechanisms:

$$\mathbf{q} = [\theta_1\ \theta_2\ \theta_3]^T. \tag{1.13}$$

   Let the following orientations be imposed to input links, $\theta_1 = -0.349$ rad, $\theta_2 = 1.745$ rad and $\theta_3 = -2.444$ rad.

Goal.

The mechanism updated configuration is calculated using the kinematic solutions of the first class driving mechanism and third-class Assur group. For the sake of brevity the H and I joints are proposed as control points through the whole procedure:

1. Third-class group joints positions, R^{A1}:

$$\begin{aligned} \mathbf{r}_H &= (-13.56, -44.78)\ \mathrm{mm}, \\ \mathbf{r}_I &= (45.56, 10.65)\ \mathrm{mm}. \end{aligned} \tag{1.14}$$

2. Flexure effective rotations Θ (Eq. (1.3))

$$\begin{aligned} \Theta_H &= -0.104\ \mathrm{rad}, \\ \Theta_I &= -0.104\ \mathrm{rad}. \end{aligned} \tag{1.15}$$

Step 2. Modular force analysis

Given:

1. The rigid-equivalent mechanism updated configuration ($\{\mathbf{r}^{D1}, \mathbf{r}^{D2}, \mathbf{r}^{D3}, R^{A1}\}$), calculated in Step 1.
2. The set P of external loads and their application points.

$$P = \{\mathbf{F}, \mathbf{r}_P\}, \tag{1.16}$$

where $\mathbf{F} = (-400, 0)$ mN and $\mathbf{r}_P$ is the middle point between M and L (see Fig. 1.10).

Goal.

The force analysis is solved using the kinetostatic modules of the third-class Assur group and first-class driving mechanism in two aspects:

1. The joint forces acting on the rigid equivalent mechanism.

$$\begin{aligned} \mathbf{F}_H &= (9.27, -41.06)\ \mathrm{mN}, \\ \mathbf{F}_I &= (131.7, 121.6)\ \mathrm{mN}. \end{aligned} \tag{1.17}$$

2. The set of driving loads $\boldsymbol{\tau}$ required to equilibrate the mechanism in the prescribed configuration:

$$\boldsymbol{\tau} = [\tau_1 \ \tau_2 \ \tau_3]^T, \tag{1.18}$$

where $\tau_1 = -0.594$ N mm, $\tau_2 = -3.485$ N mm, $\tau_3 = 6.107$ N mm.

Step 3. Large deflection analysis

Given:

1. The flexure effective rotations ($\{\Theta_E, \ldots, \Theta_M\}$), calculated in Step 1.
2. The joint forces ($\{\mathbf{F}_E, \ldots, \mathbf{F}_M\}$), calculated in Step 2.
3. The flexures geometry and material properties (Table 1.1).

Goal.

The large deflection analysis is calculated solving the differential equation (1.8), by means of a standard numerical finite difference algorithm. The solution consists of two aspects:

1. The flexures free-end position vectors ($\{\mathbf{r}_E, \ldots, \mathbf{r}_M\}$), used to update the mechanism reference configuration required in Step 1. The updated position of the fixed points H and I are selected as control points:

$$\begin{aligned} \mathbf{r}_H &= (-13.05, -44.00) \text{ mm}, \\ \mathbf{r}_I &= (43.98, 10.62) \text{ mm}, \end{aligned} \tag{1.19}$$

2. The internal moments ($\{M_E, \ldots, M_M\}$), used to update the force analysis (see Step 2). The M_H and M_I flexure moments are selected as control points:

$$\begin{aligned} M_H &= 0.468 \text{ N mm}, \\ M_I &= 1.639 \text{ N mm}. \end{aligned} \tag{1.20}$$

Finally the procedure returns to Step 1 (kinematic analysis), where new dimensions of the rigid-equivalent mechanism are calculated from the mechanism new reference configuration. Steps

(1–3) are iterated allowing for a maximal difference of $1 \cdot 10^{-6}$ N mm between two successive calculations of driving input moments $\boldsymbol{\tau}$. The problem converges after 20 iterations to the following results:

$$\begin{aligned} \boldsymbol{\tau} &= [2.207 \quad -2.286 \;\; 9.575]^T \text{ N mm}, \\ \mathbf{r}_o &= (-1.044, -0.062) \text{ mm}, \\ \psi &= -0.277 \text{ rad}, \end{aligned} \tag{1.21}$$

where $\mathbf{r}_o$ and ψ are the moving-platform center position and orientation respectively. The deflected shape of the mechanism is illustrated in Fig. 1.11.

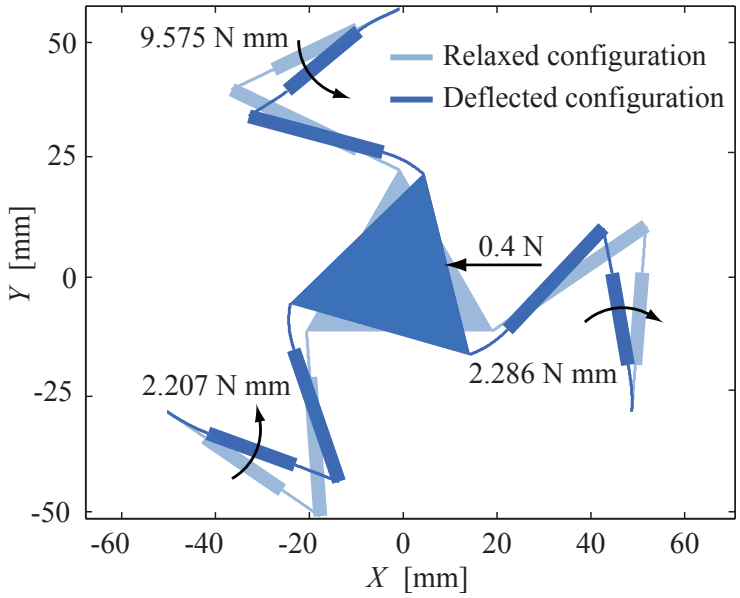

Figure 1.11: Compliant mechanism at deflected configuration

1.1.5.4 Workspace analysis and numerical validation

In this section a workspace analysis of the above described 3-*RRR* compliant mechanism is carry out both with the herein proposed technique and with non-linear FEA for numerical validation purpose. The workspace of the mechanism consists of the joint and its correspondent end-effector workspaces. The joint workspace is the set of Cartesian points $\mathbf{q} = [\theta_1 \; \theta_2 \; \theta_3]^T$, each of them representing the prescribed orientation of the mechanism at a particular configuration. Correspondently, the end-effector workspace is the set of points $[x \; y \; \psi]^T$, where x and y are the Cartesian

components of the end-effector displacement vector $(\mathbf{r}_o)$ and ψ is the end-effector orientation (see Fig. 1.10). The joint workspace carries the input data and the end-effector workspace the output one. Therefore, to each point on the joint workspace corresponds one point on the end-effector workspace. The following criteria was used in the presented study

1. Besides from the driving loads, no external loads were applied to the mechanism.
2. The workspace of the mechanism was limited to those deflected configurations in which non of the flexure hinges of the mechanism presents an axial bending stress grater that 250 MPa.
3. The prescribed rotation range for each driving mechanism was assumed to be the same, resulting from the mechanism structural symmetry and any possible prescribed orientation $\mathbf{q} = [\theta_1\ \theta_2\ \theta_3]^T$ within that range was evaluated.

To build up the mechanism joint workspace, a rotation range for each driving link of 0.44 rad was determined. Greater rotation range values led axial bending stresses that exceeded the 250 MPa limit. The ranges were divided into an arbitrary number of 22 intermediate values for a total number of 22^3 simulations accounted into the joint workspace analysis. The end-effector workspace was obtained through the evaluation of deflected configuration cause by each of the prescribed orientations $\mathbf{q}$ on the joint workspace.

A numerical validation of the obtained end-effector workspace with ANSYS®non-linear FEA was conducted. To model mechanism behavior the beam4 (suitable for large deflections) element was implemented. Each flexure was modeled using a mesh of one hundred elements in order to obtain accurate results. For the rigid segments the same type of element was implemented. However a mesh of ten elements was used to model each segment and the value assigned to their stiffness was of the order of 1000 times grater than the one of the elements used to model the flexures. Figures 1.12–1.14 illustrate both the joint and end-effector workspaces. In Fig. 1.12, the color assigned to each of the points of the workspaces represents the mechanism maximal axial bending stress at a this particular configuration. Similarly, the colormap used in Figures 1.13 and 1.14 represent the prediction error of the end-effector displacement and the orientation error respectively, between the presented method and the FEA.

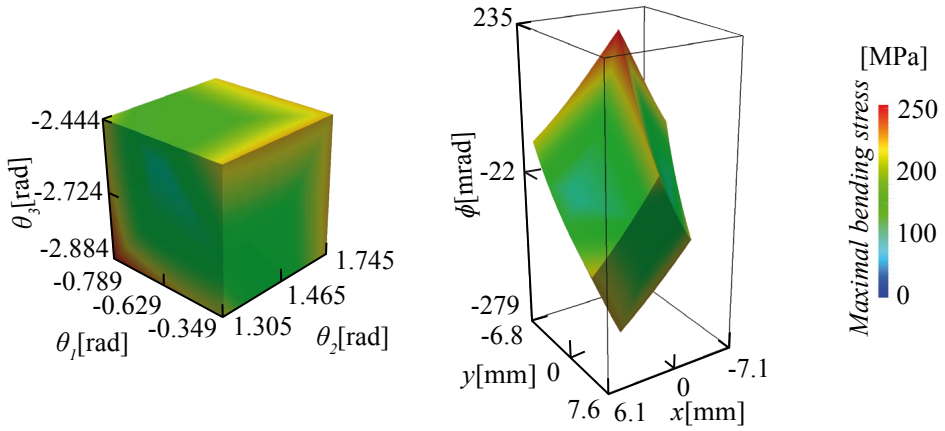

Figure 1.12: Joint and end-effector workspaces with maximal axial bending stress (colormap)

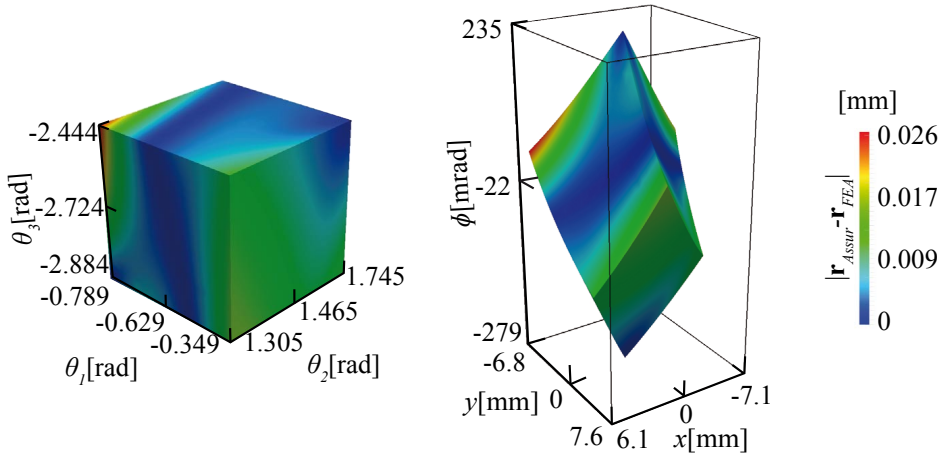

Figure 1.13: Joint and end-effector workspaces with end-effector absolute position error compared to FEA (colormap)

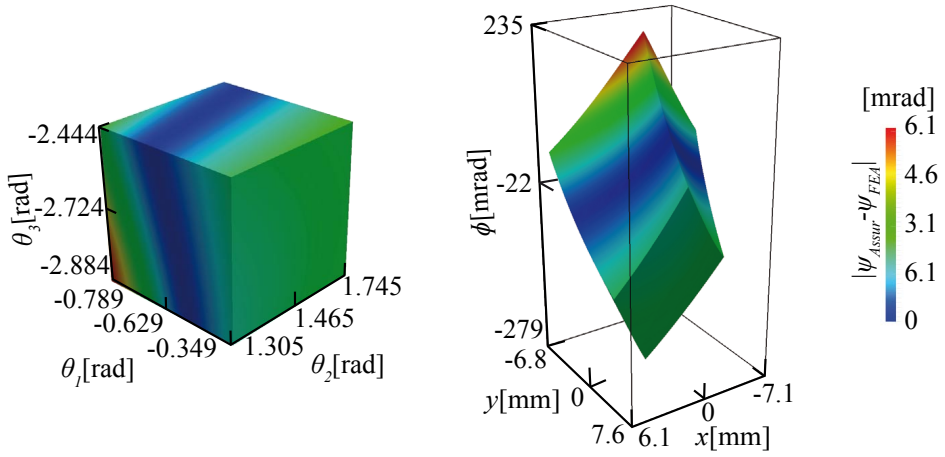

Figure 1.14: Joint and end-effector workspaces with end-effector absolute orientation error compared to FEA (colormap)

1.1.6 Conclusions

This article addresses the force-displacement model of flexure-based planar CMs considering large deflections under quasi-static conditions. Unlike other procedures, the kinematic and force analyses are solved through the decomposition of a rigid-equivalent mechanism into Assur groups. This enables for an extended analysis capability in which the force-displacement model of a wide variety of mechanisms can be assessed depending on the amount of Assur groups available in a kinematic and force analysis solution library.

To validate the performance of the proposed procedure a 3-DOF CM case study was carried out (section 1.1.5). Two simulations were conducted. First, the mechanism pose assessment under an applied load and a prescribed orientation of the driving links. Second, a workspace analysis subjected to axial bending stress restrictions.

The mechanism axial bending streets analysis (see Fig. 1.12) shows that the device presents a non-symmetrical rotational stiffness, since higher stress values arise when the mechanism is actuated to achieve counter-clockwise rotations on its end-effector. Comparisons with FEA led in general to a good match, as the maximal error values of the end-effector position and orientation were found to be 0.026 mm and 6.1 mrad through end-effector displacement and orientation ranges of 15 mm and 500 mrad respectively. The maximal position error (regarding only the end-effector displacement vector $\mathbf{r}_o$) took place at the most distant deflected configuration, as illustrated in Fig. 1.13. In the same manner, the highest orientation error occurred at the deflected configuration of maximal end-effector orientation ψ value (see Fig. 1.14). According to this, considering a more extensive workspace that conveys the mechanism to reach more distant configurations, might result into an increase in the error between the introduced technique and the FEA predictions. However, such considerations are not practical, since operating the device at this configurations might result into mechanical failure.

Scope and Future Work. Only CMs whose rigid equivalent can be dissagregated into Assur groups might be modeled with the proposed technique. No consideration of buckling effects is taken into account into the deflection analysis.

Real experimental test to validate the procedure, together with the implementation of a dynamic model, and a capable model of fully compliant mechanisms are proposals for future work.

1.2 Analytical Method for the Kinetostatic Analysis of the Second-Class RRR Assur Group Allowing for Friction in the Kinematic Pairs

Sebastián Durango, Oscar Ruiz
{sdurang1, oruiz}@eafit.edu.co
CAD CAM CAE Laboratory
EAFIT University
Medellín, Colombia

Gabriel Calle
gcalle@utp.edu.co
Mechanical Engineering College
Technical University of Pereira
Pereira, Colombia

This article was published by the Journal of the Brazilian Society of Mechanical Sciences and Engineering, Vol. 32 (3), pp. 200–207. ISSN: 1678–5878.

Abstract

The calculation of forces in the kinematic pairs of mechanisms by inverse dynamics is usually performed without friction considerations. In practice, when examination of articulated mechanisms takes into account friction, the solution of the inverse dynamics results in a complex procedure. If a modular approach for the inverse dynamics is used, then exact solutions are available, but not necessarily practical. For example, the analytical solution for a second-class first-type Assur group is a $16th$ degree equation. Previous researches proposed an approximated but practical (graphical) method to determine the forces on the kinematic pairs taking into account the friction forces. In this article, an analytical interpretation of the Artobolevski approximated method is developed for the second-class Assur group with three rotational pairs. The final results for the reactions calculated with the implemented method present a good approximation with respect to the graphical solution. Future work should consider friction forces not only in second-class groups with rotational joints but in second-class groups with prismatic joints and higher-class Assur groups.

keywords: Modular Approach, Friction, Kinetostatics, Assur Group.

Glossary

f'	Non-dimensional friction coefficient of a rotational pair.
F	Force magnitude. [N].
J	Inertial moment of mass. [kg m^2].
l	Link length. [m].
m	Mass of a link . [kg].
M	Moment of a force, force pair. [Nm].
P	Power. [W].
r	Shaft radius of a rotational pair. [m].
R	Rotational kinematic pair.
$\mathbf{R}_{AB}$	Relative position vector of point A with respect to point B.
sgn()	Sign function.
T_c	Drive input torque of a driving mechanism. [Nm].

Greek symbols

γ , δ	Angular parameters. [rad].
η	Mechanical efficiency of a mechanism.
ω	Angular velocity of a link. [rad/s].

Subscripts

$_f$	Friction component of a force or moment.
$_{h,i,j,k}$	Link h, link i, link j, link k.

Supperscripts

^{n}	Force component normal to a link.
^{t}	Force component parallel to a link.

1.2.1 Introduction

In the context of the dynamic analysis of the articulated mechanisms, it is usual to neglect friction effects in the kinematic pairs. However, when calculating performance, accurate dynamics or power consumption are required, and friction in the kinematic pairs needs to be considered.

The accurate calculation of friction forces and moments (by inverse dynamics) in the kinematic

pairs of articulated mechanisms results in a complex procedure [26]. The problem complexity is due to the non-linear character of the required models. A graphical iterative solution to the problem of inverse dynamics (kinetostatics) of planar mechanism taking into account friction was proposed by [27]. This solution is limited by its graphical nature.

This paper presents a practical alternative to the kinetostatic analysis of second-class mechanisms with rotational pairs allowing friction in the kinematic pairs. The developed approach is based on the modular concept developed by [28] for the analysis of planar mechanisms based on their structure. The approach corresponds to a chain-based general purpose program in terms of computer aided analysis of mechanical systems [24]. Major advantages of chain-based general purpose programs are flexibility and computer efficiency, being possible to analyze a great variety of mechanisms [24]. To develop a modular approach it is necessary to codify independent analytical solutions (modules) for a number of kinematic chains with a special condition (Assur groups). The analysis of a particular mechanism is performed by assembling the modules corresponding to the driving mechanisms and the Assur groups forming the mechanism.

A methodology to obtain a kinetostatic model allowing for kinematic pair friction in any structural group is proposed (see section 1.2.3, Fig. 1.18). The proposed methodology is applied to the kinetostatic modeling of the second-class first-type Assur group (see section 1.2.3.1). A four-bar mechanism formed by a driving rotational mechanism and a second-class first-type Assur group is used as a case study of the modular kinetostatic analysis (see section 1.2.4.1). Finally, conclusions are drawn and future work is proposed (see section 1.2.5).

1.2.2 Literature Review

1.2.2.1 Computer aided analysis methods for mechanical systems

Computer aided analysis methods for mechanical systems are divided into two categories [29]:

1. Special Purpose (SP).
2. General Purpose (GP).

GP methods are codified as libraries without any specific mechanism, but including the necessary elements to virtually assembly a mechanism. GP libraries could be developed over the

kinematic joint concept or over the kinematic unit concept. For planar mechanisms a kinematic unit corresponds to a structural group or Assur group.

For joint based GP programs the library contains a number of kinematic joints and bodies. Multi-body system (MBS) dynamics became the basis of joint based programs for dynamic analysis of planar and spatial mechanisms. A modern tendency in MBS dynamics is to develop modular methods and hierarchical simulations [30–32]. For planar linkages [33] present an MBS dynamic simulator that allows (Dahl) friction in the kinematic pairs. Dynamics of a planar rigid-link mechanism with rotating slider joint and simplified friction calculations are presented in [34,35]. In [36] a specific case of static analysis of spherical closed chains allowing joint friction calculations was developed. The estimation of friction is developed using a successive approximation method, however, with respect to the approach presented here, the methodology requires to formulate a new set of equations for each new mechanism structure to be analyzed.

GP programs based on kinematic units. Libraries developed using the kinematic unit GP approach contain a number of kinematic chains with a special characteristic that is, they can be assembled in some way to form a mechanism. In the case of planar chains such characteristic corresponds with the definition of Assur groups. The most important feature of this kind of programs is that it comprises the advantages of both SP programs and joint based GP programs, [24] lists them as: computational efficiency (like SP programs) and flexibility (like GP programs).

Kinematics of mechanisms by a kinematic unit GP approach are reported as follows: Reference [37] presents an iterative method for the forward kinematics of higher-class Assur groups by decomposing it into dyadic (second-class) forms. Reference [25] develops a virtual searching method for the position analysis of higher-class Assur groups, [23] presents a general and optimal numerical method to calculate the kinematics of a mechanism when its structural classification is given, [38–40] develop a position analysis in polynomial form of Assur groups of class 4 and 3 including some prismatic joints, [41] research a modular approach for the kinematic analysis of mechanisms, [42] analyze the position of an eight-link Assur group using a vector technique.

GP programs based on kinematic units for kinetostatic analysis (inverse dynamics) of mechanisms were developed by [43–45] for second-class mechanisms and [46] for second and third-class mechanisms. Friction in the kinematic pairs is neglected in those works.

Dynamics of mechanisms by a kinematic unit GP approach are reported as follows: Reference [47] presents a method for the dynamic analysis of planar mechanisms using Assur groups and a state-space formulation of the dynamics. Reference [24] develops a general method for the

dynamic analysis of mechanisms using a modular approach based on the concept of neutral (Assur) and expansion modules. There are no kinematic pair friction considerations in those programs.

The present article proposes an analytical but practical method to the inverse dynamics of Assur groups allowing friction in the kinematic pairs. The analytical and modular form of the method allows to develop a modular approach for the kinetostatic analysis of planar mechanisms.

1.2.3 Methodology

Methods for the kinematic, inverse and forward dynamic analysis based on structural groups are general and modular. A structural group can be identified as a kinematic chain without degrees of freedom with respect to the links which with it forms pairs and such that it is not possible to divide in simpler chains with the same characteristic [41]. The analysis of a structural group can be established independently and then codified as a computer function or module in a library. The variety of mechanisms that could be analyzed with a library depends on the number of modules the library includes. However, most industrial mechanisms are formed by combinations of first-class (driving) mechanisms (Fig. 1.15) and second-class structural groups (Fig. 1.16).

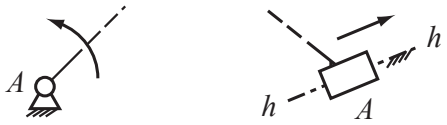

a. Rotational type (*R*) *b*. Prismatic type (*P*)

Figure 1.15: First-class (driving) mechanisms

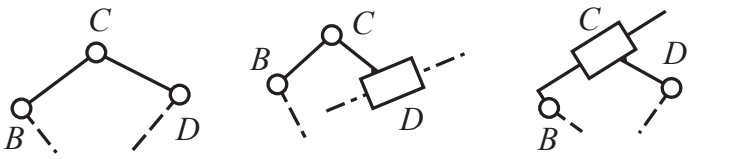

a. First type (*RRR*) *b*. Second type (*RRP*) *c*. Third type (*RPR*)

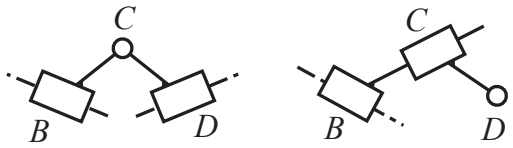

d. Fourth type (*PRP*) *e*. Fifth type (*PPR*)

Figure 1.16: Second-class structural groups

In inverse dynamics we assume that the laws of motion of the driving mechanisms are given. Therefore it is possible to stream the kinematics from group to group until the entire mechanism is solved. The solution is developed in the direction of the structural sequence of the mechanism using the required modules (Fig. 1.17). To complete the force analysis the last group in the structural sequence is isolated. The pair reactions are solved using the correspondent kinetostatic module. The solution comes from group to group in the opposite way of the structural sequence until the driving force or torque is solved (Fig. 1.17).

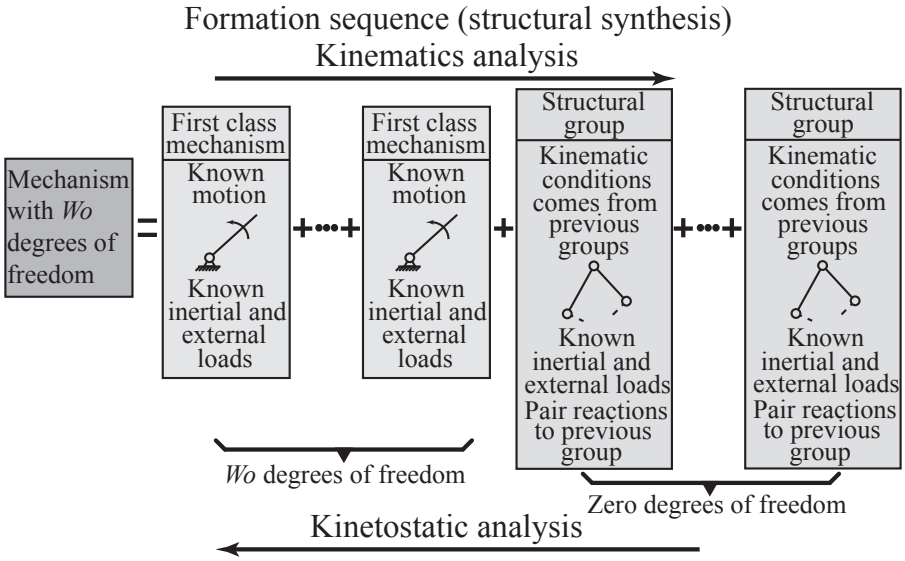

Figure 1.17: Kinematics and kinetostatic analysis of mechanisms with a modular approach

The analytical solution of the kinetostatics of structural groups without friction in the kinematic pairs results in a linear problem. However, when friction in the kinematic pairs is allowed the problem becomes non-linear and complex. In particular, for a second-class first-type structural group an exact analytical solution allowing friction results in a 16-degree equation [26]. Therefore a simpler estimation method is needed.

Reference [27] proposed a graphical approximated method for the inverse dynamics of structural groups allowing friction. This method could be implemented with a parametric CAD program, but it is not practical for the analysis of complex mechanisms nor for multiple configurations of a mechanism. [26] recommends not applying this method when the analyzed mechanism is close to a self-locking configuration. In such configuration friction forces dominate and the approximation could not be valid. In mechanisms self-locking is defined when the work of the driving forces is not enough to overcome the resistive forces different from the workloads, *e.g.* the friction forces actuating on the kinematic pairs. When a mechanism is close to a self-locking configuration its

mechanical efficiency comes to zero, Eq. 1.22.

$$\eta = \frac{W_l}{W_d} \approx 0 \tag{1.22}$$

where the mechanical efficiency η is defined as the ratio of the work of the useful resistive loads (W_l) to the work of the driving forces (W_d). To analyze complex mechanisms and for multiple configuration analysis a computer aided analytical solution is desirable.

The following methodology (see Fig. 1.18) is proposed to obtain an iterative analytical solution of the kinetostatics of a structural group allowing friction in the kinematic pairs:

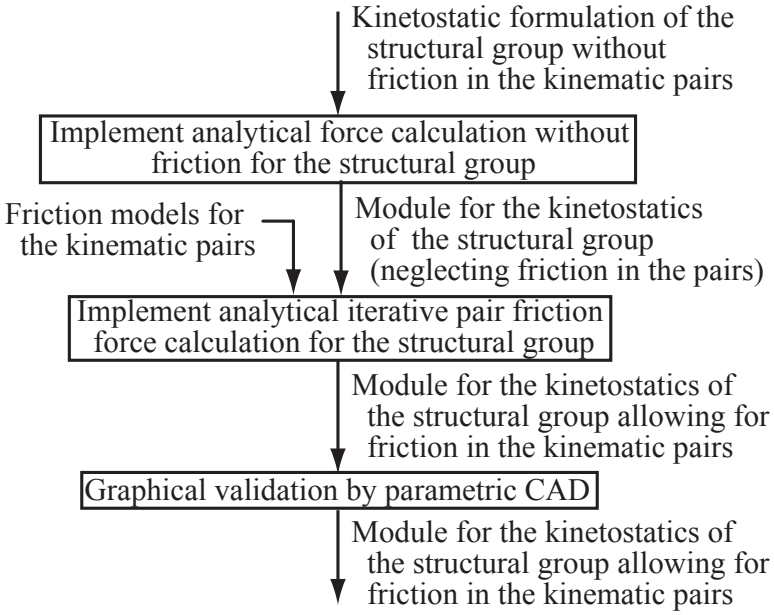

Figure 1.18: Kinetostatic modeling of structural groups allowing friction in the kinematic pairs

1. Obtain a kinetostatic (D'Alembert) formulation without friction forces and moments for the structural group. Analytical solutions of the pair reactions within the group are formulated.

2. Establish a friction model for the kinematic pairs in the structural group. Several options are acceptable for the pair friction models, from a simple Coulomb model to a Dahl one [33].

3. Include the friction forces and moments in the kinetostatic formulation (as external loads).

4. Codify an independent computer function with successive approximation process for the pair force calculation in the structural group.

5. Develop a parametric computer aided drawing (CAD) validation for pair forces in the structural group. [48] proposed a parametric CAD method for the kinematics of planar mechanisms that is expandable to kinetostatics.

As an example of the proposed methodology, the kinetostatic model allowing friction of the second-class first-type structural group is developed in section 1.2.3.1. This methodology is expandable to other second-class or higher-class Assur groups.

1.2.3.1 Kinetostatics of the second-class first-type Assur group

For the kinetostatic analysis of the second-class first-type Assur group neglecting friction in the kinematic pairs, the known parameters are:

1. The geometry of the links,
2. The kinematics of the structural group, and
3. The inertial parameters of the links.

Figure 1.19 presents a dynamic equilibrium diagram of the second-class first-type structural group neglecting friction in the kinematic pairs. Solving the dynamic equilibrium over the entire group by the *x* and *y* components:

$$F_{hi,x} + F_{i,x} + F_{j,x} + F_{kj,x} = 0 \tag{1.23}$$

$$F_{hi,y} + F_{i,y} + F_{j,y} + F_{kj,y} = 0 \tag{1.24}$$

where F_{pq} corresponds to the force of link *p* over link *q*, $pq = hi, kj$. F_i, F_j are the sum of the external and inertial forces over links *i* and *j* respectively.

Taking force moments around *C*, for links *i* and *j*:

$$R_{BC,x}F_{hi,y} - R_{BC,y}F_{hi,x} + M_i + M_{Fi,C} = 0 \tag{1.25}$$

$$R_{DC,x}F_{kj,y} - R_{DC,y}F_{kj,x} + M_j + M_{Fj,C} = 0 \tag{1.26}$$

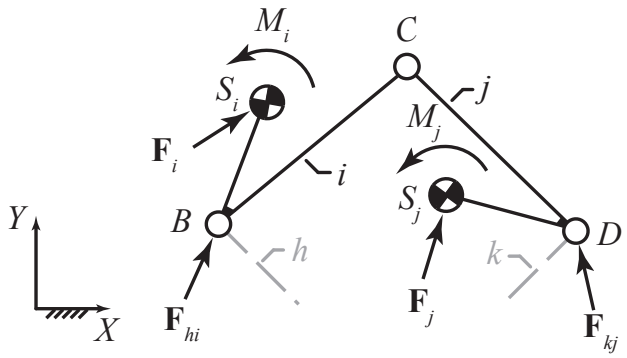

Figure 1.19: Second-class first-type Assur group, dynamic equilibrium diagram

where M_p is the sum of the external and inertial moments over link *p*, and $M_{Fp,C}$ is the sum of the force moments of external and inertial forces actuating on link *p* with respect to *C*, $p = i, j$.

Equations (1.23)–(1.26), form a linearly independent system for the reactions $\mathbf{F}_{hi}$ and $\mathbf{F}_{kj}$ neglecting friction in the kinematic pairs. To calculate the reaction on the *C* pair the sum of forces over link *i* or *j* can be solved. Taking the sum of forces over link *i* by the *x* and *y* components:

$$F_{hi,x} + F_{i,x} + F_{ji,x} = 0 \tag{1.27}$$

$$F_{hi,y} + F_{i,y} + F_{ji,y} = 0 \tag{1.28}$$

To estimate the kinematic pair reactions with friction effects it is necessary to calculate the friction moments in the kinematic pairs ($M_{hi,f}$, $M_{ij,f}$, $M_{ji,f}$ and $M_{kj,f}$, Fig. 1.20). A model for the friction in the kinematic pairs is required. A simplified Coulomb model is assumed (Eq. (1.29)). However, a sophisticated model can be used, *e.g.* a smooth (Dahl) friction model is proposed by [33]. The assumed model for friction in rotational kinematic pairs is

$$M_f = Frf' \tag{1.29}$$

where r is the radius of the cylindrical element on the pair, f' is the friction coefficient on the rotational pair and F is the load over the shaft. The friction moment is opposite with respect to the relative movement of the links forming the pair. The friction coefficient for a rotational pair is greater than the nominal friction coefficient between the materials forming the pair. An accepted estimation is to calculate it as $4/3$ of the friction coefficient between the materials [26]. However, a more sophisticated estimation of the coefficient can include mechanical characteristics of the joint, *e.g.* parameters of the bearing forming the pair. With the assumed model (Eq. 1.29) the initial

estimation of the friction moments in the kinematic pairs of the second-class first-type structural group is as follows:

$$M_{hi,f} = -\text{sgn}(\omega_i - \omega_h)\, F_{hi} f'_B r_B \tag{1.30}$$

$$M_{ji,f} = -M_{ij,f} = -\text{sgn}(\omega_i - \omega_j)\, F_{ji} f'_C r_C \tag{1.31}$$

$$M_{kj,f} = -\text{sgn}(\omega_j - \omega_k)\, F_{kj} f'_D r_D \tag{1.32}$$

were ω_p is the angular velocity of the link p, f'_Q is the friction coefficient in the rotational pair Q, sgn() is the sign function and r_Q is the radius of the cylindrical element forming the pair, $p = h,\, i,\, j,\, k$, $Q = B,\, C,\, D$. Including the friction moments in the kinetostatic formulation, Eqs. (1.25)–(1.26):

$$R_{BC,x}F_{hi,y} - R_{BC,y}F_{hi,x} + M_i + M_{Fi,C} + M_{hi,f} + M_{ji,f} = 0 \tag{1.33}$$

$$R_{DC,x}F_{kj,y} - R_{DC,y}F_{kj,x} + M_j + M_{Fj,C} + M_{ij,f} + M_{kj,f} = 0 \tag{1.34}$$

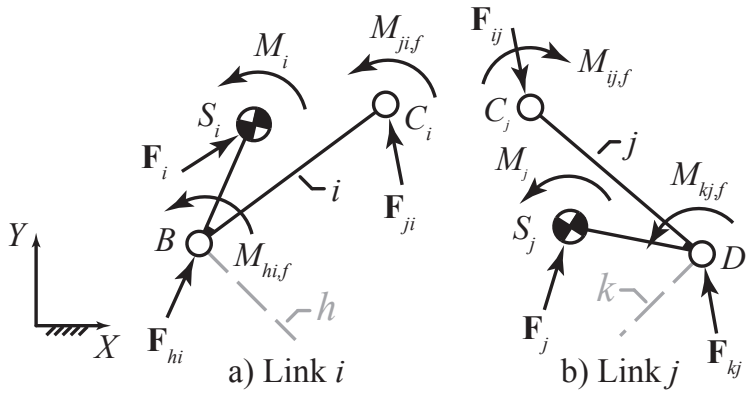

Figure 1.20: Second-class first-type Assur group, dynamic equilibrium diagrams with friction moments

In Eqs. (1.33)–(1.34) the friction moments are functions of the magnitude of the radial forces on each rotational pair. Therefore it is not possible to determine directly the reactions $\mathbf{F}_{hi}$, $\mathbf{F}_{ji}$, and $\mathbf{F}_{kj}$ by means of Eqs. (1.23), (1.24), (1.27), (1.28), (1.33) and (1.34). A practical form to solve this problem is to use a method of successive approximations:

1. For the first approximation the moments of the friction forces are equal to zero. $M_{hi,f} = 0$, $M_{ji,f} = -M_{ij,f} = 0$, and $M_{kj,f} = 0$. The problem is reduced to the solution of the kinetostatics neglecting friction by the linear set of Eqs. (1.23)–(1.28).

2. Assuming a friction simplified model Eq. (1.29), the initial estimation of the friction moments is calculated by the Eqs. (1.30)–(1.32).

3. Using the estimated values of the friction moments calculated in step 2, a new set of reactions $\mathbf{F}_{hi}$, $\mathbf{F}_{ji}$, $\mathbf{F}_{kj}$ is determined by the set of Eqs. (1.23), (1.24), (1.27), (1.28), (1.33) and (1.34).

4. Iterate the calculation process the new values for F_{hi}, F_{ji}, F_{kj} are used in step 2 for friction moments. A new set of kinematic pair reactions is determined in step 3.

5. The iteration process finishes when the difference of the magnitude of the reactions in consecutive calculations is small enough. The maximum difference can be defined depending on the units and magnitudes of the reactions calculated in the analysis. In this sense, the difference depends on the analyzed mechanism. As an example, the four-bar mechanism analyzed in section 1.2.4.1 contains a second-class first-type Assur group. The magnitude of the reactions in the Assur group is of order $1 \cdot 10^3$ N. The reference value for the difference of the reactions between calculations was defined as $1 \cdot 10^{-3}$ N.

Figure 1.21 presents a diagram for the proposed model. The obtained model for the second-class first-type Assur group can be codified as an independent module or computer function. Such function could be included in a GP chain based library for the analysis of planar mechanisms.

The method of modeling presented here for the kinetostatic analysis allowing friction in the kinematic pairs of the second-class first-type Assur group is expandable to any other second-class or high-class Assur group. Section 1.2.3.2 presents the modeling of the rotational driving mechanism allowing friction in the rotational pair.

1.2.3.2 Kinetostatics of the rotational primary mechanism

Figure 1.22 presents the dynamic equilibrium diagram for a rotational driving mechanism with a torque input and friction moment in the rotational pair. The sum of forces for the dynamic equilibrium is:

$$\mathbf{F}_{0h} + \mathbf{F}_h = 0 \tag{1.35}$$

where $\mathbf{F}_h$ is the sum of the external and inertial forces over link *h* and $\mathbf{F}_{0h}$ is the reaction in the rotational pair. The effect of other links forming pairs with link *h* is included as an external force and moment.

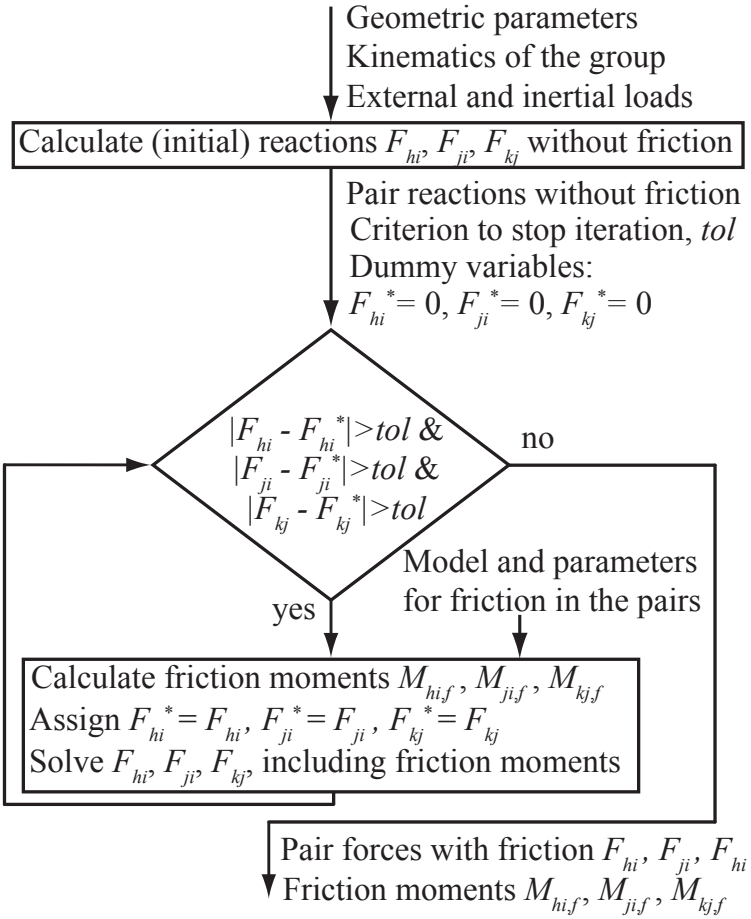

Figure 1.21: Kinetostatic model of a second-class first-type Assur group allowing friction in the kinematic pairs

It is possible to solve the reaction $\mathbf{F}_{0h}$ using directly the Eq. (1.35). Once the reaction is solved it is possible to determine the required input torque for dynamic equilibrium. Calculating the sum of moments with respect to A (Fig. 1.22):

$$T_c + M_{0h,f} + M_h + M_{Fh,A} = 0 \tag{1.36}$$

where T_c is the required input torque for the dynamic equilibrium, M_h is the sum of the external and inertial moments and $M_{Fh,A}$ is the sum of the force moments of the inertial and external forces with respect to *A*.

The friction moment $M_{0h,f}$ can be determined assuming a model for the friction in the rotational pair. Assuming a simplified friction model, Eq. (1.29), and including the sign function to

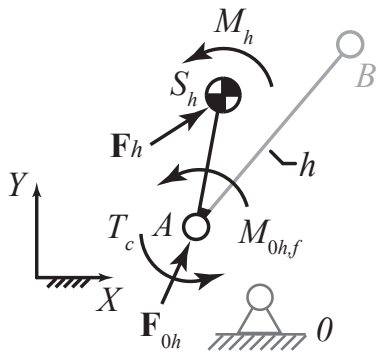

Figure 1.22: Rotational primary mechanism: dynamic equilibrium diagram allowing friction in the rotational pair

determine the direction of the friction moment:

$$M_{0h,f} = -\text{sgn}(\omega_h - \omega_0)\, F_{0h} f'_A r_A \tag{1.37}$$

where ω_p is the angular velocity of link p, f'_A is the friction coefficient on the pair, r_A is the radius of the cylindrical element on the pair, and $p = 0, h$. The input torque (T_c) can be solved directly from Eq. (1.36).

Equations (1.35)–(1.37) can be codified as an independent module or computer function. Such function could be included in a chain-based GP library for the analysis of planar mechanisms.

As an application and validation the inverse dynamics of a four-bar mechanism allowing friction in the rotational kinematic pairs is developed in section 1.2.4.

1.2.4 Results

In this paper a kinetostatic model of the second-class first-type Assur group is presented. The model allows friction in the kinematic pairs. The pair reactions are calculated using an iterative method avoiding non-linearities and complicated solutions. Although the obtained model is for the second-class first-type structural group, it is possible to extend the method of modeling (Fig. 1.18) to any second-class or higher-class structural group.

A simplified friction model is assumed to estimate the friction moments in the rotational pairs (Eq. 1.29); however, other models are allowed, *e*.g. a Dahl model for friction in rotational pairs [33].

Analytical models for the kinematics and kinetostatics of first-class mechanisms and second-class structural groups were codified as modules of a computer library. If a graphic user interface (GUI) is used to develop the modules, then each structural group or driving mechanism is represented by a block. The structural sequence of the mechanism can be established wiring properly the blocks, Fig. 1.23.

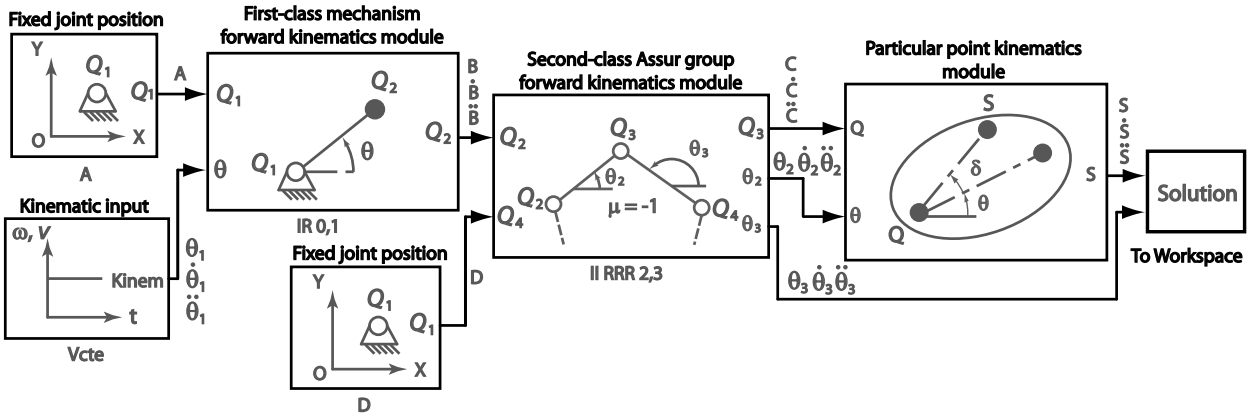

Figure 1.23: Kinematic modular analysis of a four-bar mechanism using a graphic user interface (GUI). Structural sequence: $I^{R}_{0,1} \rightarrow I^{RRR}_{2,3}$

A computer aided graphical validation of the presented modules was developed using a parametric CAD software (SolidWorks). SolidWorks is a product of Dassault Systèmes SolidWorks Corp. A second-class mechanism including a first-class rotational mechanism and a second-class first-type structural group is used as a validation model (section 1.2.4.1).

1.2.4.1 Modular kinetostatics of a four-bar mechanism

Figure 1.24 presents a four-bar mechanism with parameters specified in Table 1.2. For the analysis, the mechanism is assumed to be in steady state. The input angular velocity is assumed to be constant ($\omega_1 = 10\,\mathrm{rad/s}$). The structural classification of the four-bar mechanism is:

$$I^{R}_{0,1} \rightarrow II^{RRR}_{2,3} \tag{1.38}$$

where I^{R} is for a driving mechanism with a rotational pair and II^{RRR} is for a second-class first-type Assur group.

We assume that the kinematics of the four-bar mechanism is given. The kinetostatic analysis

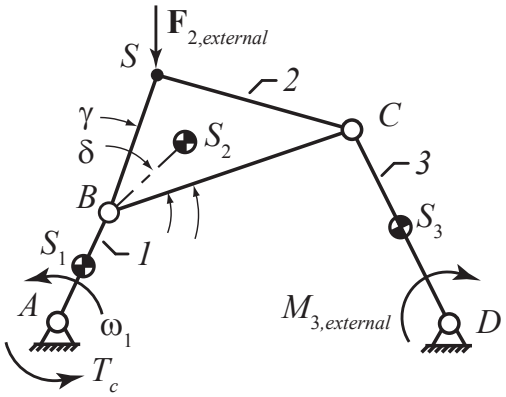

Figure 1.24: Four-bar mechanism

Parameter	Magnitude	Parameter	Magnitude	Parameter	Magnitude
l_{AB}	$2.00\,\mathrm{m}$	l_{DS3}	$1.50\,\mathrm{m}$	$\mathbf{F}_{2,external}$	$1.0\,\mathrm{kN}\downarrow$
l_{BC}	$6.00\,\mathrm{m}$	m_1	$4.8\,\mathrm{kg}$	$M_{3,external}$	$-250\,\mathrm{N\,m}$
l_{CD}	$3.00\,\mathrm{m}$	m_2	$30.0\,\mathrm{kg}$	J_1	$1.70\,\mathrm{kg\,m^2}$
l_{AD}	$5.50\,\mathrm{m}$	m_3	$7.2\,\mathrm{kg}$	J_2	$48.80\,\mathrm{kg\,m^2}$
l_{BS2}	$2.80\,\mathrm{m}$	δ	$0.152\,\mathrm{rad}$	J_3	$5.50\,\mathrm{kg\,m^2}$
l_{BS}	$2.50\,\mathrm{m}$	γ	$\pi/6\,\mathrm{rad}$	f' (a)	0.40
l_{AS1}	$1.00\,\mathrm{m}$			r (a)	$7.50\,\mathrm{mm}$

(a) Same radius and friction coefficient for all joints

Table 1.2: Four-bar mechanism: geometric and inertial parameters

is developed for the range of movement of the input link with evaluations each $\pi/180$ rad. The modular kinetostatic analysis allowing friction in the kinematic pairs of the four-bar mechanism is as follows:

1. Solve the kinetostatics of the second-class structural group formed by links *2* and *3*. The module for the kinetostatics of the second-class structural group corresponds with the codification of the methodology described in section 1.2.3.1.

2. Stream the solutions in step 1 to the first-class mechanism and solve the input drive torque and reactions. The module for the kinetostatics of the first-class mechanism corresponds with the codification of the solution of the set of Eqs. (1.35)–(1.37), section 1.2.3.2.

Figure 1.25 shows the kinetostatic analysis process of the four-bar mechanism.

The results of the inverse dynamic analysis of the four-bar mechanism are presented in Figures 1.26, 1.27 and 1.28. Three solutions are calculated:

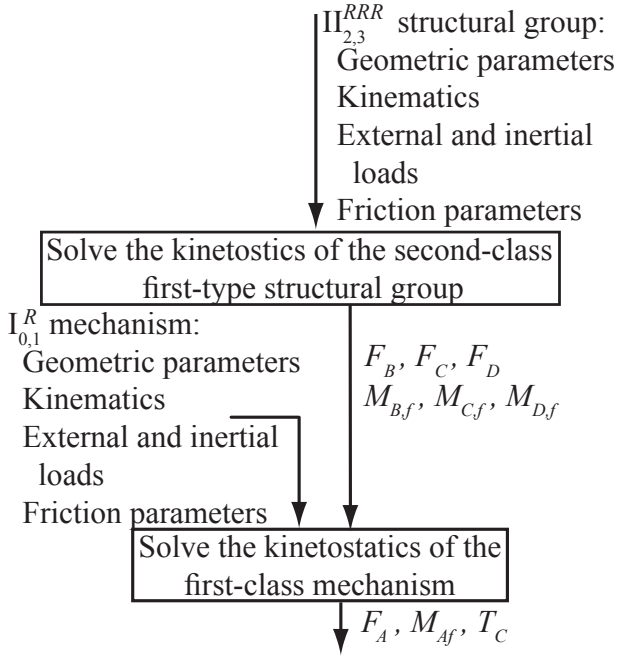

Figure 1.25: Kinetostatic analysis of a four-bar mechanism with a modular approach

1. Calculating pair friction effects using a modular approach and the successive approximation method proposed here,

2. Calculating pair friction effects using a joint-based MBS dynamic program (rough calculation of pair friction forces without iteration in SimMechanics). Most of commercial MBS simulation software uses an approximate calculation of friction forces without iteration, e.g. classical (stiction) friction.

3. Neglecting friction in the kinematic pairs.

The presented outputs are: the required driving torque (Fig. 1.26), the required power to overcome the friction in the kinematic pairs (Fig. 1.27), and the reaction at pair D (Fig. 1.28). The criterion for breaking the iteration process was established as $1 \cdot 10^{(-3)}$ N for the difference on consecutive calculations of the magnitude of the pair reactions in the II^{RRR} structural group. SimMechanics is a product of the MathWorks Inc. The results solving the inverse dynamics problem by the method of successive approximation developed here and by using an MBS dynamic simulator are basically coincident. However, the solution presented here is straightforward with respect to the MBS dynamic simulation because it does not require the solution of any differential equation of movement.

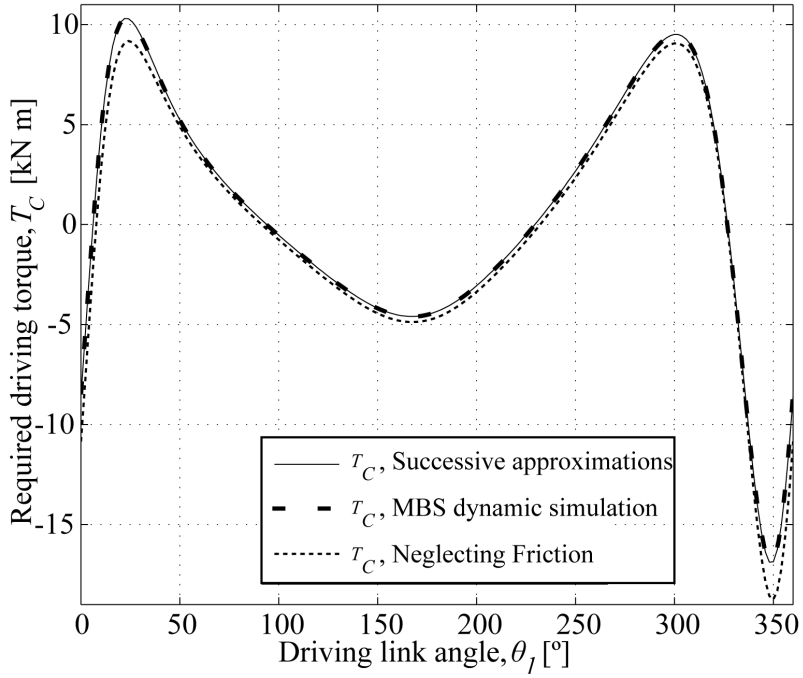

Figure 1.26: Kinetostatic analysis of a four-bar mechanism. Required driving torque

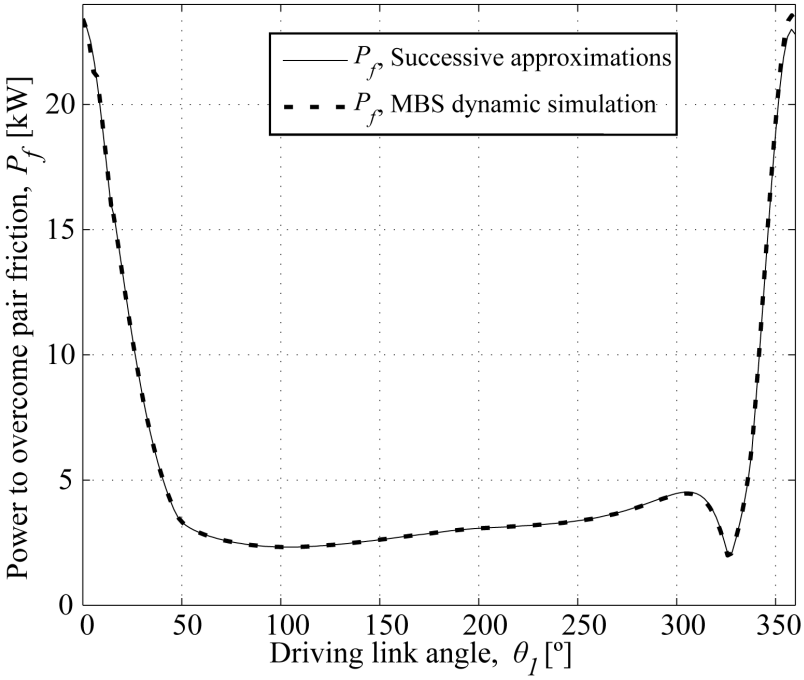

Figure 1.27: Kinetostatic analysis of a four-bar mechanism. Required power to overcome pair friction

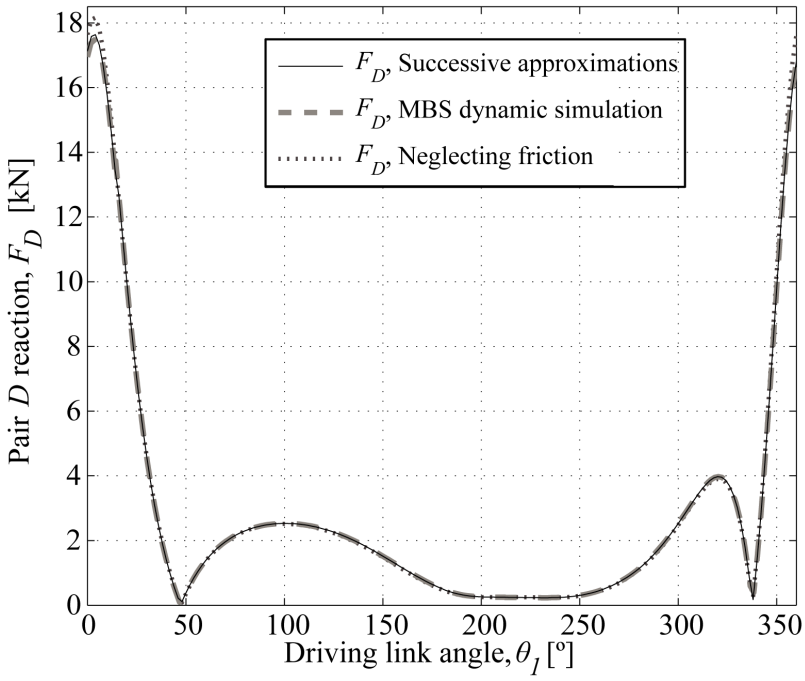

Figure 1.28: Kinetostatic analysis of a four-bar mechanism. Pair *D* reaction

1.2.4.2 Computer aided graphical validation

A computer aided graphical solution using a parametric CAD software (SolidWorks) was developed as a validation of the second-class first-type structural group module. Such validation uses the successive approximation method by [27] with three iterations. The validation was performed using the four-bar mechanism proposed in section 1.2.4.1. Ten equally-spaced configurations of the driving mechanism were evaluated for the reactions at pairs *B*, *C* and *D*. The maximum difference between the calculation of the pair reactions using the analytical method of successive approximations proposed here and the graphical method with 3 iterations was lower than $0.1\,\%$.

1.2.4.3 Known limitations

The analytical method for the kinetostatic analysis of Assur groups allowing friction in the kinematic pairs presented here is not adequate in cases in which the mechanism is close to a self-locking configuration. Self-locking occurs when the work of the driving forces is not enough to overcome the resistive forces different from the workloads. In such configurations the influence of friction forces is important and an approximated estimation leads to big calculation errors [26].

The proposed analysis method does not consider singular configurations of the mechanism. The definition of singular configurations adopted here corresponds to the definition of [49]. For serial singular configurations the analysis is not adequate if the mechanism is near to self-locking. For parallel and architectural singular configurations the proposed kinetostatic analysis method must be avoided.

1.2.5 Conclusions and Prospective

The performance of a mechanism during its periodic movement depends on the work needed to overcome the productive and non-productive resistances. Usually non productive resistances are mainly the result of friction. In mechanisms, the calculation of reactions with friction usually leads to a non-linear problem. Therefore, approximated methods of calculation as the one developed here (section 1.2.3) are practical and useful.

The analytical solutions for the kinetostatics of structural groups allowing friction in the kinematic pairs presented in this paper correspond to the so called general purpose programs based on chains (modular approach). The modular approach allows codifying computer functions with emphasis in making input data structure easy to understand. Therefore, very complex planar linkages may be described using a simple and familiar form of the input data.

For the development of the kinetostatic analytical models for structural groups allowing friction in the kinematic pairs a methodology was proposed (section 1.2.3, Fig. 1.18). Such methodology is based in an iterative but practical solution. With respect to commercial software, the proposed modular approach for the kinetostatic analysis of mechanisms has the following advantages:

1. The modules for mechanism analysis developed by this method preserve the characteristics of the GP programs based on kinematic chains: computational efficiency and flexibility. In consequence, with respect to commercial MBS simulation software the flexibility is comparable. In the case of MBS simulation software the complexity of the mechanisms that can be analyzed depends on the number of joints that are coded. In the case of the modular approach the complexity depends on the structural groups that are coded. However, most of industrial mechanisms are formed only by driving mechanisms and second-class structural groups.

2. With respect to commercial MBS simulation software the proposed methodology is straight-

forward because it does not require the solution of any differential equation of movement.

Future work is proposed developing modules for the analysis of higher-class structural groups, structural groups with prismatic joints, and the inclusion of more elaborated friction models of the kinematic pairs.

1.3 "Erratum to A Novel Technique for Position Analysis of Planar Compliant Mechanisms [Mech. Mach. Theory 40, 2005, pp. 1224–1239]"

Authors of the Erratum:
Jorge Correa, Oscar Ruiz, Sebastián Durango
{jcorre20, oruiz, sdurang1}@eafit.edu.co
CAD CAM CAE Laboratory
EAFIT University
Medellín, Colombia

Authors of the original article:
S. Venanzi[a], P. Giesen[b], V. Parenti-Castelli[a]
[a] DIEM Department of Mechanical Engineering, University of Bologna
[b] TNO TPD, Institute of Applied Physics, DOI Division Optical Instrumentation

This article was published in Mechanism and Machine Theory 45 (5), 2010, p. 811,
ISSN 0094-114X.

By kind information of the below cited authors of the present errata, the following two errors have been found:

1. In Section 4 of paper [11], end of first paragraph, the correct external load compatible with the results reported in the case study is $F_R = (-0.3, 0.0)$ N instead of $F_R = (0.5, 0.0)$ N.
2. In Section 4.2, the correct expression for the angle θ_3 is $\theta_3 = -(\gamma - \gamma_0 - \beta + \beta_0)$ instead of $\theta_3 = \gamma - \gamma_0 - \beta + \beta_0$.

The authors of the original paper thank the commentators for their detailed analysis and for kindly conveying this information both to them and to the readers of this journal.

Authors of the errata:

Jorge E. Correa, Oscar E. Ruiz, Sebastián Durango

Chapter 2

Force-Displacement Model of Compliant Mechanisms by Design of Computer Experiments

This chapter is devoted to the *force-displacement model of compliant mechanisms* (CMs) by *Design of Computer Experiments* (DOCE). Different from chapter 1, this contribution is available not only for flexure-based CMs but for CMs with distributed flexibility and spatial movement.

The contribution is presented through the article 2.1 corresponding to an invitation to rework the paper [8] for republication in the Special Issue of the Journal of Engineering with Computers (Elsevier) on “Engineering Analysis and Simulations Based on Virtual Prototypes”.

2.1 Design of Computer Experiments Applied to Modeling Compliant Mechanisms

Sebastián Durango, David Restrepo, Oscar Ruiz
{sdurang1, drestr21, oruiz}@eafit.edu.co
CAD CAM CAE Laboratory
EAFIT University
Medellín, Colombia

Diego A. Acosta
dacostam@eafit.edu.co
DPP Research Group
EAFIT University
Medellín, Colombia

This article was submitted to the Journal of Engineering with Computers (ISSN:0177-0667) corresponding to an invitation for republication of paper [8] in the Special Issue Engineering Analysis and Simulations Based on Virtual Prototypes.

Abstract

This article discusses a procedure for force-displacement modeling of Compliant Mechanisms (CMs) by using Design-Of-Computer Experiments (DOCE). The application discussed produces a force-displacement meta-model, or closed analytic vector function, that aims at controling CMs in real-time. In our work the meta-modeling (factorial and space-filling DOCE) of CMs is supported on FEA. The procedure discussed is used to model the HexFlex mechanism functioning under quasi-static conditions. The HexFlex is a parallel CM for nano-manipulation that allows six degrees of freedom (x, y, z, θ_x, θ_y, θ_z) of its moving platform. In the multi-linear model fit of the HexFlex the products or interactions proved to be negligible, therefore yielding a linear model for the operating range. The accuracy of the meta-model was calculated conducting a set of computer experiments with random uniform distribution of the input forces. Three error criteria were recorded comparing the meta-model prediction with respect to the results of the FEA experiments by determining: *i*) maximum of the absolute value of the error, *ii*) relative error, and *iii*) root mean

square error. The maximum errors of our model are lower than high-precision manufacturing tolerances. These errors are also lower than those reported by other researchers who have tried to fit meta-models to the HexFlex mechanism.

keywords: Design of Computer Experiments, Design of Experiments, Compliant Mechanism, Meta-modeling, Plackett-Burman Design, Uniform Design.

Glossary

XYZ	Fixed reference coordinate system
$\mathrm{T1}$	Input force port on Tab1
$\mathrm{T2}$	Input force port on Tab2
$\mathrm{T3}$	Input force port on Tab3
$\mathrm{D1}$	Direction parallel to the connection beams in the HexFlex
$\mathrm{D2}$	Direction perpendicular to the plane that contains the HexFlex on its relaxed position
τ	Vector of input forces and torques
$\mathbf{r}$	End-effector pose vector
x, y, z	Coordinates of a point in XYZ frame
$\theta_x, \theta_y, \theta_z$	Set of Euler angles
DOE	Design of Experiments
DOCE	Design of Computer Experiments
CM	Compliant Mechanism
DOF	Degrees of Freedom

2.1.1 Introduction

In traditional mechanisms movement is achieved using kinematic joints (cylindrical, spherical, prismatic, etc.) and links that are as rigid as possible. In contrast, Compliant Mechanisms (CMs, [50]) are mechanical devices which undergo elastic deflections to transmit motion, force or energy from specified input ports to output ports. The main advantage of CMs with respect to traditional rigid-link mechanisms is that fewer parts, and assembly processes, and no lubrication are required. However, due to the complexity of their motion (which is actually a deflection), CMs cannot be designed and analyzed by traditional kinematic methods [51].

In addition, CMs' force-displacement (Input/Output or I/O) model is required for a significant number of applications. In particular, closed form models are required in real-time control applications.

A common tool in designing a CM is the optimization of its geometry or topology according to a proposed performance function. Achieving "good" values of the performance functions closely relates to a "desirable" structure, both geometrically and topologically [52–54]. Each instance of the CM produces values of the function to be optimized, and the search of a desirable geometry or topology is therefore a minimization problem. This approach reduces human intervention in the design but gives as a result structures that can be impossible to build [55], (*e.g.* because they might have unconnected components).

Two methods are used to relate CM deflections against forces and/or torques [12]: 1- Pseudo Rigid Body Model (PRBM) and 2- Numerical methods (FEA).

PRBM considers a CM as being a traditional static structure where the joints are produced by concentrated elasticity zones [11, 56, 57] which produce the flexibility or *lumped compliance* while the rest of the mechanism may be considered rigid. To be useful, PRBM must deal with lumped compliance zones which have closed analytic solutions relating force/torque vs. deflection. This aspect considerably limits the applicability of PRBM. On the other hand, if FEA is used to model CMs, the designer is basically solving solid mechanics differential equations by numerical methods. Since each run of the solution requires considerable numerical processing, numerical methods are not suitable for time-critical applications (*e.g.* real-time control). In general, the lack of tools to model CMs is recognized as an open research problem [11].

This article presents a methodology to synthesize a Force (Input) - Displacement (Output) model of CMs working under quasi-static conditions. It is required that the model be suitable for real-time applications and therefore it must be a low degree polynomial Multi-Input Multi-Output (MIMO), which we will refer to as *meta-model*. Besides being fast, the sought model is able to address both lumped and distributed compliance. Obviously, to determine such a model using Design-Of-Experiments (DOE) methodologies, series of experiments must be conducted. In our case, we will call *experiment* an FEA simulation of force/torque vs. displacements. This is a Design-of-Computer-Experiments (DOCE) methodology.

The layout of this article is as follows: section 2.1.2 presents a literature review and compares it with the contributions of this work; section 2.1.4 presents the proposed methodology and its scope for force-displacement modeling of CMs under quasi-static conditions. The case study "HexFlex"

CM is developed in section 2.1.5, and section 2.1.6 concludes the article.

2.1.2 Literature Review. Modeling of Compliant Mechanisms

2.1.2.1 Meta-models

The term *meta-model* in computer experiments represents a surrogate model based on the use of statistical techniques to yield mathematical equations that approximate the results rendered by computer algorithms such as FEA [58]. If the true nature of a computer analysis code is $u = w(\mathbf{v})$ where $\mathbf{v}$ are the inputs and u are the outputs of the computer code then a surrogate model or *meta-model* of the analysis code is $\widehat{u} = z(\mathbf{v})$ where $\widehat{u}$ is an approximation of the outputs of the computer code so that $\widehat{u} = u + \epsilon$ with ϵ being the approximation error.

Meta-models have benefits in screening variables, reducing design costs and optimizing designs [59]. They are applied here to model the quasi-static behavior of the HexFlex mechanism. The HexFlex is a six degrees of freedom parallel CM with distributed compliance for nano-manipulation created at MIT by Martin L. Culpepper and Gordon Anderson [60, 61].

2.1.2.2 Analysis and Design of Compliant Mechanisms

Topology and geometry optimization methods applied to CMs allow to tune up shapes, dimensions and connectivities to achieve a good numerical value of a function which evaluates the efficiency of the CM. The optimization (see [12]) relies in any case on the possibility of relating forces/torques vs. positions/deflections in the mechanism. For such a purpose, structural optimization uses either PRBM or numerically solved differential equations (FEA).

2.1.2.3 Topology Optimization

Topology optimization consists of finding the optimal connectivity and geometry of a loaded structure within a specified region and with specified performance criteria. Reference [62] discusses

the topology optimization method for designing CMs. Reference [63] proposes honeycomb tessellation and material-mask overlay methods to obtain optimal single-material compliant topologies. Topology optimization methods based on material distribution are reported to be usually ill-posed [50]. Alternatives to this problem are proposed in the form of homogenization [64], the Solid Isotropic Material with Penalization method (SIMP, [65]) and level set methods [50]. Reference [66] uses topology optimization methods to develop constant output force CMs for a given actuator characteristic. Reference [62] proposes a method for non-linear optimization based on geometric and material non-linearities to obtain a desired displacement under a specific load.

The topology optimization methods are limited to the design stage. The majority of the methods that use topology optimization for the synthesis of CM are applied about a particular operation point of the mechanism. Topology optimization requires relating force/torque conditions with position/deflection of mechanisms/structures. To find this relation, PRBM and FEA are used, as discussed next.

2.1.3 Pseudo Rigid Body Modeling

PRBM is used to design *static structures* which behave as *movable mechanisms*. In the structure, local regions (*e.g.* flexural joints, notch hinges) are chosen and intentionally weakened so that they undergo large deflections having what is called *lumped compliance*. In this way, the structure behaves as a mechanism (*i.e.* has degrees of freedom) although strictly speaking no kinematic joints are present.

In the designed structure the PRBM differentiates stiff from flexible components. The former are modeled as completely rigid while the latter provide mobility to the mechanism (displacement and torsional springs, non-linear elastic beams, etc.). These hyper-flexible members can be analyzed with closed differential equations (*e.g.* flexural cantilever beam). In the PRBM model the stiff members do not deflect, so that deflected ones absorb the whole angular displacement becoming *rotational* joints.

A key step of the PRBM is to estimate the equivalent application point and equivalent elastic constant of the spring represented by the flexible cantilever beam.

The PRBM approach is mathematically addressed under linear and non-linear strain formulations. This means that the strains are expressed in terms of linear and non-linear displacements.

From theory of elasticity, strains can be formulated as functions of the partial derivatives of the displacement functions, and higher-order partial derivatives are usually involved. The linear formulation neglects partial derivatives that have an order or power larger than one. The following articles present linear PRBM as fundamental part of their formulation: In [67], an analytical scheme for the displacement analysis of micro-positioning stages with flexural hinges is presented. The scheme replaces the hinges by linear springs, allowing the creation of simple I/O models of the mechanisms based on their elastic energy equations. Analytical models of rotational and translational compliant joints are presented in [68]. In [69], PRBM is applied to predicting the behavior of a nano-scale parallel guiding mechanism which uses two carbon nano-tubes as flexural links. The kinematic behavior was reported 92,7% accurate with respect to a molecular simulation. Reference [70] presents the design of a three degree of freedom planar CM based on the 3RRR rigid mechanism. The design of bistable CMs based on the PRBM and calculations of the potential energy and moment required to move it to a particular position is presented in [71]. In reference [72] the kinematic and force analysis of compliant driven robotic mechanisms is made based on equations that relate joint torques, joint angles and displacements. The I/O model of a 3RRR compliant micro-motion stage replacing its flexures with a set of equivalent springs is presented in [16].

Non-linear PRBM is based mainly on the application of Euler beam models or deflection models based on the Castigliano's second theorem to model the flexible members of the CM solving higher order partial derivatives of the strain formulation. The following articles present non-linear PRBM as part of their formulation: Reference [73] discusses conic section flexure hinges using Euler beam model and Castigliano's second theorem. Reference [74] develops an extension of the Frenet-Serret beam equations to apply it on the synthesis of CMs. Reference [75] introduces an analytical approach to corner filleted flexure hinges using the Castigliano's second theorem. In [18] a PRBM is developed and solved for the tip deflection of flexible beams under combined loads. It uses a numerical technique to solve the large-deflection Euler-Bernoulli beam equation. Reference [57] develops a synthesis and analysis PRBM for the limit positions of a four-bar mechanism with an output compliant link (one end pinned to the coupler, one end fixed to the ground). The lumped compliance is modeled by non-linear beam theory, allowing for large non-linear deflections of the pinned end of the compliant link. The model only applies for a given topology. In [11], PRBM is enhanced to allow large deflections of elastic hinges. Four elastic hinges (leaf spring, cross, notch, and Haberland) are modeled and a joint-based modular approach is obtained. The modeling technique reported reduces the time needed for off-line modeling and design but not enough for real-time control. Reference [76] presents the mathematical model, derived from the second Castigliano's theorem, for a 6 DOF CM. The forward and inverse analyses of an open loop CM are developed in [77] by using numerical methods to solve large deflections of the mechanism.

Reference [78] develops a mathematical dynamic model, based on large-deflection beam models, for compliant constant force compression mechanisms.

In general, PRBM is useful to model lumped compliance. Models obtained with linear PRBM can be applied in real-time control but is restricted in precision engineering applications because of its low accuracy [11, 50]. Non-linear PRBM is suitable for accurate modeling and design, but it is not computationally efficient for real-time control. At any rate, PRBM requires that the geometry and loads of the elastic links allow for a closed-form analytic solution. These considerations seriously hinder the application of PRBM.

2.1.3.1 Numerical Methods

PRBM works when parts of the structure analyzed are significantly weaker than others in the body. The weaker ones concentrate the movement. The stiffer ones are considered totally rigid. In addition, the weaker parts must have a geometry that accepts close forms of force-deflection equations [11]. When the mechanism hinges do not accept closed analytical force/deflection solutions, and computing time is not an issue, FEA is applicable for their analysis and simulation. Reference [79] presents a procedure for the optimal design of flexural hinges for compliant micromechanisms. The optimal design is developed by coupling an FEA model to an optimization algorithm. The optimization is intended to maximize the rotation of the hinges under kinematic and strain constrains of the material of the hinge. Because of its time expenses, a pure FEA modeling of CMs is restricted to the design stage of the mechanism, being excluded from real-time control applications.

Reference [80] presents a localized application of FEA in CMs. In the design stage, two main steps are taken to complete a force/deflection model: 1- The elastic properties of the hinges are estimated by an independent 3D FEA. 2- The FEA-estimated properties are incorporated into a general CM model by the use of equivalent beams. This hybrid model may be applied in a reduced manner for real-time I/O models of CMs. However, the method is limited because the geometry of the zones in which the equivalent flexible beam meets the rigid parts has a considerable influence on the predictions of deflections and stress concentrations of the CM.

Reference [81] presents the synthesis of CMs. The merit of the article is that, unlike others, it extensively presents the usage of highly non-linear Finite Elements, allowing the modeling of very large deflections.

Reference [22] describes the design of a compliant robotic wrist able to perform spherical motions. The inverse and direct kinematics and the design of flexures of the spherical compliant mechanisms are computed by FEA. In [82], the stiffness properties of a (compliant) notch hinge are computed using FEA relating the initial and final positions of the mechanisms under known loads. The procedure is only used to find the properties of the flexures and not to find an I/O model of the CM.

In [83], a synthesis method for spatial CMs is proposed. The mechanisms are modeled as a set of connected three dimensional *wide curves*. A three dimensional *wide curve* is a spatial curve with variable cross section. Deformation and performance of the mechanism are evaluated by an iso-parametric degenerate-continuum nonlinear FEA procedure. Notice that no analytical force-deflection model is sought in this reference.

Summarizing, numerical methods such as FEA are useful in determining the deflection and stresses in CMs because they allow to analyze CMs that have a geometry that is not easily modeled using methods like the PRBM. However, FEA cannot be used in a real-time scenario to control CMs. For this purpose, an intermediate I/O model must be estimated. This is the purpose of our current investigation.

2.1.3.2 Contribution of this Article

This article presents a new general procedure for modeling CMs under quasi-static conditions by DOCE methodology. The proposed approach allows to model CMs that have lumped or distributed compliance. The main advantages of the proposed approach with respect to traditional modeling methods (PRBM, topology optimization, FEA) are:

1. The methodology is general enough to cover both lumped and distributed CMs.
2. The obtained I/O model might be simple enough to be used in real-time control.
3. Real experimentation is replaced by computer simulations reducing costs in product development.

It is clear to us that DOCE does not replace DOE (*i.e.* with physically conducted experiments). However, the pre-fitting of the model by using DOCE serves to identify and avoid ranges, interactions and limitations that would make the DOE extremely expensive.

As an application of the methodology, the 6 DOF CM HexFlex is modeled by finding an accurate model with respect to FEA simulations.

The differences in application domains between PRBM, FEA and DOCE techniques should be emphasized here: PRBM is only applicable to mechanisms whose geometry can be decomposed into links for which an analytical expression for force/torque vs. deflections is possible. PRBM is fast and accurate but its application domain is reduced. FEA presents no restrictions in the geometry of the mechanisms or bodies being analyzed. However, it is a slow method and definitely not suited for real-time applications. DOCE allows to calibrate systems (not only mechanisms) and to obtain an I/O model which is fast and accurate for the particular operation point chosen. In our case, DOCE uses FEA as a subsidiary tool to carry the computer experiments and therefore allows to tune up the I/O model. In DOCE, if the mechanism or the operating point are changed, a new DOCE model is required. In a typical application of DOCE for mechanisms, a given mechanism is calibrated or modeled via computer experiments. Next, it is installed in the host device and then controlled via the analytical I/O model previously obtained.

2.1.4 Methodology for Meta-modeling of Compliant Mechanisms.

2.1.4.1 Workflow and Used Software Packages

Figure 2.1 displays the assembly of computational tools to fit the DOCE model. This model is a set of hypersurfaces (r_1, r_2, etc.) in the multidimensional space of the input variables $\tau_1, \tau_2, ...$ (Eq. (2.1)), as shown in the upper right corner. The statistical fitting of the model (upper left corner of Fig. 2.1) is carried out with MATLAB© code, by using a Plackett-Burman DOE shown in Table 2.2. Such values are calculated by a number of FEA simulations in ANSYS© (lower row of Fig. 2.1) controlled from the MATLAB© programs. ANSYS© , therefore, acts in this case as a FEA server subordinated to MATLAB© programs.

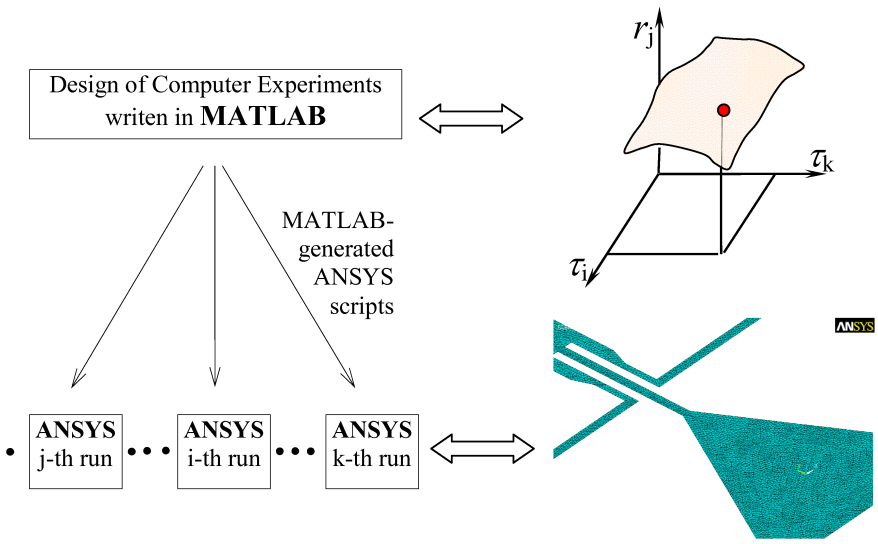

Figure 2.1: ANSYS© as a FEA server controlled from MATLAB©

2.1.4.2 Design of Computer Experiments

In Meta-modeling of CMs we are looking for a function f that relates the input forces and torques (τ) with translations and rotations of the end-effector ($\mathbf{r}$) under quasi-static conditions:

$$\begin{aligned} f &: \tau \rightarrow \mathbf{r}, \\ \tau &= \begin{bmatrix} \tau_1 & \tau_2 & \cdots & \tau_n \end{bmatrix}^T, \\ \mathbf{r} &= \begin{bmatrix} r_1 & r_2 & \cdots & r_m \end{bmatrix}^T, \end{aligned} \tag{2.1}$$

where $m \leq n$.

For an end-effector taking an arbitrary pose, we have $m = 6$. We assume that the mechanisms are not redundant (*i.e.* $m = n$).

To model CMs under quasi-static condition using meta-models from computational experiments, the methodology presented in Fig. 2.2 is proposed and summarized as follows:

1. Define the CM topology. The set of factor parameters is the vector of input forces and torques (τ).

2. Propose a virtual model of the CM. This model is usually MIMO polynomial model, calculated in the vicinity of the operating point.

3. Use a Fractional Factorial DOE (*e.g.* Plackett-Burman) to screen variables. The main factors and interactions are obtained by virtual experiments.

4. Use an Space Filling DOE (*e.g.* Uniform Design [84]) to fine-tune the mathematical model of the mechanism by virtual experiments.

5. Construct the surrogate model of the kinematics of the CM.

6. Verify the accuracy of the meta-model using extra experiments [58].

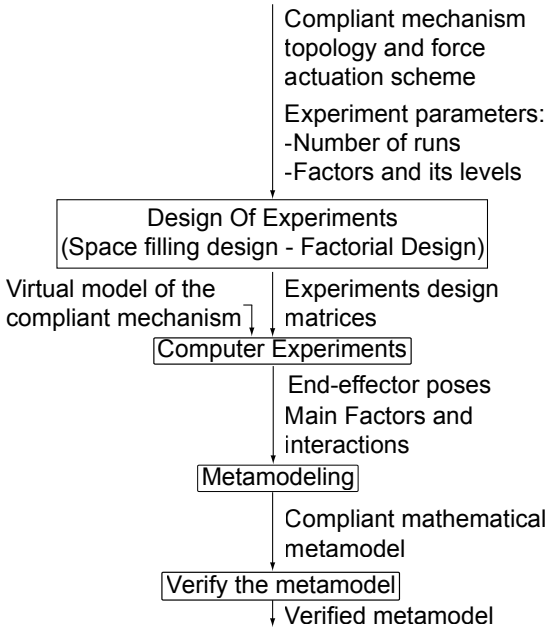

Figure 2.2: Methodology for force-displacement meta-modeling of compliant mechanisms

The previous steps define the scope of our article. However, it must be kept in mind that actual experiments must be conducted to fit an industrially applicable meta-model. Our contribution permits to execute this material experiments with a minimum of cost overhead.

In section 2.1.5 the proposed methodology is applied to obtain a mathematical meta-model of the HexFlex parallel CM. The developed meta-model relates the actuator forces at the input ports with the position and orientation of the end effector.

2.1.4.3 Methodology Scope

The presented methodology for modeling CMs is limited to:

1. CMs that allows small displacements of its end-effector.
2. Input forces and moments slowly varying in time (quasi-static conditions).
3. The model is restricted to the neighborhood of the the operation point for which was calculated.
4. Although the proposed methodology is general for CMs, the obtained force-displacement models are specific for each individual case.

In spite of these limitations, the proposed force-displacement modeling of CMs by DOCE is relevant for a wide range of applications because most CMs are designed for small displacements of its end-effector under quasi-static conditions, specially in compliant parallel nano-manipulating mechanisms.

It must be pointed out that the DOCE methodology applied in this article is specifically prescribed when an I/O model is required of a largely or totally unknown phenomenon or system. We fit a DOCE model which relates forces (Inputs) to end-effector positions (Outputs) of a mechanism. The application scenario of such a model is the real-time control of the mechanism, in the neighborhood of an operating point. Because one is interested in real-time control, an accurate but slow FEA model is out of question. The DOCE model might be a linear, quadratic, cubic, etc. approximation around the operating point. DOCE allows to trim the polynomial model by neglecting high level interactions if their statistical significance is low. In this article this trimming led to a linear meta-model.

Section 2.1.5 shows the meta-modeling of the HexFlex CM under quasi-static conditions.

2.1.5 Case Study. Force-displacement Meta-modeling of the HexFlex Mechanism

Applying the procedure described in section 2.1.4 the HexFlex parallel CM is meta-modeled.

The meta-model of the HexFlex mechanism is developed in detail as follows: in section 2.1.5.1 the mechanism is described. The input factors (input forces) and its levels are determined. Section 2.1.5.2 develops the Fractional DOE to determine the main factors and interactions. Section 2.1.5.3 presents the Space Filling DOCE and the meta-modeling of the HexFlex CM by conducting FEA

tests. Finally, section 2.1.5.5 successfully validates the meta-model just obtained by running 1000 FEA tests and comparing their results against the meta-model predictions.

2.1.5.1 The HexFlex Mechanism

The topology and dimensions of the HexFlex mechanism are shown in Fig. 2.3. This mechanism allows the moving platform translation and rotation of the X, Y and Z axes as shown in Fig. 2.4. The HexFlex is consist of a triangular moving platform, three tabs to provide an interface with the actuators, and six connection beams between the moving platform and the grounded zone (Fig. 2.3(a)).

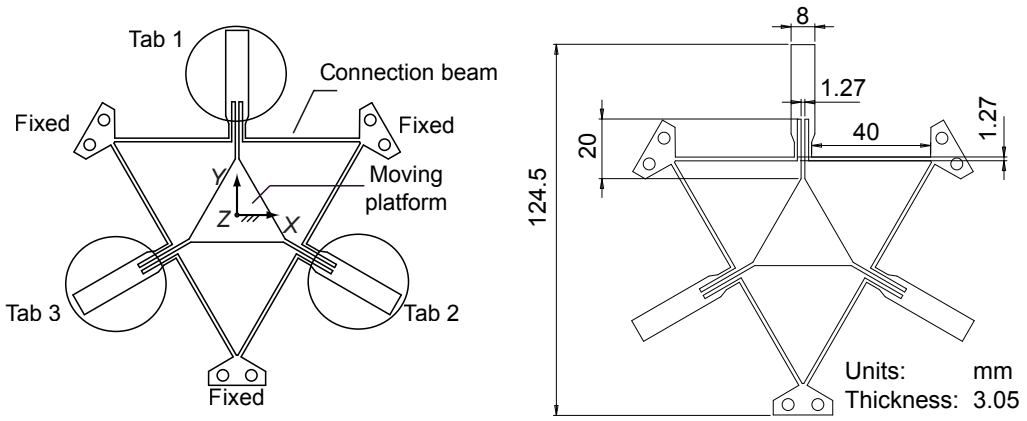

(a) HexFlex components (b) HexFlex main dimensions

Figure 2.3: Six DOFs compliant mechanism [85]

To control the moving platform there are two actuators in the external edge of each tab. For each tab, one actuator acts in direction parallel to the connection beams (called direction one and denoted $\mathrm{D1}$) and, the other actuator acts perpendicular to the tab (Z direction, $\mathrm{D2}$) as shown in Fig. 2.5. The tabs are denoted T1, T2, T3. The motion of specific actuator is denoted by the tab followed by the direction using the convention shown in Fig. 2.5.

The actuators used in the experiments allow a force of 1 N. The positive direction of actuators for $\mathrm{D2}$ coincides with the direction in which Z is positive, and for $\mathrm{D1}$ the positive direction of actuators is as shown in Fig. 2.5. Slowly varying in time forces are assumed for the experiments (quasi-static experiments). Planar and non-planar displacements may be made simultaneously. The material selected to model the mechanism is Aluminum 7075.

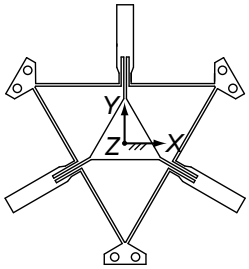

(a) HexFlex mechanism in relaxed position.

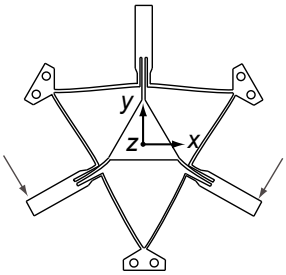

(b) HexFlex mechanism. In-plane translations.

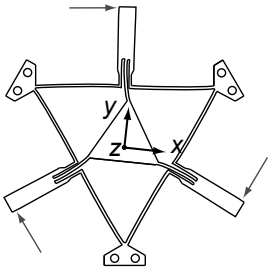

(c) HexFlex mechanism. In-plane rotations.

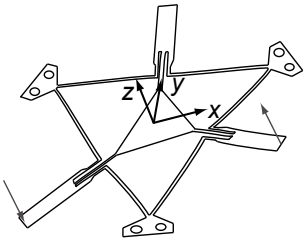

(d) HexFlex mechanism. Out-plane rotations.

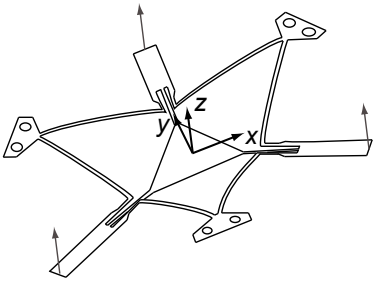

(e) HexFlex mechanism. Out-plane translations.

Figure 2.4: Six DOFs complaint mechanism in deflection

To define the meta-model function, the vector of input forces (τ) and pose of the end-effector ($\mathbf{r}$) are defined by:

$$\tau = \begin{bmatrix} \text{T1D1} & \text{T1D2} & \text{T2D1} & \text{T2D2} & \text{T3D1} & \text{T3D2} \end{bmatrix}^T, \tag{2.2}$$

$$\mathbf{r} = \begin{bmatrix} x & y & z & \theta_x & \theta_y & \theta_z \end{bmatrix}^T, \tag{2.3}$$

where the end-effector pose (position and orientation) is defined by three translational components (x, y, z) and three differential Euler XYZ angles ($\theta_x,\ \theta_y,\ \theta_z$), and the input forces correspond to the actuators in the tabs. Differential Euler angles are commutative and therefore the order of the x, y and z rotations do not affect the final orientation [86].

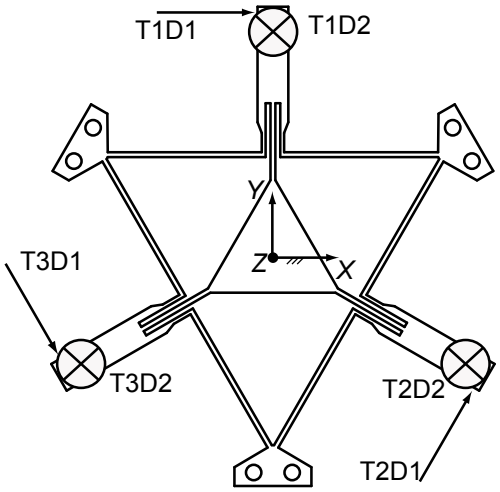

Figure 2.5: HexFlex actuators direction

The reference frame or World Coordinate System is chosen to be at the center of gravity of the moving platform in its relaxed position (Fig. 2.6). The moving platform coordinate frame is attached at its centroid. Therefore, in a relaxed position the reference frame and the moving frame coincide.

Using the symmetry of the mechanism and the dimensions shown on Fig. 2.3(b), a sixth part of the mechanism was modeled and meshed to make a geometric FEM model of the mechanism (Fig. 2.6(a)). Using geometric transformations, the mechanism was completed developing a symmetrical mesh. Then the mesh was exported to ANSYS© (Fig. 2.6(b)) using quad shell elements to run the virtual DOE . For a given set of input loads in the tabs, the computer experiments produce the position and orientation of the moving frame on the mechanism.

Operation Ranges. The selection of operation ranges for the DOCE is based on the recommendations of the HexFlex mechanism designers [85], corresponding to a force range of ± 1 N. As for the operating point for the HexFlex mechanism, we adopted the usual one in the literature, which is $x = 0$, $y = 0$, $z = 0$, $\theta_x = 0$, $\theta_y = 0$, and $\theta_z = 0$. It must be pointed out that, in addition to the reviewed literature, the ranges, convenience of the operating point, and elimination of high degree and crossed-influence terms were verified by the series of computer experiments carried out by the methodology applied in this article.

The upper and lower levels of each factor for the Fractional Factorial and Space Filling DOE are displayed on Table 2.1. The factors or inputs of the experiments are defined by Eq. (2.2) and correspond to the actuation forces of the mechanism, which are the controllable input variables (*i.e.* factors) of the experiment.

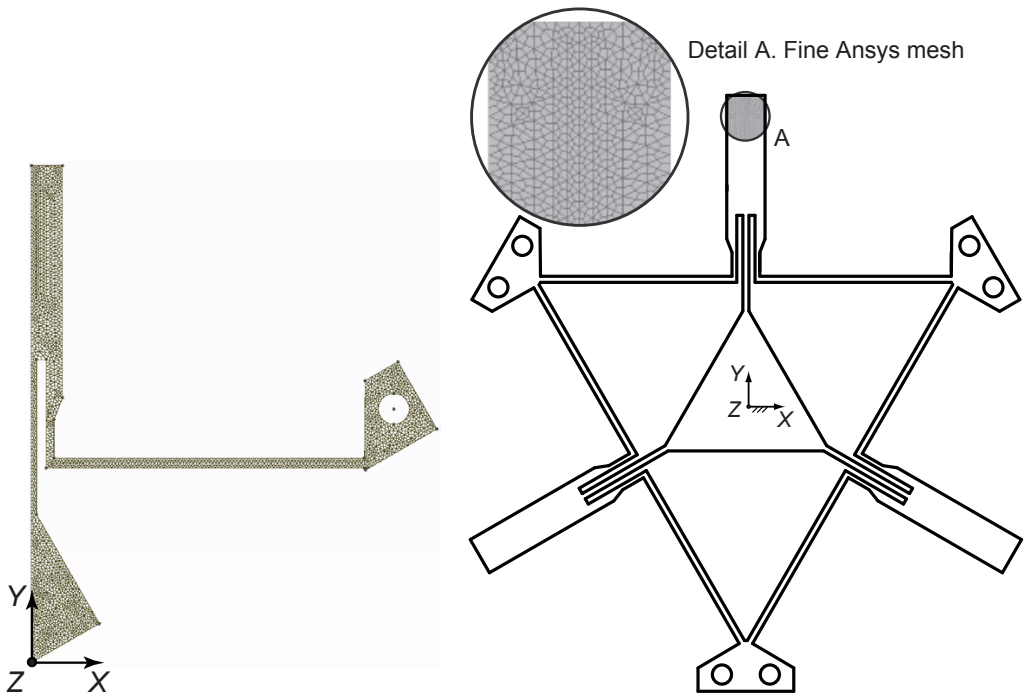

(a) Sixth part of the mesh (b) FEM model in ANSYS©

Figure 2.6: FEA model of the HexFlex Mechanism

Factor	Low level	High level
T1D1	-1 N	$+1$ N
T1D2	-1 N	$+1$ N
T2D1	-1 N	$+1$ N
T2D2	-1 N	$+1$ N
T3D1	-1 N	$+1$ N
T3D2	-1 N	$+1$ N

Table 2.1: Studied Factors. Forces in Tabs of the HexFlex

Sections 2.1.5.2 and 2.1.5.3 develop the Factorial and Space Filling DOCE defining the meta-model of the HexFlex.

2.1.5.2 Fractional Factorial DOE

To screen factors a Plackett-Burman DOE (see [87, 88]) with 12 runs is made. Plackett-Burman designs are very economical and efficient when only main effects are of interest. A script was

developed to automatically generate the virtual experiments and their results. The DOE matrix and the results of each response are shown on Table 2.2.

Design Matrix						**Responses**					
T1D1 [N]	**T1D2** [N]	**T2D1** [N]	**T2D2** [N]	**T3D1** [N]	**T3D2** [N]	x [μm]	y [μm]	z [μm]	θ_x [μrad]	θ_y [μrad]	θ_z [μrad]
1	−1	1	−1	−1	−1	115056	0,6	−862976	0,0001	−0,0001	3,10176
−1	−1	1	1	1	−1	−57529	99636,5	−287659	−39,3596	−68,0656	3,10183
1	−1	−1	−1	1	1	−3	−0,6	−287655	−39,2665	68,1194	−9,30545
−1	−1	−1	−1	−1	−1	−57525	−99636,5	−862976	0,0001	−0,0001	3,10186
1	1	−1	1	1	−1	−3	−0,6	287655	39,2665	−68,1194	−9,30545
1	1	1	−1	1	1	57525	99636,5	287659	39,3596	68,0656	−3,10186
−1	−1	−1	1	1	1	−115056	−0,6	287662	−78,6262	0,0539	−3,10176
−1	1	−1	−1	−1	1	−57525	−99636,5	287659	39,3596	68,0656	3,10186
−1	1	1	1	−1	1	3	0,6	862976	−0,0001	0,0001	9,30545
−1	1	1	−1	1	−1	−57529	99636,5	−287662	78,6262	−0,0539	3,10183
1	1	−1	1	−1	−1	57529	−99636,5	287655	39,2665	−68,1194	−3,10183
1	−1	1	1	−1	1	115056	0,6	287662	−78,6262	0,0539	3,10176

Table 2.2: Plackett-Burman DOE Matrix for Six factors and 12 runs

To analyze the results of the Plackett-Burman DOE, Half Normal Probability (HNP) (Fig. 2.7) and Pareto (Fig. 2.8) plots are made. These analyzes provide a simple way to examine the response variables (*i.e.* x, y, z, etc) and the relative importance of the factors and interactions of the experiment.

The Pareto charts results coincide with Half Normal Probability (HNP) showing that the main effects are consistent with the symmetries of the topology of the mechanism (Fig. 2.5). The symmetries of the mechanism also caused that some effects had the same value.

In addition to the Pareto charts and HNP analysis, another way of looking at the resulting effects consists of using Lenth's plots [89]. The absolute values of the aliasing of the effects are sorted in ascending order to calculate the median (ν). Once the median is calculated a pseudo-standard error (S_0) is estimated using the formula: $S_0 = 1.5\nu$. The pseudo-standard error serves to define the margin of error (ME) and the simultaneous margin of error, by using the 0.975-quantile and $t_{g,m/3}$ of the t-student distribution allowing fractional degrees of freedom. The results for these analyses are displayed on Table 2.3 and indicate which independent variables (T1D1, T1D2, T2D2, T3D2, T2D1, T3D1) have effects on which dependent variables ($x, y, z, \theta_x, \theta_y, \theta_z$). Because this is a fractional factorial design, we can only screen at this point the existence of such dependency. Later on, using a Space Filling technique we will confirm and quantify them. The responses are affected as follows:

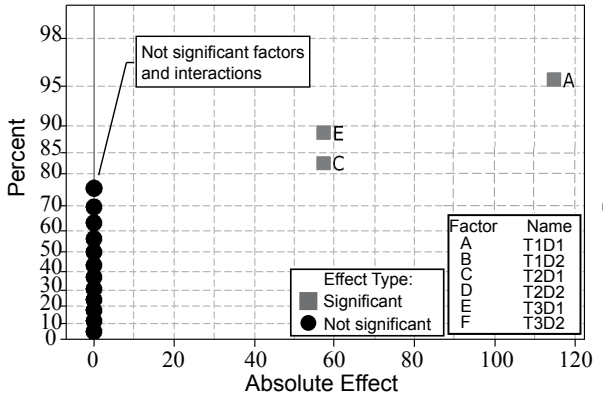

(a) Half Normal Plot for x translation

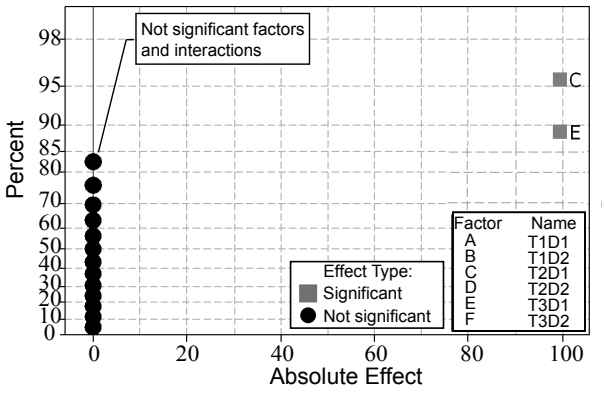

(b) Half Normal Plot for y translation

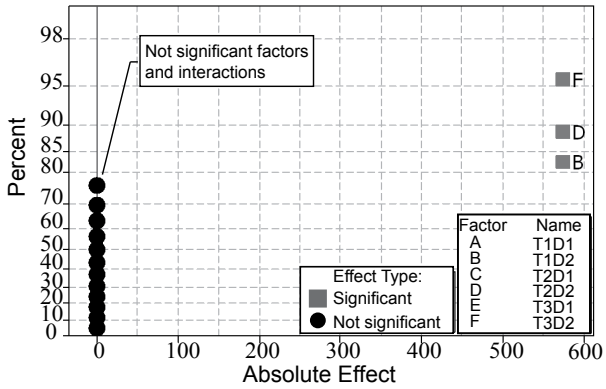

(c) Half Normal Plot for z translation

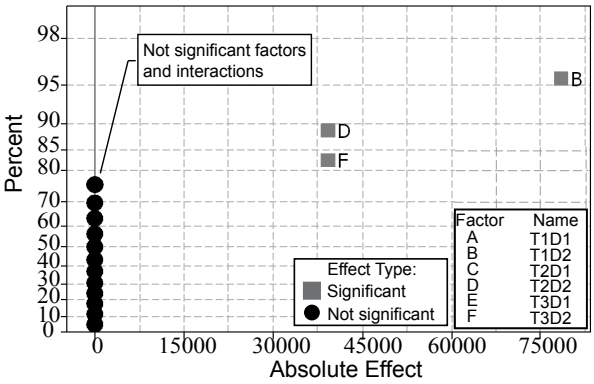

(d) Half Normal Plot for θ_x rotation

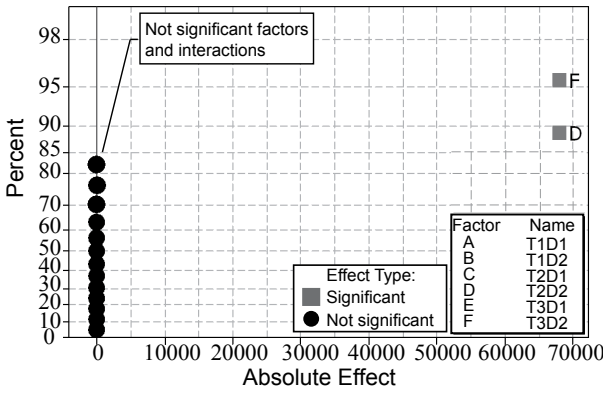

(e) Half Normal Plot for θ_y rotation

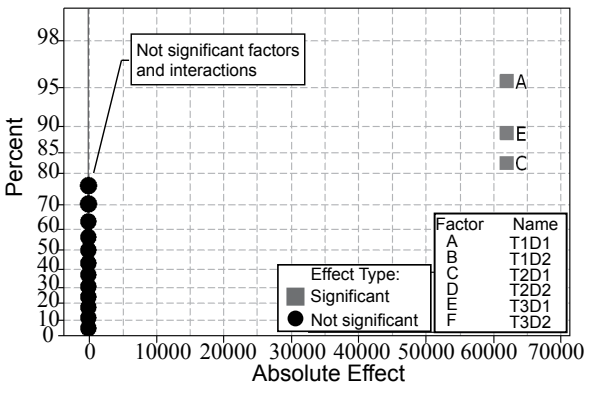

(f) Half Normal Plot for θ_z rotation

Figure 2.7: Half Normal Probability Plots. Placket-Burman DOE for 12 runs and 6 factors for HexFlex quasi-static conditions

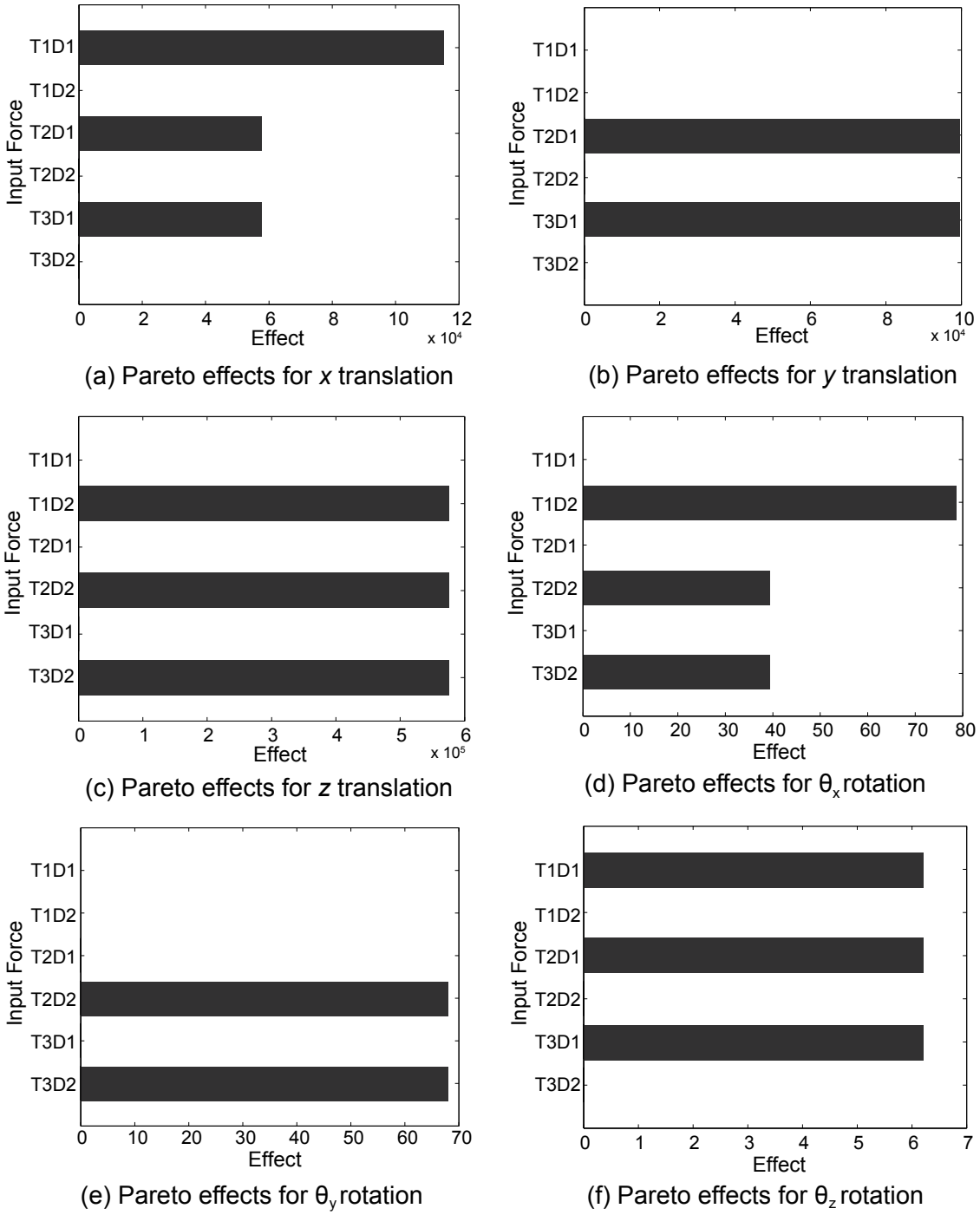

(a) Pareto effects for *x* translation

(b) Pareto effects for *y* translation

(c) Pareto effects for *z* translation

(d) Pareto effects for θ_x rotation

(e) Pareto effects for θ_y rotation

(f) Pareto effects for θ_z rotation

Figure 2.8: Pareto Charts. Placket-Burman DOE for 12 runs and 6 factors for HexFlex quasi-static conditions

1. x and θ_z are mainly affected by $T1D1$, $T2D1$, and $T3D1$.
2. z and θ_x are mainly affected by $T1D2$, $T2D2$, and $T3D2$.
3. y is mainly affected by $T2D1$ and $T3D1$.
4. θ_y is mainly affected by $T2D2$ and $T3D2$.

	x [μm]	y [μm]	z [μm]	θ_x [μrad]	θ_y [μrad]	θ_z [μrad]
T1D2	0,17	0	575314	78,63	0,05	0
T2D2	0,17	0	575317	39,36	68,07	0
T3D2	0,17	0	575321	39,27	68,12	0
T2D1	57527,50	99637,1	0	0	0	6,20
T3D1	57531,50	99635,9	0	0	0	6,2
T1D1	115053,50	0	0	0	0	6,20
ν	19,63	0	287657	19,63	0,03	3,10
S_0	29,45	0	431486	29,45	0,04	4,70
ME	110,73	0	0	0	0	0
SME	265,34	0	0	0	0	0

Table 2.3: Lenth's analysis of Six DOF HexFlex Mechanism

Also, it is evident that to obtain in-plane displacements (x, y, θ_z) the actuators should exert force in direction one (D1) and that out-of-plane displacements (z, θ_x, θ_y) are generated when actuators act in direction two (D2).

2.1.5.3 Space Filling DOE and Meta-model of the HexFlex

To generate a valid meta-model of the HexFlex mechanism a Uniform DOE (see [90]) with six factors and six levels is used (see Table 2.1). A Uniform Design is a modification of fractional factorial designs that provides scatter design points in the experimental domain space. The design matrix and the FEA output displacements found using Ansys© are shown on Table 2.4.

2.1.5.4 HexFlex Mechanism Meta-modeling

After running the space filling DOE (section 2.1.5.3), the next step consists of choosing an appropriate approximation model.

Design Matrix						**Responses**					
T1D1 [N]	**T1D2** [N]	**T2D1** [N]	**T2D2** [N]	**T3D1** [N]	**T3D2** [N]	x [μm]	y [μm]	z [μm]	θ_x [μrad]	θ_y [μrad]	θ_z [μrad]
0,6	-0,2	-1,0	-1,0	1,0	-0,2	-23,00	0,00	-403,37	15723,33	27294,40	-8057,19
-0,6	-0,6	0,2	1,0	-1,0	0,2	0,00	-39,85	172,88	-47310,09	-27294,38	5583,32
-0,2	0,2	-0,2	-1,0	-1,0	0,6	11,5	-59,78	-57,63	15769,99	54588,86	3098,05
-1,0	-0,2	1,0	0,6	-0,2	1,0	-23,01	39,85	403,37	-39390,09	13647,29	6831,66
1,0	0,2	1,0	1,0	0,6	0,2	69,02	79,71	403,37	-15723,33	-27294,40	-1883,93
-1,0	-1,0	-0,2	-1,0	-0,2	-1,0	-57,52	-19,93	-864,35	-116,71	-0,06	3120,86
-0,6	0,2	-1,0	1,0	0,2	0,6	-69,02	-39,85	518,61	-23596,69	-13647,16	-1838,28
0,6	-0,6	0,6	0,6	0,2	-1,0	46,01	39,85	-288,11	-15816,67	-54588,89	-635,59
-1,0	1,0	-0,6	-0,2	-0,6	0,2	-57,52	-59,78	288,10	39483,43	13647,20	3120,87
0,2	1,0	0,2	1,0	-0,2	-0,6	23,01	0,00	403,35	31610,14	-54588,88	612,76
-0,6	0,6	0,2	-1,0	0,2	1,0	-34,51	19,93	172,86	23690,01	68236,09	1872,51
1,0	-1,0	-0,2	0,6	-0,6	-0,2	69,02	-39,85	-172,86	-47356,77	-27294,41	-1883,92
-1,0	0,6	-0,2	0,6	0,6	-0,2	-80,53	19,93	288,11	15816,74	-27294,44	646,99
-1,0	0,2	0,6	-0,6	1,0	-0,6	-69,02	79,71	-288,12	31516,73	-0,05	1883,92
1,0	1,0	0,6	-1,0	-0,2	0,2	80,52	19,93	57,61	55230,10	40941,61	-646,99
1,0	0,6	-1,0	0,2	0,2	-0,6	23,01	-39,85	57,61	31563,44	-27294,47	-6831,66
0,2	1,0	-0,6	-0,6	0,6	-1,0	-23,01	0,00	-172,89	70976,84	-13647,30	-4334,97
0,6	0,6	-0,6	0,6	-1,0	1,0	46,02	-79,71	633,86	-7803,34	13647,27	-635,57
0,2	0,2	0,6	0,2	-0,6	-0,2	46,01	0,00	57,62	7896,70	-13647,22	3086,63
0,6	-0,2	0,2	-0,6	-1,0	-0,6	69,02	-39,85	-403,37	15723,35	-0,04	1838,29
0,6	-0,6	1,0	-0,6	-0,6	0,6	80,52	19,93	-172,86	-23690,10	40941,67	3075,22
0,2	-1,0	0,2	0,2	1,0	1,0	-11,50	59,78	57,64	-63103,51	27294,51	-3098,05
-0,2	0,6	1,0	-0,2	-1,0	-1,0	46,01	0,00	-172,88	47310,13	-27294,50	6808,84
-0,6	-1,0	1,0	-0,2	0,6	-0,2	-23,01	79,71	-403,35	-31610,10	0,00	3109,44
-0,2	-0,6	-0,6	-0,6	0,2	0,2	-34,51	-19,93	-288,11	-15816,74	27294,44	-1849,69
-0,2	-0,6	-0,6	1,0	1,0	-0,6	-57,52	19,93	-57,62	-31563,37	-54588,85	-4323,57
-0,6	-0,2	-1,0	0,2	-0,6	-1,0	-46,01	-79,71	-288,12	7850,04	-40941,69	635,59
-0,2	1,0	0,6	0,2	1,0	0,6	-23,01	79,71	518,60	23736,74	13647,23	-612,77
1,0	-0,2	-0,2	-0,2	0,6	1,0	34,51	19,93	172,88	-23643,42	40941,70	-5594,73
0,2	-1,0	-1,0	-0,2	-0,2	0,6	-11,50	-59,78	-172,85	-47356,81	27294,48	-3098,03

Table 2.4: Uniform DOE and results of the Experiments

Low-order polynomials have been used effectively to build approximations in a variety of applications including force-displacement modeling [91]. Here a second order polynomial with interactions is used for meta-modeling an input-output of the HexFlex mechanism.

The chosen polynomial model for the input-output meta-model of the HexFlex mechanism is shown in Eq. (2.4).

$$\mathbf{r}_i = \beta_0 + \sum_{i=1}^{k} \beta_i \tau_i + \sum_{i=1}^{k} \beta_{ii} \tau_i^2 + \sum_{i=1}^{k} \sum_{j=1}^{k} \beta_{ij} \tau_i \tau_j, \tag{2.4}$$

where $i = 1, \ldots, 6$, $j = 1, \ldots, 6$, $i < j$, and τ and $\mathbf{r}$ are defined in Eq. (2.2) and Eq. (2.3) respectively.

The Placket-Burman DOE analysis reveals out which interactions of the behavior of the mechanism are not important and are therefore negligible in Eq. (2.4). Also, preliminary experiments showed that the quadratic terms of Eq. (2.4) do not influence the behavior of the mechanism and are therefore neglected. The resulting force-displacement meta-model of the HexFlex mechanism is shown on Eq. (2.5).

$$\begin{bmatrix} x & y & z & \theta_x & \theta_y & \theta_z \end{bmatrix}^T = S_T \begin{bmatrix} \text{T1D1} & \text{T1D2} & \text{T2D1} & \text{T2D2} & \text{T3D1} & \text{T3D2} \end{bmatrix}^T, \quad (2.5)$$

where the matrix S_T (Eq. (2.6)) represents the I/O matrix of the mechanism. Each term of S_T is found using a penalized least-squares regression [92, 93]. The units associated to the elements S_T for the HexFlex are as follow: rows 1 to 3 $\mu\text{m/N}$ and rows 3 to 6 $\mu\text{rad/N}$.

$$S_T = \begin{bmatrix} 57,5 & 0 & 28,8 & 0 & -28,8 & 0 \\ 0 & 0 & 49,8 & 0 & 49,8 & 0 \\ 0 & 287,7 & 0 & 287,7 & 0 & 287,7 \\ 0 & 39313,0 & 0 & -19679,9 & 0 & -19633,3 \\ 0 & 0 & 0 & -34032,0 & 0 & 34060,2 \\ -3101,8 & 0 & 3101,8 & 0 & -3101,8 & 0 \end{bmatrix}. \quad (2.6)$$

2.1.5.5 Validation of the HexFlex Meta-model

To validate the accuracy of the the meta-model, 1000 random experiments with uniform distributions and factor levels between -1 N and 1 N are made. The found forward model is used to compare the pose estimations using meta-modeling against the FEA software Ansys©. The precision of the model is calculated using three error criteria:

1. The maximum absolute error ($MAXABS$ Eq. (2.7)).
2. The relative error between the meta-model and the FEA model.
3. The root mean square error ($RMSE$ Eq. (2.8)) over the set of experiments.

The $MAXABS$ and relative $\%$ of error, allows the calculation of the local error. The $RMSE$ provides good estimate of the global error. The error between meta-model predictions and the Ansys© results is shown in Table 2.5. The deformed shape of the mechanism for one of the

experiments made to validate the accuracy of the meta-model is shown in Fig 2.9.

$$MAXABS = max\left\{\left|\psi_i - \widehat{\psi_i}\right|\right\}_{i=1,\ldots,n_{error}}, \tag{2.7}$$

$$RMSE = \sqrt{\frac{\sum_{i=1}^{n_{error}}(\psi_i - \widehat{\psi_i})^2}{n_{error}}}. \tag{2.8}$$

	$MAXABS$	MAX $\%error$	$RMSE$
x [μm]	4,01E-04	1,08E-03	8,67E-05
y [μm]	4,18E-04	3,59E-04	2,07E-05
z [μm]	2,85E-04	2,41E-04	4,19E-05
θ_x [μrad]	2,41E-02	2,26E-03	9,78E-04
θ_y [μrad]	4,16E+00	6,21E-01	5,57E-03
θ_z [μrad]	2,10E-02	2,30E-03	2,23E-03

Table 2.5: Error between meta-model estimations and Ansys© simulations for 1000 random experiments with uniform distribution

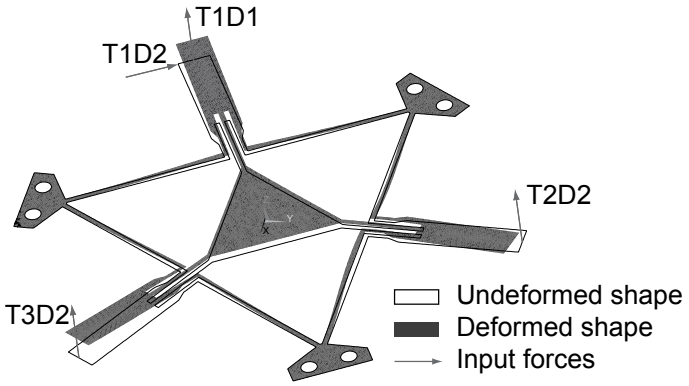

Figure 2.9: Deflected shape of the HexFlex mechanism for one meta-model validation experiment

2.1.6 Conclusions

This article presented a computer-based meta-modeling methodology for the force-displacement modeling of CMs under quasi-static conditions using DOCE. The methodology is applied to obtain

a force-displacement model of the six degrees of freedom HexFlex CM. To obtain the meta-model of the HexFlex, virtual experiments based on Plackett-Burman and Uniform DOEs are performed using FEA. The obtained meta-model of the HexFlex is linear for the movement range of the mechanism. The accuracy of the meta-model was calculated by running 1000 FEA-based computer experiments. The values found in the experiment were compared against those generated by the meta-model. The results of the comparison can be observed in Table 2.5. These results led us to conclude that the meta-model is sound for the ranges and operating point chosen.

Performing Factorial DOE it was possible to identify characteristics of the behavior of the mechanism, such as the presence of symmetries in the actuation and the quasi-static behavior of the mechanism. A Uniform DOE was employed to fine tune the model of the mechanism. The mechanism was modeled using a low-order polynomial, because of its quasi-static behavior and small displacements. The model found allows to have an I/O model of the mechanism yielding a transfer function for developing real-time control. It should be noticed that the (linear) model obtained is easily invertible, which adds to its applicability. However even if the model obtained was not linear, its invertibility is guaranteed because it is a polynomial approximation around the vicinity of the operating point.

Nonetheless DOCE is not intended to replace real-experiment-based DOE but to forecast / ignore possible interactions and to fine-tune ranges, thereby reducing costs of experimentation and model/product development.

Scalability and Symmetry. The scalability and symmetry of the discussed method deserve the following comments: 1- A scaled copy of the mechanism does not have the scaled I/O function of the original mechanism. A reason for this behavior is that size has effects on the flexibility of the material. 2- A scaled copy of the mechanism accepts the same DOCE methodology propose, to reach its I/O function. 3- The DOCE method applied here does not make use of symmetries of the modeled mechanism. However, we did use symmetries in checking the values of the obtained coefficients (Eq. (2.5) and Eq. (2.6)) with the purpose of finding possible modelingor calculation errors. Symmetries helped us to find and correct such procedural errors, reaching a meaningful equation. Although it was not a goal for this article, future work might include the consideration of mechanism symmetries to find the coefficients (not only to check them).

Applicability to Other Mechanisms. DOE, and DOCE in particular, are methods that can be applied to complex systems whose I/O function is fully or partially unknown. A mechanism is not different, in this sense, to a chemical or a biotechnological process. DOCE methodology is able to model other mechanisms, even if they are not of the HexFlex types. The numerical models

obtained for different mechanisms will indeed be different in the classification of input and output variables, sensitivities, etc. However, *the DOCE methodology* will still be valid to find the I/O function of such mechanisms.

Chapter 3

Kinematic Identification of Parallel Mechanisms

This chapter is devoted to the *kinematic identification of parallel mechanisms*. Its contribution is a new Divide-and-Conquer (DC) protocol for the kinematic identification of parallel mechanisms based on the inverse calibration method introduced by [4]. Different from available kinematic identification methods, the proposed protocol exploits the structural symmetries of parallel mechanisms in order to set a symmetrical-independent identification for each leg.

Two articles are presented. In article 3.1 the new DC protocol is developed. The protocol includes the novel symmetrical aspects of kinematic identification. However, it is centered on the identification itself. Article 3.2 is focused on the symmetrical observability of leg parameters what represents its novel contribution. Kinematic identification is proposed as a natural application of symmetrical observability.

Both articles 3.1 and 3.2 are based on the published conference paper [10]. Article [10] is not included in this dissertation, nevertheless its content is covered in articles 3.1 and 3.2.

3.1 A Divide-and-Conquer Protocol for Kinematic Identification of Parallel Mechanisms Using Symmetric Groups

Sebastián Durango, David Restrepo, Oscar Ruiz
{sdurang1, drestr21, oruiz}@eafit.edu.co
CAD CAM CAE Laboratory
EAFIT University
Medellín, Colombia

John Restrepo-Giraldo, Sofiane Achiche
{jdrg, soac}@man.dtu.dk
Engineering Design and Product Development
Technical University of Denmark
Lyngby, Denmark

This article was accepted by the Journal of Mechanisms and Robotics (ASME), ISSN: 1942-4302. Note: this article is an extension of the published conference paper [10].

Abstract

This article presents a new kinematic identification protocol suitable for symmetrical parallel mechanisms, with the following contributions: (i) a Divide-and-Conquer (DC) strategy in which the kinematic identification is developed independently on each leg of the mechanism using the inverse calibration method, and (ii) a symmetric groups application that takes advantage of the symmetrical observability of the leg parameters sets. Compared to traditional identification methods, the main advantages of the proposed DC protocol are: (i) cost reduction in the design of identification poses using observability symmetries. The pose selection is carried out only for a reference leg, allowing the poses of the remaining $(n_{legs} - 1)$ legs to be dictated by symmetrical operations performed on the selected poses, and (ii) improvement of the numerical efficiency of the procedure for the selection of optimal identification poses. We adopted a pose selection algorithm supported on determinant-based index instead of traditional eigenvalue-based ones, reducing the computation complexity of the optimal identification poses. The kinematic identification of a 3

degrees-of-freedom symmetrical parallel mechanism is discussed as a case study, and the performance of the calibrated mechanism is evaluated through forward kinematic simulations.

keywords: Kinematic Identification, Parallel Mechanism, Divide-and-Conquer Strategy, Symmetric Group, Symmetrical Observability.

Glossary

$\mathbf{C}$	Jacobian identification matrix
F	Constraint kinematic equation
G	Group
$L,\ l$	Length of a link
N	Number of identification poses
$\mathbf{Q}$	Column matrix of active-joint configurations
$\underline{\mathbf{Q}}$	Q matrix of a QR decomposition
$\mathbf{P}$	Column matrix of parametric representations of the end-effector orientation
$\mathbf{R}$	Column matrix of end-effector position vectors
$\underline{\mathbf{R}}$	R matrix of a QR decomposition
$\underline{R}RR$	Rotational - rotational - rotational kinematic structure
V	Polygon
g	Inverse kinematic equation
k	Gain of an active-joint sensor
n_{DOF}	Number of degrees of freedom
n_{legs}	Number of legs of a parallel mechanism
n_{φ}	Number of parameters to be identified
q	Active joint variable
$\mathbf{q}$	Vector of active joint variables
$\mathbf{r}$	Position vector
s	Singular value

Greek symbols

α, β	Planar angles
γ	Offset of an active-joint sensor
φ	Set of kinematic parameters of a parallel mechanism
λ	Symmetry operation

θ	Active-joint angle
ρ	Parametric representation of an orientation, *e.g.* a set of Euler angles
σ	Standard deviation
ψ	Reading of an active-joint sensor

Subscripts

$_C$	Symmetrical observability
$_M$	Mechanism
$_Q$	Active joints
$_W$	Workspace
$_i$	Indexing variable
$_\kappa$	κth leg of a parallel mechanism

Superscripts

^{T}	Transpose
^{j}	jth pose of the mechanism

3.1.1 Introduction

In mechanisms and manipulators, the accuracy of the end-effector critically depends on the knowledge of the kinematic parameters that rule the control model, [4]. Thus, the kinematic parameters of a mechanism have to be estimated precisely to improve its accuracy [7]. The process of estimating the kinematic parameters and updating the kinematic model is formally known as kinematic identification or kinematic calibration [6, 7].

This article addresses the kinematic identification of symmetrical parallel mechanisms which are defined as follows:

1. The number of legs equals to the number of degrees of freedom of the mechanism.
2. Each leg is controlled by one actuator.
3. Each leg has the same pattern of joints and links.
4. In at least one particular pose the kinematic structure of the mechanism defines a symmetric group G_M [94]. A group is a set G equipped with an internal operation $\odot$, such that the

operation is associative, has closure, and has both a neutral and an inverse element in G [95]. A particular example of a symmetric group is the one of all the rigid motions λ such that $\lambda(V) = V$, V being a polygon [94].

Most industrial parallel mechanisms can be classified as symmetrical [94].

We updated the Divide-and-Conquer (DC) kinematic identification protocol presented in [10] with a symmetrical pose selection procedure. The DC protocol requires independently identifying the legs using the inverse calibration method proposed in [4, 7], this allows the design of experiments to optimize the observability of the set of parameters on each leg [10]. However, by the symmetries of the mechanism it is possible to express leg parameters in coordinate systems which allow symmetrical observability, and as a result, symmetrical pose selection. Consequently, this article presents a contribution to improve the pose accuracy in symmetrical parallel mechanisms using a new DC kinematic identification protocol based on inverse kinematic modeling and a symmetrical planning of the identification experiments.

Compared to traditional identification methods, the main advantages of the proposed DC identification protocol are:

1. Cost reduction in the design of identification experiments by the use of observability symmetries. The pose selection is carried out on a reference leg and for the remaining $(n_{legs} - 1)$ legs the poses are determined by symmetrical operations performed on the poses of the reference leg.

2. Improvement of the numerical efficiency of the procedure for the selection of optimal identification poses by the adoption of the active robot calibration algorithm of Sun and Hollerbach [96]. Traditional pose selection algorithms are based on observability indexes that are calculated through eigenvalue decomposition of the covariance observability matrix, whereas the active robot calibration algorithm is determinant-based, resulting in higher computational efficiency.

The layout for the rest of the article is: section 3.1.2 which develops a literature review on inverse calibration and analysis of symmetries in parallel mechanisms; section 3.1.3 presents the new DC kinematic identification protocol for symmetrical parallel mechanisms. Results are summarized in section 3.1.4 through the simulated kinematic identification of a 3*RRR* symmetrical parallel mechanism using the DC protocol. Finally, concluding remarks are presented in section 3.1.5.

3.1.2 Literature Review

Parallel mechanisms are reported to bear higher loads, at higher speed and often with a higher repeatability compared to open-loop kinematic chains [7]. However, the accuracy of parallel mechanisms is usually restricted by the knowledge of the kinematic parameters that rule their control models. [4]. Therefore, when working with parallel mechanisms it is essential to calibrate the kinematic models with estimated parameters so that accurate motion at high-speed rates can be achieved [7]. The following categories of kinematic identification are proposed by [7] in the case of parallel mechanisms:

1. Constrained calibration. This method relies on the use of mechanical systems that constrain the end-effector or the legs motion during calibration. The workspace size is reduced by the constraints which restrict the identification pose selection and the identification efficiency [6, 7].

2. Self calibration. These methods rely on the use of redundant metrology. Some passive-joints are instrumented in addition to the active-joints. The redundant metrology replaces the information provided by external measurement devices. However, the actual task of adding the redundant sensors to the passive-joints is quite complex [7, 97].

3. Forward kinematics calibration. These methods are directly adapted from the serial mechanisms calibration methods [98]. The identification is performed by minimizing the difference between an end-effector pose measurement and its corresponding value, calculated from measured active-joint values through the forward kinematics model. A major drawback of this approach is the instability associated with the numerical evaluation of the forward kinematics of parallel mechanisms which does not have an analytical solution [7, 99].

4. Inverse calibration method. This method developed by [4], is accepted as the natural [4, 7] and most numerically efficient [6] among the identification algorithms for parallel mechanisms. The kinematic parameters are estimated by minimizing the difference between measured and computed active-joint variables calculated through the inverse kinematics of the end-effector pose measurements. In this article, we adopt this method for the calibration of symmetrical parallel mechanisms.

A set of inverse kinematics equations are used as constraint equations in the inverse calibration method. These equations can be linearized in terms of the unknown parameters, producing a differential error model with an identification Jacobian matrix that allows the measurement of the

observability of the parameters [4, 96]. This observability matrix is usually block diagonal on parallel mechanisms, with each block depending only on the parameters of one leg, allowing the independent leg identification [4].

In [7] the inverse calibration method is updated for the vision-based calibration of parallel robots, identifying camera parameters in addition to the kinematic ones. In [3] a kinematic calibration method for parallel kinematic machine-tools that replaces the end-effector position measurements by measurements on a dedicated machined part is presented. This method is aimed at process calibration and is performed only on a sub-region of the workspace, resulting in a part-dedicated calibration. Reference [100] presents the kinematic calibration problem as a non-linear constrained optimization problem formulated in a geometric context. Geometrically, the kinematic calibration consists of determining a best fitting parametrized multi-dimensional surface to a given set of measured points in the environment (joint variables and parameters) and task (end-effector pose) space manifolds. The formulation is general enough to cover most of the allowable identification methods, including inverse calibration.

In [10] a DC kinematic identification protocol based on the inverse calibration method is presented. The identification experiments are independently planned for each leg, optimizing the observability of leg parameters. Compared to traditional identification methods, the protocol has reported the following advantages:

1. The identification poses are optimized for the estimation of reduced sets of parameters (the sets corresponding to each leg).

2. The independent identification of the set of parameters of each leg improves the numerical efficiency of the identification algorithms.

The calibration of the kinematic model with the identified set of parameter achieves a better end-effector accuracy as a result of (1) and (2) .

A common characteristic of [3, 4, 7, 10, 100] is the lack of use of the kinematic structure symmetries present in most parallel mechanisms. These symmetries have been used for workspace and singularity analysis of parallel mechanisms, but not for kinematic identification.

The fundamentals of workspace analysis of symmetrical parallel mechanisms are presented in [94, 101], where a theorem that reveals a relation between the mechanism symmetries and the workspace symmetries is formalized. The use of the theorem allows to reduce the computational

cost of workspace calculations to $\frac{1}{n}$ of a full search, n being the order of the symmetries. In [102] the symmetric theorem is used to analyze the symmetrical characteristics of the singularities of symmetrical parallel mechanisms. The special case of workspace and singularity symmetries of parallel spherical mechanisms is presented in [103].

In this article we extended the use of symmetries to express sets of leg parameters in coordinate systems, allowing symmetrical observability of kinematic parameters for identification. This enables the updating of the DC kinematic identification protocol with a symmetrical pose selection procedure that reduces the cost of the experimental design. In this sense, the main contributions of the article are:

1. A DC kinematic identification strategy suitable for symmetrical parallel mechanisms (section 3.1.3.1)
2. A set of conditions to obtain symmetrical observability of the sets of leg parameters of symmetrical parallel mechanisms (section 3.1.3.2).

Contributions (1) and (2) result in a new DC kinematic identification protocol for symmetrical parallel mechanisms, which is presented in section 3.1.3.

3.1.3 Divide-and-Conquer Kinematic Identification Protocol for Symmetrical Parallel Mechanisms

The set of conditions that define a symmetrical parallel mechanism are summarized as follows:

1. The number of legs (n_{legs}) is equal to the number of degrees of freedom (n_{DOF}) of the mechanism.
$$n_{DOF} = n_{legs} \tag{3.1}$$
2. All the legs have an identical kinematic pattern. That is, each leg has the same number of active and passive joints, and the joints are arranged in an identical pattern.
3. The constraint kinematic equations (F_κ) for each leg of the mechanism can be expressed in their implicit form:
$$F_\kappa = g_\kappa(\varphi_\kappa, \mathbf{r}, \rho) - q_\kappa = 0 \qquad (\kappa = 1, 2, \ldots, n_{legs}), \tag{3.2}$$

where κ denotes the κth leg, g_κ is an inverse kinematic function, φ_κ is the set of kinematic parameters, $\mathbf{r}$ is the position vector of the end-effector, ρ is a parametric representation of the platform orientation (*e.g.* a set of Euler angles), and q_κ is the active-joint variable. The set of constraint equations for the complete mechanism is defined in the following manner:

$$F(\mathbf{q}) = \begin{bmatrix} F_1(q_1) \\ F_2(q_2) \\ \vdots \\ F_{n_{legs}}(q_{n_{legs}}) \end{bmatrix} = \begin{bmatrix} g_1(\varphi_1, \mathbf{r}, \rho) - q_1 \\ g_2(\varphi_2, \mathbf{r}, \rho) - q_2 \\ \vdots \\ g_{n_{legs}}(\varphi_{n_{legs}}, \mathbf{r}, \rho) - q_{n_{legs}} \end{bmatrix}, \tag{3.3}$$

where $\mathbf{q} = [q_1 \; q_2 \; \cdots q_{n_{legs}}]^T$ is the vector of active joint variables.

4. The kinematic structure of the mechanism describes a symmetric group G_M on a particular pose of the end-effector.

In a practical way, the definition of symmetrical parallel mechanism covers most of the industrial parallel manipulators.

Conditions (1) to (4) configure a symmetrical workspace and are necessary for the symmetrical planning of the kinematic identification experiments. The symmetry of the workspace of spatial parallel mechanisms is proved in [94]. In addition to the conditions of the symmetrical mechanism, we assume the following condition to obtain a symmetrical active-joint workspace:

5. The active-joints reference systems are defined in such a way that the active-joint variables are also symmetrical in the particular pose defining the symmetric group of the kinematic structure (G_M). For the active-joints this implies to have the same value in the symmetrical configuration. The symmetric group of the active-joint variables is denoted as G_Q.

If the active-joint workspace is symmetrical, then the following relation holds:

$$F(\lambda_i(\mathbf{q})) = \lambda_i(F(\mathbf{q})) \qquad (i = 1, 2, \ldots, n_{legs}), \tag{3.4}$$

where F is the set of constraint kinematic equations of the mechanisms (Eq. (3.3)), and $\lambda_i \in G_Q$ is a symmetric operation of the active-joint workspace symmetric group.

The proof of Eq. (3.4) is analogous to the forward kinematics of parallel mechanisms: it requires the solution of the constraint kinematic equations given the vector of joint variables. In

general it is not possible to express the forward kinematics of parallel mechanisms in an analytical manner [7]. In consequence, a proof of the symmetric conjecture of active-joint workspace is not straightforward and is not provided in this article. However, in section 3.1.4.1 the conjecture is validated through a numerical analysis of the workspace and active-joint workspace of a three-degrees-of-freedom parallel mechanism formed only by rotational joints.

3.1.3.1 Kinematic identification by a divide-and-conquer strategy

A kinematic identification based on inverse kinematics and independent estimation of the sets of leg parameters (DC strategy) is stated as follows:

Given

1. A set of nominal kinematic parameters (φ_κ) for the κth leg. n_φ parameters are assumed to be identified:
$$\varphi_\kappa = \begin{bmatrix}\varphi_{\kappa,1} & \dots & \varphi_{\kappa,n_\varphi}\end{bmatrix}^T \qquad (\kappa = 1, 2, \dots, n_{legs}). \tag{3.5}$$

2. An inverse kinematic function (g_κ) that relates the κth active joint variable (q_κ) with the end-effector position $(\mathbf{r})$ and orientation (ρ). For the jth pose of the mechanism the inverse function of the κth leg is defined to be:
$$g_\kappa^j : \varphi_\kappa \times (\mathbf{r}^j \times \rho^j) \rightarrow q_\kappa^j \qquad (j = 1, 2, \dots, N). \tag{3.6}$$

3. A set of end-effector measured poses $\{\hat{\mathbf{R}}_\kappa, \mathbf{P}_\kappa\}$:
$$\begin{aligned}\hat{\mathbf{R}}_\kappa^T &= \left[(\hat{\mathbf{r}}_\kappa^1)^T \cdots (\hat{\mathbf{r}}_\kappa^N)^T\right] \qquad (\kappa = 1, 2, \dots, n_{legs}),\\ \hat{\mathbf{P}}_\kappa^T &= \left[(\hat{\rho}_\kappa^1)^T \cdots (\hat{\rho}_\kappa^N)^T\right] \qquad (\kappa = 1, 2, \dots, n_{legs}),\end{aligned} \tag{3.7}$$

   where $\hat{\mathbf{R}}_\kappa$ is a column matrix of N measured position vectors and $\hat{\mathbf{P}}_\kappa$ is a column matrix of N measured end-effector parametric representations of the orientation. Here, we assume that all unconstrained end-effector degrees of freedom are measured, and that its number equals the number of actuated legs (see Eq. (3.1)).

4. A set $(\hat{\mathbf{Q}}_\kappa)$ of N measurements of the κth active-joint variable, corresponding to the set of

end-effector measurements:

$$\hat{\mathbf{Q}}_\kappa = \begin{bmatrix} \hat{q}_\kappa^1 & \cdots & \hat{q}_\kappa^N \end{bmatrix}^T \qquad (\kappa = 1, 2, \ldots, n_{legs}). \tag{3.8}$$

Goal

1. To find the set of unknown kinematic parameters $(\bar{\varphi}_\kappa)$ that minimizes the error between the measured set of active-joint variables $(\hat{\mathbf{Q}}_\kappa)$ and its corresponding estimated set $(\bar{\mathbf{Q}}_\kappa)$ calculated from the measured end-effector poses through the inverse kinematic model (g_κ). The problem can be formally stated as the following non-linear minimization:

$$\begin{aligned} &\min_{\varphi_\kappa} \sum_{j=1}^{N} \left(g_\kappa^j(\varphi_\kappa, \hat{\mathbf{r}}^j, \hat{\rho}^j) - \hat{q}_\kappa^j \right)^2 \qquad (\kappa = 1, 2, \ldots, n_{legs}), \\ &\text{subject to : } \mathbf{r}^j \in \mathbf{R}_\kappa,\ \rho^j \in \mathbf{P}_\kappa \qquad (j = 1, 2, \ldots, N), \end{aligned} \tag{3.9}$$

   where $\{\mathbf{R}_\kappa, \mathbf{P}_\kappa\}$ is the set of identification poses, $\mathbf{R}_\kappa \subset \mathbf{R}$, $\mathbf{P}_\kappa \subset \mathbf{P}$, and $\{\mathbf{R}, \mathbf{P}\}$ is a singularity-free workspace that constrains the optimization problem.

A kinematic identification protocol for parallel symmetrical mechanisms based on the DC identification strategy and kinematic structure symmetries is proposed in section 3.1.3.3. It is necessary to set the kinematic parameters before performing the identification protocol in order to obtain a symmetrical observability of the legs. The conditions for the symmetrical observability are summarized in section 3.1.3.2.

3.1.3.2 Symmetrical observability of leg parameters

The kinematic identification planning of a parallel mechanism could be symmetrical if its kinematic parameters are carefully set in order to meet conditions (1) to (4) of section 3.1.3 required for a symmetrical workspace. Moreover, the planning of the kinematic identification experiments may be reduced according to a subset (G_C) of the symmetric group (G_M), of the kinematic structure (Eq. (3.10)). The subset G_C is defined by the symmetry operations that allow to super-impose a reference leg with the κth leg ($\kappa = 1, 2, \ldots, n_{legs}$):

$$G_C = \left\{ \lambda_1, \lambda_2, \ldots, \lambda_{n_{legs}} \right\} \qquad (G_C \subseteq G_M), \tag{3.10}$$

where $\lambda \in G_M$ is a symmetry operation of the mechanism kinematic structure symmetric group.

In order to design a symmetrical kinematic identification, we assume the following conditions:

1. The symmetries of the kinematic structure are described by the symmetric group G_M.
2. The mechanism has a symmetrical workspace characterized by a symmetric group G_W.
3. The geometric method is adopted for the kinematic modeling of the mechanism. An independent vector-loop kinematic constraint equation is written for each leg in the form of Eq. (3.2). Consequently, the following hypotheses are assumed to be valid:
   (a) Each U-joint forming a leg is modeled as perfect.
   (b) Each spherical joint forming a leg is modeled as perfect.
   (c) Each prismatic joint is modeled as perfectly assembled to its neighboring joints (U-joints, spherical joint, rotational joints, etc.).
   (d) The axis of each rotational joint is modeled as perfectly orientated.
   (e) If the mechanism is planar, then all the links are modeled as constrained in a plane.

   The hypotheses (3a) to (3e) are consequent with realistic operational conditions, where the influences of defects in the joints have a minor effect on pose accuracy compared with errors in the location of the joints [97].
4. The position of each base fixed point A_κ (U-joint, spherical joint, etc.) is defined by three parameters (see Fig. 3.1, $\kappa = 1, 2, \ldots, n_{legs}$):
   (a) The magnitude of the $\overline{OA_\kappa}$ segment.
   (b) The angle α_κ of the $\overline{OA_\kappa}$ segment with respect to the Z axis of the base reference system.
   (c) The angle β_κ of the projection of the segment $\overline{OA_\kappa}$ on plane XY with respect to the X axis of the base reference system.
5. The position of each platform point b_κ (U-joint, spherical joint, etc.) is described by three parameters defined analogously to the base fixed points (Fig. 3.1). The $ouvw$ reference system is analogous to the $OXYZ$. The three parameters are denoted as $\overline{ob_\kappa}$, α_{b_κ}, and β_{b_κ} ($\kappa = 1, 2, \ldots, n_{legs}$).

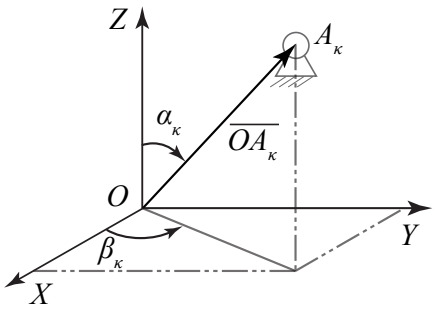

Figure 3.1: Position of fixed point A_κ

We assume a linear model for the active joints of the mechanism (Eq. (3.11)), requiring the estimation of two additional kinematic parameters for each leg: the joint gain (k), and the joint offset (γ). Therefore, additional symmetrical conditions are required to allow a symmetrical kinematic identification:

6. Each active joint has the same nominal gain k_κ ($\kappa = 1, 2, \ldots, n_{legs}$).

7. The mechanism has configured a symmetrical active-joint workspace characterized by a symmetric group G_Q. The conditions to configure a symmetrical active-joint workspace are proposed in conditions (1) to (5) of section 3.1.3.

The linear active-joint model is defined by:

$$\theta_\kappa = k_\kappa \psi_\kappa + \gamma_\kappa \qquad (\kappa = 1, 2, \ldots, n_{legs}), \tag{3.11}$$

where θ is the active joint angle, ψ is the sensor reading, k is the gain in the active-joint, and γ is the offset of the sensor.

To plan a symmetric identification, the observability of the ith kinematic parameter of the κth leg in the jth mechanism pose must be the same that the observability of its corresponding parameter of a reference leg in a symmetrical pose. To compute the observability we calculate the Jacobian identification matrix of each leg independently. That is

$$\begin{aligned} \mathbf{C}_\kappa^T &= \begin{bmatrix} (\mathbf{C}_\kappa^1)^T & (\mathbf{C}_\kappa^2)^T & \cdots & (\mathbf{C}_\kappa^N)^T \end{bmatrix} \qquad (\kappa = 1, 2, \ldots, n_{legs}), \\ \mathbf{C}_\kappa^j(\varphi_\kappa, \mathbf{r}^j, \rho^j) &= \frac{\partial F_\kappa(\varphi_\kappa, \mathbf{r}^j, \rho^j)}{\partial \varphi_\kappa^T} \qquad (j = 1, 2, \ldots, N), \end{aligned} \tag{3.12}$$

where the F_κ function is the κth constraint kinematic equation of the set of Eqs. (3.3), and each row of the Jacobian matrix $\mathbf{C}_\kappa$ corresponds to an identification pose of the mechanism. To calculate

the observability of the parameters we adopt the QR decomposition of the Jacobian identification matrix (Eq. (3.12)) presented in [6]:

$$\underline{\mathbf{Q}}^T \mathbf{C}_\kappa = \begin{bmatrix} \underline{\mathbf{R}} \\ \mathbf{0} \end{bmatrix}, \tag{3.13}$$

where $\underline{\mathbf{Q}}$ is a $N \times N$ orthogonal matrix, $\underline{\mathbf{R}}$ is a $n_\varphi \times n_\varphi$ upper triangular matrix, $\mathbf{0}$ is a $(N - n_\varphi) \times n_\varphi$ zero matrix, and n_φ is the number of parameters to be estimated.

The observability of the ith parameter is estimated by its corresponding element on the diagonal of the $\underline{\mathbf{R}}$ matrix, stating the symmetrical observability for the independent kinematic identification of the legs as:

$$|\underline{\mathbf{R}}^\kappa_{ii}\left(\mathbf{C}_\kappa(\varphi_\kappa, \mathbf{R}, \mathbf{P})\right)| = \left|\underline{\mathbf{R}}^1_{ii}\left(\mathbf{C}_1\left(\varphi_1, \lambda_\kappa(\mathbf{R}), \mathbf{P}\right)\right)\right| \\ (i = 1, 2, \ldots, n_\varphi)(\kappa = 1, 2, \ldots, n_{legs}), \tag{3.14}$$

where, without loss of generality, the first leg is assumed as the reference and λ_κ is the κth symmetrical operation of G_C that is applied individually over each end-effector position on $\mathbf{R}$. The smaller the norm of the parameter,the lower the observability, and the non-observable parameters are those for which $|\underline{\mathbf{R}}_{ii}| = 0$.

Section 3.1.3.3 proposes a kinematic identification of symmetrical parallel mechanisms protocol based in the symmetrical observability of the legs, and the DC identification strategy.

3.1.3.3 Kinematic identification of symmetrical parallel mechanisms protocol

For the DC kinematic identification protocol we assume:

1. The parallel mechanism is symmetric (see conditions (1) to (5) of section 3.1.3).
2. The kinematic parameters of the mechanism are set so as to obtain a symmetrical observability of the legs and the symmetric observability group (G_C) is specified (see section 3.1.3.2).

The DC identification protocol is presented in Fig. 3.2 and stated in the following procedures (DC steps):

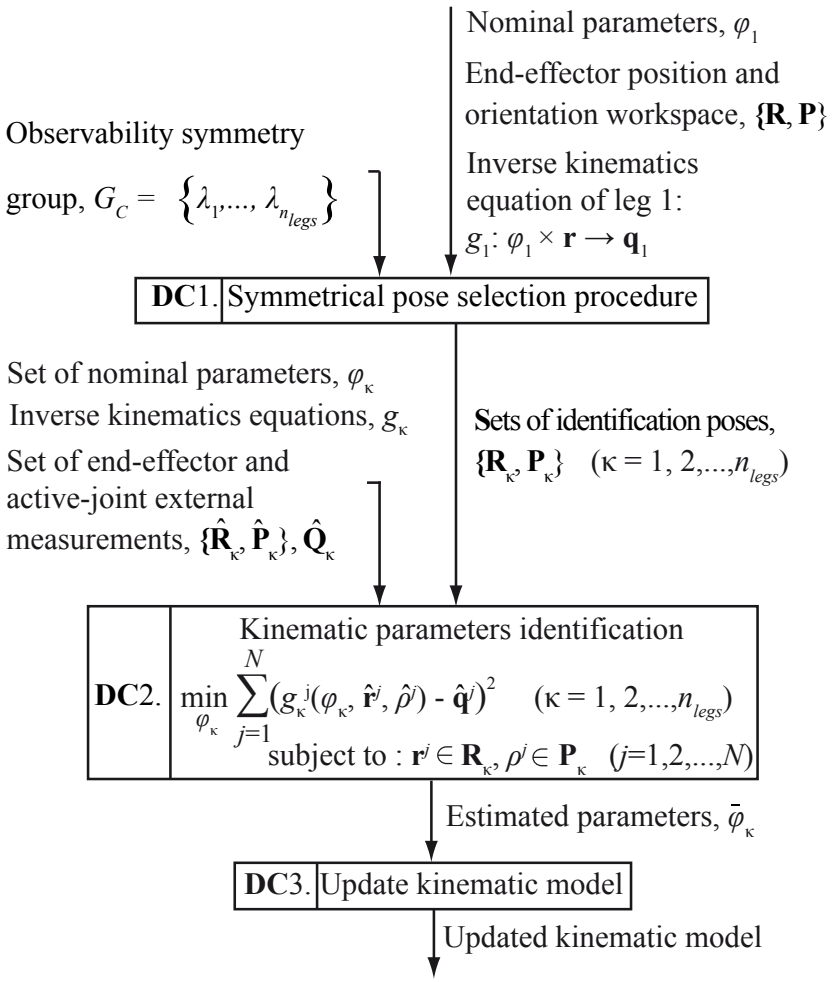

Figure 3.2: Divide-and-conquer kinematic identification of symmetrical parallel mechanisms protocol

DC1. Symmetrical pose selection. This step is detailed in Fig. 3.3.

(a) Calculation of the Jacobian identification matrix. Given the nominal parameters (φ_1) for a reference leg, the corresponding kinematic function (F_1), and a representative set of postures of a workspace without singularities $\{\mathbf{R}, \mathbf{P}\}$; the Jacobian identification matrix $(\mathbf{C}_1^{\mathbf{R}})$ is calculated as:

$$\mathbf{C}_1^{\mathbf{R}}(\varphi_1, \mathbf{R}, \mathbf{P}) = \frac{\partial F_1(\varphi_1, \mathbf{R}, \mathbf{P})}{\partial \varphi_1^T}. \tag{3.15}$$

here, the calculation of the Jacobian matrix can be performed analytically or numerically. For parallel mechanisms the constraint kinematic function F is usually available for the analytical (symbolic) calculation of the Jacobian matrix. A procedure for the

numerical calculation of the Jacobian matrix is proposed in [104].

(b) Pose selection by active robot calibration algorithm. Given the Jacobian identification matrix calculated in step (DC 1a) to select an optimal set of postures $\{\mathbf{R}_1, \mathbf{P}_1\}$ for the kinematic identification of the reference leg. We adopt the active calibration algorithm developed by Sun and Hollerbach [96] to optimize the poses. The optimized identification set of poses is determined by solving the problem:

$$\begin{aligned} &\max_{\{\mathbf{R_1},\mathbf{P_1}\}} O_1, \\ &\text{subject to} : \mathbf{R}_1 \subset \mathbf{R}, \mathbf{P}_1 \subset \mathbf{P}, \end{aligned} \tag{3.16}$$

were O_1 is an observability index of the identification matrix defined as follows,

$$O_1(\mathbf{C}_1(\varphi_1, \mathbf{R}_1, \mathbf{P}_1)) = \frac{(s_1\ s_2 \cdots s_{n_\varphi})^{1/n_\varphi}}{n_\varphi}, \tag{3.17}$$

where n_φ is the number of parameters to be identified, and s_i^2 $(i = 1, 2, \ldots n_\varphi)$ are the eigenvalues of the covariance matrix $\mathbf{C}^T\mathbf{C}$. The effective criterion is the product of all non-zero eigenvalues, being the determinant of $\mathbf{C}^T\mathbf{C}$ because n_φ is constant. This allows to solve the optimization problem (Eq. (3.16)) by using a recursive (exchange - add - exchange pose) determinant instead of eigenvalue calculation, thus reducing the computation complexity and enabling the consideration of more candidate pose sets in the optimal pose set search [96]. As rule of thumb, the number of identification poses should be two or three times larger than the number of parameters to be estimated [105].

(c) Symmetrical pose selection. Given the selected set of identification poses of the reference leg $\{\mathbf{R1}, \mathbf{P1}\}$ and the observability symmetric group (G_C), find the sets of identification poses of the remaining $(n_{legs} - 1)$ legs:

$$\begin{aligned} \mathbf{R}_\kappa &= \lambda_\kappa(\mathbf{R_1}) \qquad (\kappa = 2, \ldots, n_{legs}), \\ \mathbf{P}_\kappa &= \mathbf{P_1} \qquad (\kappa = 2, \ldots, n_{legs}). \end{aligned} \tag{3.18}$$

where the symmetry operation λ operates onto the end-effector workspace. Here the end-effector workspace is defined as the volume within which the end-effector point (i.e. the geometry center of the moving stage) can be reached [94]. The symmetry operation does not operate onto the orientation of the end-effector.

DC2. Estimation of kinematic parameters. Given the optimized set $\{\mathbf{R}_\kappa, \mathbf{P}_\kappa\}$ of identification

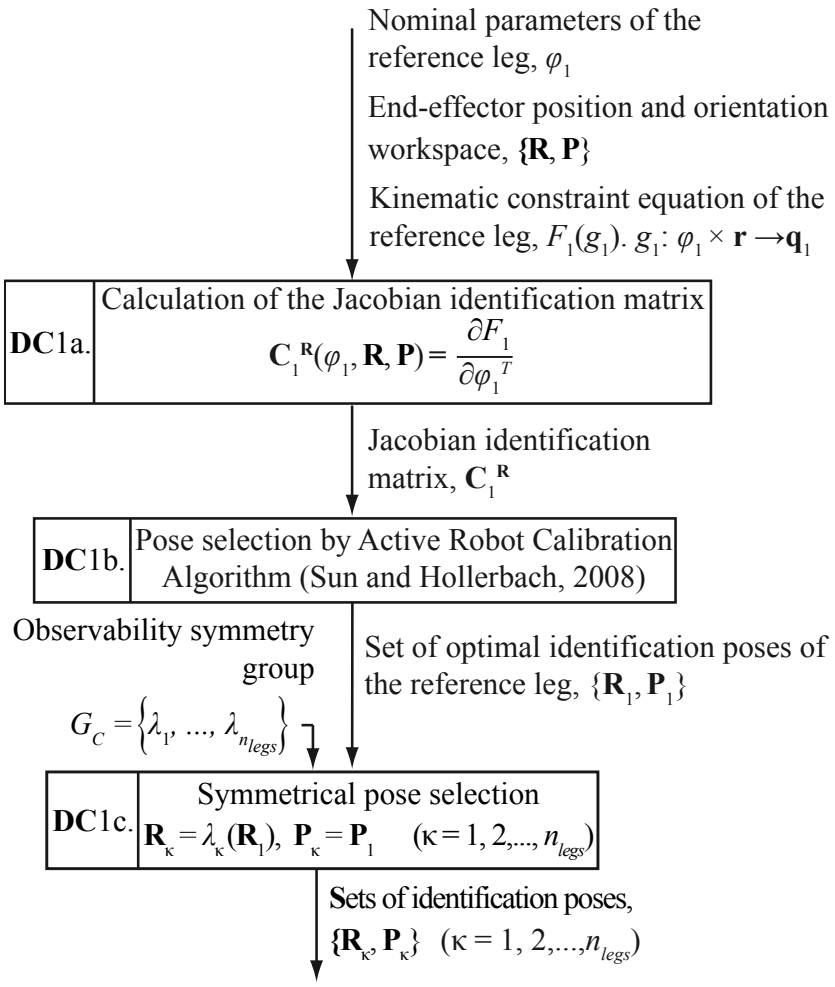

Figure 3.3: Symmetrical pose selection procedure

poses obtained in (DC 1) and its corresponding sets $(\hat{\mathbf{Q}}_\kappa, \{\hat{\mathbf{R}}_\kappa, \hat{\mathbf{P}}_\kappa\})$ of active-joint and end-effector measurements, estimate the set of kinematic parameters (φ_κ) so that the optimization problem defined by Eq. (3.9) is solved $(\kappa = 1, 2, \ldots, n_{legs})$.

DC3. Kinematic model update. Given the identified sets of parameters obtained in (DC 2), update the kinematic model of the parallel mechanism.

The DC identification protocol is used in the simulated kinematic identification of a $3\underline{R}RR$ symmetrical parallel mechanism in section 3.1.4. The calibration results are compared with a traditional inverse kinematic calibration.

3.1.4 Results

The kinematic identification of a $3\underline{R}RR$ parallel mechanism is simulated to evaluate the performance of the DC identification protocol. The mechanism consists of an equilateral moving platform $(b_1b_2b_3)$ that is connected by three identical rotational - rotational - rotational kinematic chains $(A_\kappa C_\kappa b_\kappa,\ \kappa = 1, 2, 3)$, to an equilateral fixed base $(A_1A_2A_3)$ (see Fig. 3.4(a)). The mechanism has three degrees of freedom actuated from three active-joints that are located on the fixed base. To simulate the kinematic behavior of the mechanism, the nominal kinematic parameters are disturbed by adding random errors following a normal distribution with a standard deviation of $\sigma = 5 \cdot 10^{-5}$ m and $\sigma = 5 \cdot 10^{-5}$ rad for the longitudinal and angular dimensions respectively. The following set of nominal parameters is assumed:

1. Dimensions of the links: $\overline{A_1A_2} = \overline{A_2A_3} = \overline{A_1A_3} = 6.00$ m, $\overline{b_1b_2} = \overline{b_2b_3} = \overline{b_1b_3} = 1.50$ m, $l = L = 1.50$ m.

2. Configuration of the legs (dyads): $[-1\ -1\ -1]$. Each leg is considered as a dyad that can be configured as $+1$ or -1 according to the convention described in Fig. 3.4(b).

3. Nominal gain of the active-joints: $k_1 = k_2 = k_3 = 1$.

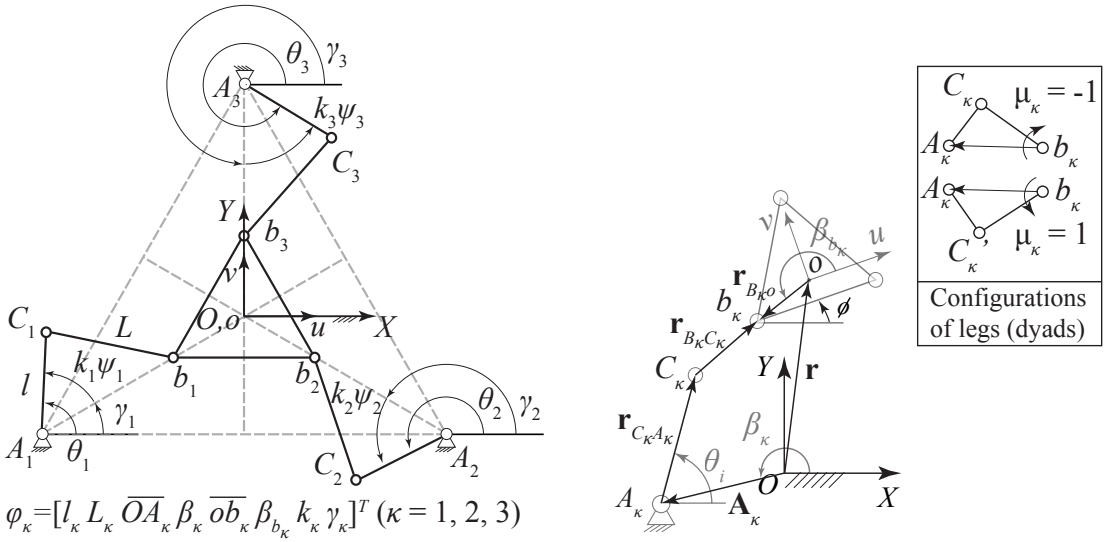

(a) Mechanism in symmetric pose

(b) Kinematic loop of the κth leg

Figure 3.4: $3\underline{R}RR$ symmetrical parallel mechanism. Kinematic parameters and constraint loop

The end-effector measurements $(\hat{\mathbf{R}}_\kappa)$ are simulated from their corresponding active-joint measurements $(\hat{\mathbf{Q}}_\kappa)$ through a forward kinematics model to which a normally distributed random dis-

turbances have been added and were defined as follows:

$$\begin{aligned} \sigma_r &= 5.00 \cdot 10^{-6}\ \mathrm{m}, \\ \sigma_\rho &= 5.00 \cdot 10^{-6}\ \mathrm{rad}, \end{aligned} \tag{3.19}$$

where σ_r and σ_ρ are the standard deviations in length and orientation measurements respectively. Prior to the kinematic identification, a symmetry analysis and a declaration of symmetrically observable sets of leg parameters are performed in sections 3.1.4.1 and 3.1.4.2.

we assume that the origin of the fixed coordinate frame is located at the geometric center of the fixed base $A_1A_2A_3$ in order to carry out the kinematics modeling, symmetry analysis, and kinematic identification. The X-axis points along the direction of A_1A_2, and the Y-axis is perpendicular to A_1A_2 (see Fig. 3.4(a)). A moving frame is attached to the geometric center of the platform. The u-axis of the platform frame points along the line b_1b_2, and the v-axis is perpendicular to b_1b_2 (see Fig. 3.4(a)). The location of the moving platform is specified by the coordinates of the platform center and the orientation angle of the moving frame with respect to the fixed frame:

$$\begin{aligned} \mathbf{r} &= [x \ \ y \ \ 0]^T, \\ \rho &= \phi. \end{aligned} \tag{3.20}$$

3.1.4.1 Symmetry analysis

The $3\underline{R}RR$ symmetrical parallel mechanism satisfies the workspace symmetry conditions (1) to (4) of section 3.1.3:

1. The mechanism has three legs (dyads) and three corresponding degrees-of-freedom.
2. Each leg of the mechanism has an identical $\underline{R}RR$ pattern.
3. The kinematic constraint equation of each leg is expressed by a closed loop (see Fig. 3.4(b)) in the following manner:

$$\|\mathbf{r} - \mathbf{A}_\kappa\| - \|\mathbf{r}_{C_\kappa A_\kappa} + \mathbf{r}_{BC_\kappa} - \mathbf{r}_{B_\kappa o}\| = 0 \qquad (\kappa = 1, 2, 3). \tag{3.21}$$

4. The kinematic structure symmetric group (G_M) is specified by inspection (Fig. 3.4(a)) and defined as:

$$G_M = \{\lambda_1, \lambda_2, \lambda_3, \lambda_4, \lambda_5, \lambda_6\}, \tag{3.22}$$

where the first three elements represent the following rotations about the Z-axis: 0 rad, $2\pi/3$ rad, and $4\pi/3$ rad. The last three elements denote reflections about OA_1, OA_2, and OA_3 respectively.

The actuation of G_M on the end-effector workspace will cause the workspace to superimpose on itself. The symmetrical workspace theorem for this mechanism is proved in [94, 101]. We assume a linear active-joint model (Eq. (3.11) with $n_{legs} = 3$ legs). In consequence, to design a symmetrical kinematic identification, it is also necessary to satisfy the condition (5) for active-joint workspace symmetry (section 3.1.3):

5. Figure 3.4(a) presents the symmetrical pose of the $3\underline{R}RR$ mechanism that determines the symmetry of the active-joint workspace, with the active-joint variables being vector defined as $\mathbf{q} = [\psi_1, \psi_2, \psi_3]^T$. The pose is obtained by setting the active-joints measure systems in the following manner:

$$\gamma_1 = \pi/6 \text{ rad}, \ \gamma_2 = 5\pi/6 \text{ rad}, \ \gamma_3 = -\pi/2 \text{ rad}. \tag{3.23}$$

where n_{legs} equals 3 for the $3\underline{R}RR$ mechanism, then the active joints symmetric group defined by Eq. (3.4) is as follows:

$$G_Q = \{\lambda_1, \lambda_2, \lambda_3\} \tag{3.24}$$

where the elements of G_Q correspond to rotations of 0 rad, $2\pi/3$ rad, and $4\pi/3$ rad around the axis $\psi_1 = \psi_2 = \psi_3$.

The active-joint workspace symmetry is numerically validated by comparing a workspace obtained by inverse kinematics with a workspace obtained by symmetrical operations λ_i (Eq. (3.24)) performed onto $1/3$ of the complete workspace. The maximal difference (obtained by comparing 33 000 corresponding active-joint configurations) is $1.2 \cdot 10^{-14}$ rad, which can be interpreted as a numerical zero. The active-joint workspace is presented in Fig. 3.5.

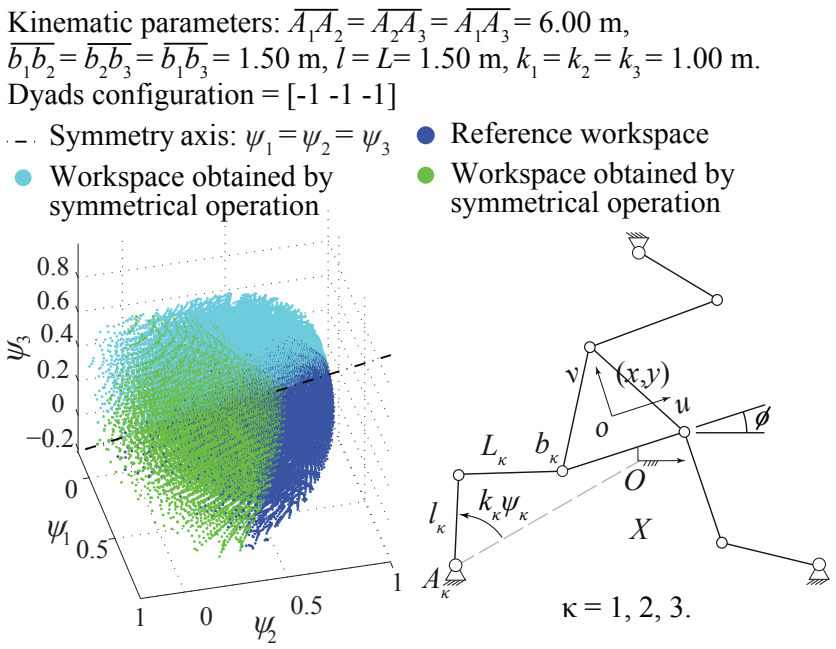

Figure 3.5: 3*RRR* symmetrical parallel mechanism. Active-joint workspace obtained by symmetrical operations

3.1.4.2 Denotation of symmetrically observable sets of kinematic parameters

Nominally, the set of kinematic parameters is defined by the position of base fixed points $(\mathbf{A}_\kappa)$, the position of platform points $(\mathbf{b}_\kappa)$, the leg lengths $(l_\kappa,\ L_\kappa)$, and the joint gain and offset (k_κ and ψ_κ) $(\kappa = 1, 2, 3)$. Consequently with the conditions (1)–(7) of the symmetrical observability, section 3.1.3.2, we express this set of parameters to be symmetrically observable: The base and platform points are modeled as constrained on the mechanism plane and defined by the magnitude of the $\overline{OA_\kappa}$ and $\overline{ob_\kappa}$ segments and angles β_κ and β_{b_κ} respectively (see Fig. 3.4). A linear model is assumed for the active joints (Eq. (3.11)). In consequence, the set of parameters to be identified is:

$$\varphi_\kappa = \left[l_\kappa\ L_\kappa\ \overline{OA_\kappa}\ \beta_\kappa\ \overline{ob_\kappa}\ \beta_{b_\kappa}\ k_\kappa\ \gamma_\kappa\right]^T \qquad (\kappa = 1, 2, 3). \tag{3.25}$$

The symmetric observability group $(G_C \subseteq G_M)$ is formed by the symmetrical operations that allow the leg 1 to superimpose with the κth leg $(\kappa = 1, 2, 3)$:

$$G_C = \{\lambda_1, \lambda_2, \lambda_3\} \qquad (G_C \subseteq G_M), \tag{3.26}$$

where G_M is the symmetric group of the mechanism kinematic structure (Eq. (3.22)).

3.1.4.3 Symmetrical kinematic identification

We implement the DC protocol for kinematic identification (see section 3.1.3.3). The mechanisms meets conditions (1) and (2) of section 3.1.3.3 that are required for symmetrical identification and that are as follows:

1. The mechanism is symmetrical as proven in section 3.1.4.1.
2. The kinematic parameters of the mechanism are specified to obtain a symmetrical observability, and the corresponding symmetric observability group is specified (Eq. (3.25) – Eq. (3.26), see section 3.1.4.2).

The execution of the DC identification protocol is summarized:

DC1. Symmetrical pose selection.

(a) Calculation of the identification matrix $(\mathbf{C}_1^{\mathbf{R}}(\varphi_1, \mathbf{R}, \mathbf{P}))$ by means of Eq. (3.15). The nominal set of parameters (φ_1) is given by the set of conditions (1)–(3) of section 3.1.4, the constraint kinematic function (F_1) is given by Eq. (3.21) with $\kappa = 1$, and the useful workspace $\{\mathbf{R}, \mathbf{P}\}$ is given by a set of 33 000 singularity-free poses of the end-effector.

(b) Selection of optimal identification poses by robot calibration algorithm [96]. The algorithm was executed 25 times using initial random sets of $8/33000$ poses and by performing the exchange - add - exchange pose strategy, resulting in the set $\{\mathbf{R}_1, \mathbf{P}_1\}$ $(\mathbf{C}_1^{\mathbf{R}})$ (see Fig. 3.6) that minimizes the variance of the kinematic parameters of leg 1. The algorithm performance is presented in Fig. 3.7.

(c) Symmetrical pose selection. The optimal sets of identification poses for the second and third legs are dictated by symmetrical operations performed on the set of poses $\{\mathbf{R}_1, \mathbf{P}_1\}$:

$$\begin{aligned} \mathbf{R}_\kappa &= \lambda_\kappa(\mathbf{R}_1) \qquad (\kappa = 2, 3), \\ \mathbf{P}_\kappa &= \mathbf{P}_1 \qquad (\kappa = 2, 3), \end{aligned} \tag{3.27}$$

where the symmetrical operations (λ_κ) are defined by Eq. (3.26). In Fig. 3.8 the symmetrical observability of the legs is verified by the calculation of the observability index (Eq. (3.14)) for the sets of optimal poses.

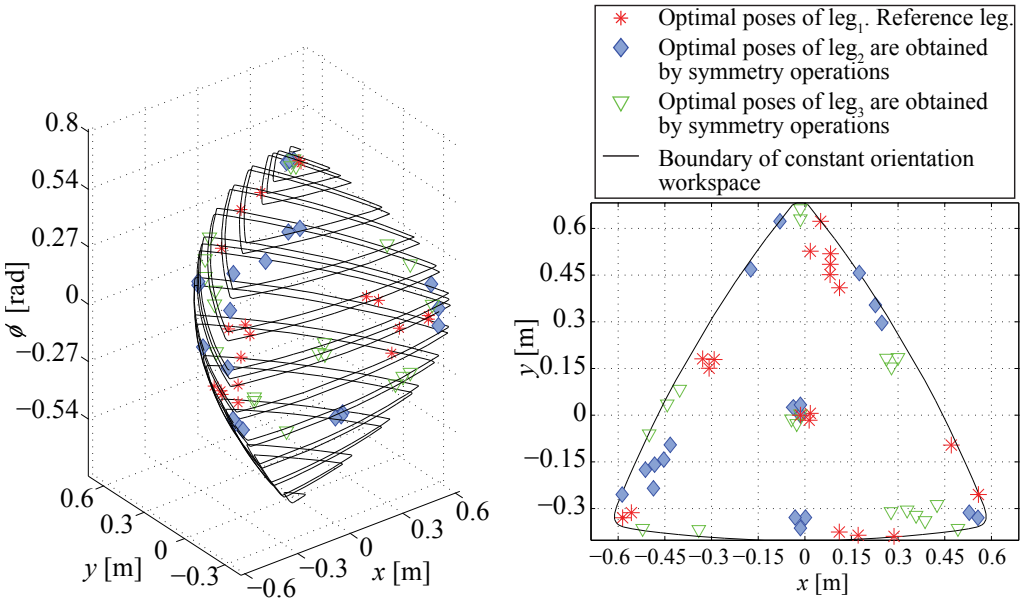

(a) End-effector workspace (b) Proyected end-effector workspace

Kinematic parameters:
$\overline{A_1A_2} = \overline{A_2A_3} = \overline{A_1A_3} = 6.00$ m,
$\overline{b_1b_2} = \overline{b_2b_3} = \overline{b_1b_3} = 1.50$ m,
$l = L = 1.50$ m,
$k_1 = k_2 = k_3 = 1.00$ m,
Dyads configuration = [-1 -1 -1]

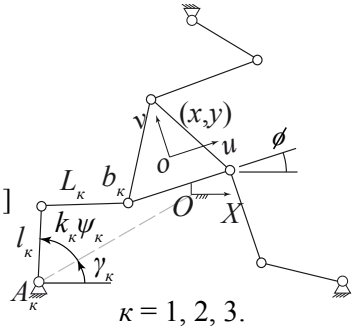

Figure 3.6: 3*RRR* symmetrical parallel mechanism. Optimal postures for kinematic identification

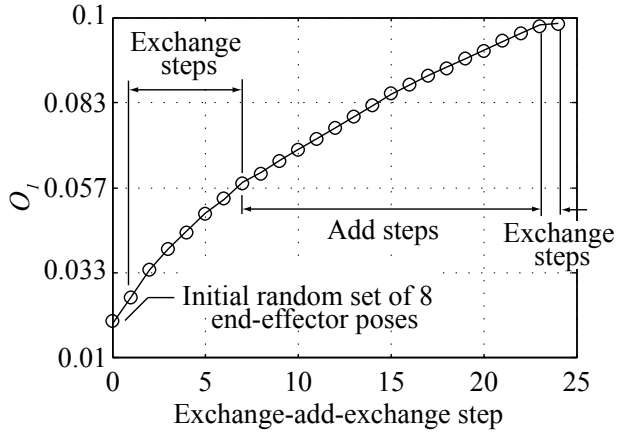

Figure 3.7: 3*RRR* symmetrical parallel mechanism. Active robot calibration algorithm performance

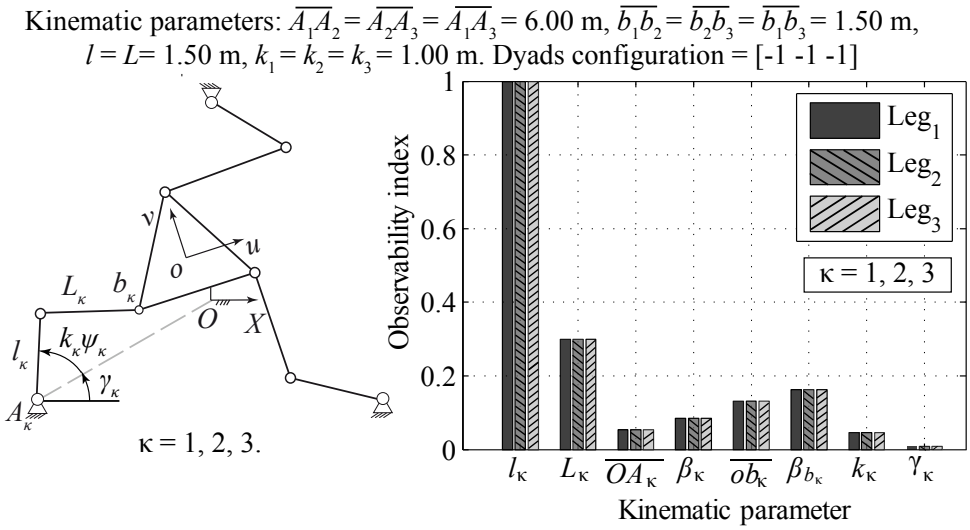

Figure 3.8: 3*RRR* symmetrical parallel mechanism. Observability of kinematic parameters corresponding to symmetrical optimal sets of identification poses

DC2. Estimation of kinematic parameters. A linearization of the inverse kinematics is used to solve the non-linear optimization problem of each leg (Eq. (3.9)). The linearization is defined in the following manner:

$$\Delta\mathbf{Q}_\kappa = \mathbf{C}_\kappa(\varphi_\kappa, \mathbf{R}_\kappa, \mathbf{P}_\kappa)\Delta\varphi_\kappa \qquad (\kappa = 1, 2, 3), \tag{3.28}$$

where $\Delta\mathbf{Q}_\kappa = \mathbf{Q}_\kappa(\varphi_\kappa, \hat{\mathbf{R}}_\kappa, \hat{\mathbf{P}}_\kappa) - \hat{\mathbf{Q}}_\kappa$ is the error in the active joint variables and $\Delta\varphi_\kappa$ is the error in the set of parameters to be estimated. All the unconstrained end-effector degrees of freedom (x, y, ϕ, Eq. (3.20)) are measured. The estimation is achieved by a least-squares solution of Eq. (3.28):

$$\Delta\varphi_\kappa = (\mathbf{C}_\kappa^T\mathbf{C}_\kappa)^{-1}\mathbf{C}_\kappa^T\Delta\mathbf{Q}_\kappa \qquad (\kappa = 1, 2, 3), \tag{3.29}$$

where the estimation is iterated until the corrections $\Delta\varphi_\kappa$ to φ_κ are small enough ($\Delta\varphi < 1 \cdot 10^{-8}[\mathrm{m} - \mathrm{rad}]$).

DC3. Update the kinematic model. The kinematic model is corrected with the set of estimated parameters ($\Delta\varphi_\kappa$):

$$\overline{\varphi}_\kappa = \varphi_\kappa + \Delta\varphi_\kappa \qquad (\kappa = 1, 2, 3), \tag{3.30}$$

where $\overline{\varphi}$ is the set of corrected parameters and φ is the nominal one.

The performance of the identification is evaluated after the kinematic calibration by calculating the Root Mean Square Error (RMSE) between the commanded end-effector position and orientation $\{\mathbf{R}, \mathbf{P}\}$ and their corresponding set of simulated measurements $\{\hat{\mathbf{R}}, \hat{\mathbf{P}}\}$. The set of measured poses corresponds to the set of 33 000 singularity-free poses used to design the identification experiments. An alternative traditional inverse kinematic calibration is performed by using 24 poses optimized for the identification of the complete set of parameters of the mechanism. The set of optimal poses is selected by means of the same active robot calibration algorithm as in the case of the DC identification. The results are registered in Fig. 3.9 for local end-effector position errors estimated on a constant orientation workspace ($\phi = 0.4$ rad) and Figures 3.10 – 3.11 for end-effector position and orientation RMSE estimated on the singularity-free workspace .

Concluding remarks of the DC kinematic identification protocol are presented in section 3.1.5.

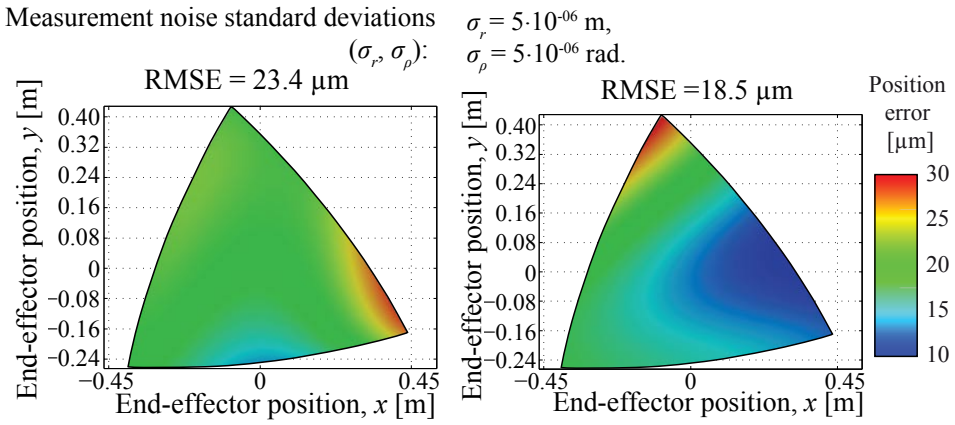

(a) Kinematic model updated with traditional identification

(b) Kinematic model updated with divide-and-conquer identification

Kinematic parameters:
$\overline{A_1A_2} = \overline{A_2A_3} = \overline{A_1A_3} = 6.00$ m,
$\overline{b_1b_2} = \overline{b_2b_3} = \overline{b_1b_3} = 1.50$ m,
$l = L = 1.50$ m,
$k_1 = k_2 = k_3 = 1.00$ m,
Dyads configuration = [-1 -1 -1]

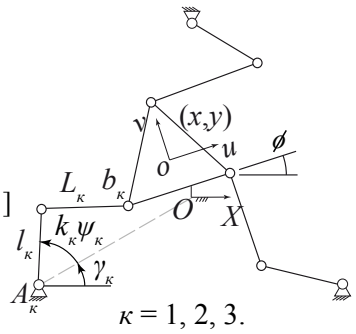

Figure 3.9: 3*RRR* calibrated symmetrical parallel mechanism. End-effector position error estimated for constant orientation $\phi = 0.4$ rad

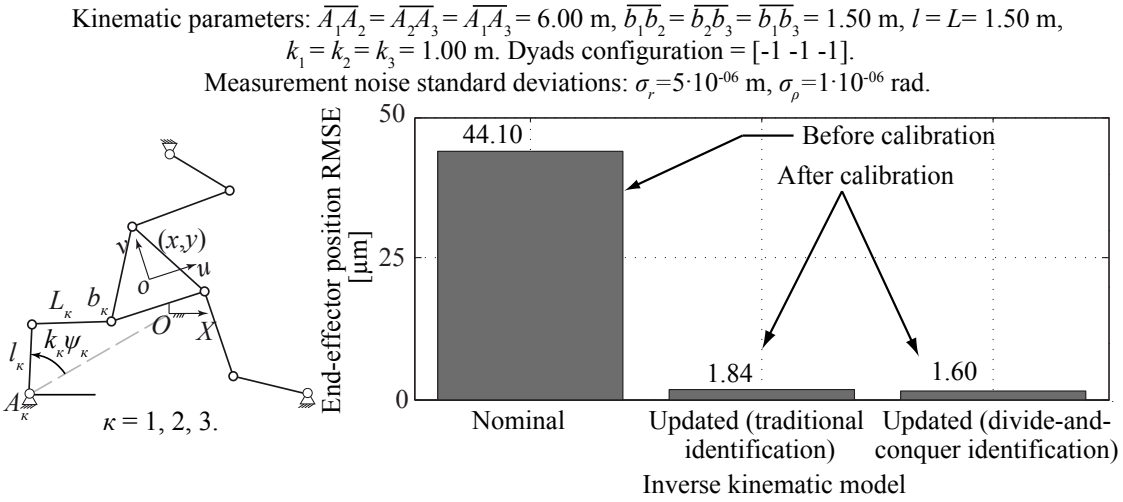

Figure 3.10: 3*RRR* symmetrical parallel mechanism. Estimated Root Mean Square Error of the end-effector position for a singularity-free workspace

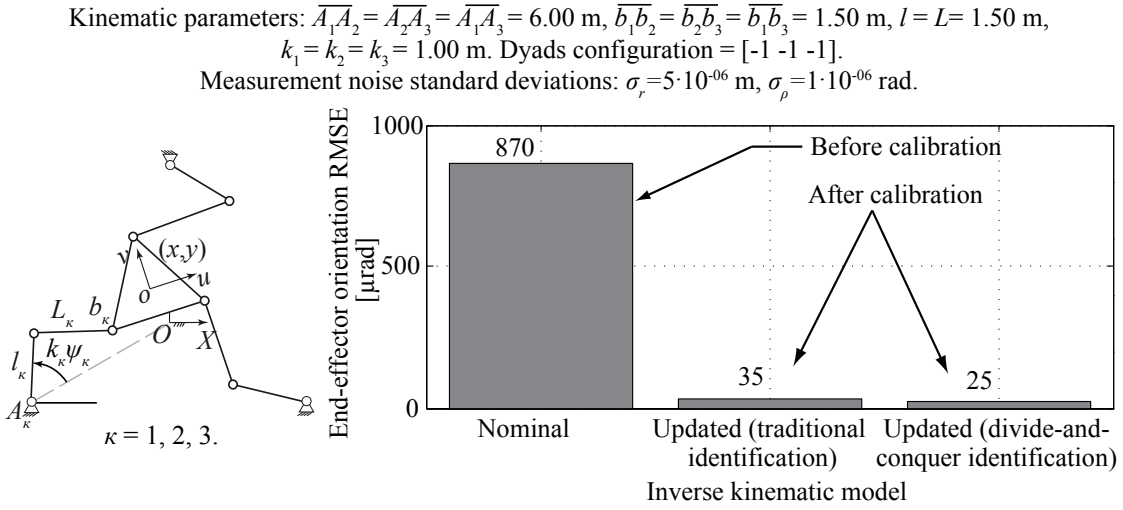

Figure 3.11: 3*RRR* symmetrical parallel mechanism. Estimated Root Mean Square Error of the end-effector orientation for a singularity-free workspace

3.1.5 Conclusions

This article presents a new DC protocol for the identification of symmetrical parallel mechanisms. The protocol exploits two characteristics of parallel mechanisms:

1. Independent solution of the inverse kinematics of each leg. It allows to propose a DC identification strategy (see section 3.1.3.1) used to optimize the identification planning of reduced sets of parameters (the sets of parameters corresponding to each leg).

2. Symmetrical kinematic structure. A set of necessary conditions to configure coordinate systems that allows to express symmetrically observable sets of leg parameters is presented in section 3.1.3.3. The symmetrical observability is the keystone to symmetrically designing the identification experiments.

The proposed kinematic identification protocol has the following advantages compared to traditional inverse calibration methods, such as [4, 7, 100]:

1. Cost reduction in the design of identification experiments by the use of observability symmetries. The pose selection is carried out only for a reference leg and for the $(n_{legs} - 1)$ remaining legs the identification poses are calculated by symmetry operations performed on the poses of the reference leg.

2. The improvement of the numerical efficiency of the protocol for the selection of optimal identification poses by the adoption of the active robot calibration algorithm [96].

If a linear least-squares estimation of the kinematic parameters (Eq. (3.29)) is used to solve the identification problem (Eq. (3.9)), then the computational cost of the matrix inversion $(\mathbf{C}^T\mathbf{C})^{-1}$ is reduced proportionally to the square of the number of legs of the mechanism (see Table 3.1).

	Traditional kinematic identification	Divide-and-conquer identification
Regressor	$(\mathbf{C}^T\mathbf{C})_{n_{legs}\cdot n_\varphi \times n_{legs}\cdot n_\varphi}$	$(\mathbf{C}_\kappa^T\mathbf{C}_\kappa)_{n_\varphi \times n_\varphi}$
Computational cost (matrix inversion)	$\propto {n_{legs}}^3 \cdot {n_\varphi}^3$	$\propto n_{legs} \cdot n_\varphi^3$
Measurement cost	$2N \cdot n_{legs}$	$N \cdot n_{legs}(n_{legs}+1)$

n_φ is the number of parameters to be identified corresponding to 1 leg.

Table 3.1: Computational and measurement cost of kinematic identification

As a result of 1 and 2, the kinematic identification performance is improved. The measurement cost of the DC protocol is incremented compared to traditional methods (see Table 3.1), which is required for the independent identification of the legs: different from traditional identification each leg requires its own set of end-effector measurements. For the DC protocol, the measurement cost is defined in the following manner: N measurements for each active-joint sensor added to N measurements for each end-effector coordinate for each leg. This leads to $N \cdot n_{legs}(n_{legs}+1)$ (see

Table 3.1) because the number of legs equals the number of end-effector degrees of freedom on symmetrical parallel mechanisms.

Real tests can be conducted to validate the DC protocol in a industrial context. Moreover, additional case studies will enable the protocol to be validated for other kinds of parallel symmetrical mechanisms.

3.2 Symmetrical Observability of Kinematic Parameters in Parallel Mechanisms

Sebastián Durango, David Restrepo, Oscar Ruiz
{sdurang1, drestr21, oruiz}@eafit.edu.co
CAD CAM CAE Laboratory
EAFIT University
Medellín, Colombia

John Restrepo-Giraldo, Sofiane Achiche
{jdrg, soac}@man.dtu.dk
Engineering Design and Product Development
Technical University of Denmark
Lyngby, Denmark

This article was submitted to the Journal of Control Engineering Practice (Elsevier), ISSN: 0967-0661. Note: this article is an extension of the published conference paper [10].

Abstract

This article presents an application of symmetric groups in symmetrical observability of kinematic parameters of parallel mechanisms. The devised concepts are used in the domain of Kinematic Identification. The investigation takes advantage of the mechanism structural symmetries and presents the following contributions: (*i*) a conjecture that allows mapping the symmetries of the mechanism into the active-joint workspace, (*ii*) the necessary conditions to express leg parameters in coordinate systems which allow symmetrical observability, and (*iii*) a procedure for exploiting symmetries in pose selection for KI that reduces the design-of-experiments cost to $(1/n_{legs})$ when compared to a KI procedure in which each leg poses are selected independently. An application of the symmetrical observability is presented through the simulated KI of a $3\underline{R}RR$ symmetrical parallel mechanism.

keywords: Symmetrical Observability, Parameter Identification, Kinematic Identification, Parallel Mechanism, Robot Manipulator.

Glossary

$\mathbf{C}$	Jacobian identification matrix
D_{2n}	Dihedral group of a n-vertices regular polygon
F	Constraint kinematic equation
G	Group
$L,\ l$	Length of a link
N	Number of identification poses
$\mathbf{Q}$	Column matrix of active-joints configurations
$\underline{\mathbf{Q}}$	Q matrix of a QR decomposition
$\mathbf{P}$	Column matrix of parametric representations of the end-effector orientation
$\mathbf{R}$	Column matrix of end-effector position vectors
$\underline{\mathbf{R}}$	R matrix of a QR decomposition
$\underline{R}RR$	Rotational - rotational - rotational kinematic structure
V	Polygon
g	Inverse kinematic equation
k	Gain of an active-joint sensor
n_{DOF}	Number of degrees of freedom
n_{legs}	Number of legs of a parallel mechanism
n_{φ}	Number of parameters to be identified
q	Active joint variable
$\mathbf{q}$	Vector of active joint variables
$\mathbf{r}$	Position vector
s	Singular value

Greek symbols

Σ	Symmetric group
α, β	Planar angles
γ	Offset of an active-joint sensor
φ	Set of kinematic parameters of a parallel mechanism
λ	Symmetric operation
θ	Active-joint angle
ρ	Parametric representation of the end-effector orientation, *e.g.* a set of Euler angles
σ	Standard deviation
ψ	Reading of an active-joint sensor

Subscripts

$_C$	Symmetrical observability
$_M$	Mechanism
$_Q$	Active joints
$_W$	Workspace
$_i$	Indexing variable
$_\kappa$	κth leg of a parallel mechanism

Superscripts

^{T}	Transpose
^{j}	jth pose of the mechanism

3.2.1 Introduction

Parallel mechanisms are instances of closed-loop mechanisms typically formed by a moving platform connected to a fixed base by several legs. Most parallel mechanisms are formed by a symmetrical structure. Symmetrical parallel mechanisms are defined in the following manner [94, 101]:

1. the number of legs equals the number of degrees of freedom of the mechanism,
2. each leg is controlled by one actuator,
3. each leg is formed by an identical kinematic chain, and
4. in at least one particular configuration the kinematic structure defines a symmetric group G_M.

Structural symmetries have been used for workspace and singularity analyses of symmetrical parallel mechanisms [94, 101–103]. In this article the use of structural symmetries is extended addressing the problem of expressing symmetrically observable sets of leg parameters. A set of necessary conditions to express leg parameters in coordinate systems which allow symmetrical observability is presented in section 3.2.5. A main condition is the workspace symmetry that was proved for symmetrical parallel mechanisms in [94, 101]. If a linear model with joint gain and offset is assumed for the active joints, then the active-joint workspace symmetry is required too.

The proof of an active-joint symmetrical workspace theorem is analogous to the forward kinematics problem of parallel mechanisms that in general has only numerical solution [7]. Therefore, a conjecture for the active-joint workspace symmetry is proposed in section 3.2.4.

A natural use of symmetrical observability would be a divide-and-conquer (DC) kinematic identification (KI) in which the identification experiments are planed for a reference leg only and extended to the remaining legs by symmetry operations. For KI the DC protocol by [10] was updated with a symmetrical pose selection procedure in section 3.2.5.1.

The layout for the rest of the article is as follows: Section 3.2.2 presents literature review on the application of symmetries in parallel mechanism analysis. Section 3.2.3 presents fundamentals of symmetric group theory. A theorem on the symmetrical workspace of symmetrical parallel mechanisms is extended on section 3.2.4, proposing a conjecture for symmetrical active-joint workspace. The symmetrical observability of sets of leg parameters is proposed in section 3.2.5, and its application in symmetrical pose selection for KI is presented in section 3.2.5.1. Results are presented in section 3.2.6 through a $3\underline{R}RR$ parallel mechanical manipulator case study in which an application of symmetrical observability of sets of leg parameters is used in a simulated KI. Concluding remarks are presented in section 3.2.7.

3.2.2 Literature Review

Structural symmetries are a common characteristic of most parallel mechanisms [94]. However, the analysis of the symmetry characteristics of parallel mechanisms is a poorly studied problems. The literature is restricted to workspace and singularity analyses.

Reference [101] presents a symmetry theorem on the workspace for symmetrical parallel mechanisms. The theorem reveals an analogous relationship between the workspace shape and the symmetry structure. This theorem is proposed to estimate geometry characteristics of the workspace and to guide the conceptual design of spatial parallel manipulators. The theorem is limited to mechanisms in which every identical kinematic chain (leg) remains always collinear. In [94], the symmetrical workspace theorem is strengthened to include a general category of symmetrical parallel mechanisms in which the permanent collinearity of the legs is not required. Reference [102] presents an application of the symmetrical workspace theorem that addresses the symmetrical calculation of singularities of symmetrical parallel mechanisms. A common characteristic of references [94, 102] is the use of symmetric group theory to prove the symmetry theorems. Different

from [94, 101, 102], reference [103] presents a methodology based on a parametric representation of the workspace orientation and singularity symmetrical analyses of spherical parallel mechanisms.

This article extends the use of structural symmetries in parallel mechanisms, addressing the problem of formulating symmetrically observable sets of leg parameters. Symmetrical observability has direct applications in kinematic identification by means of the symmetrical planning of independent identification experiments for each leg. The DC protocol in [10] was equipped with a symmetrical pose selection procedure. With respect to traditional identification methods the protocol has reported the following advantages:

1. The identification poses are optimized for the identification of reduced sets of parameters (the sets corresponding to each leg).
2. The independent identification of the set of parameters of each leg improves the numerical efficiency of the identification algorithms.
3. By (1) and (2) calibrating the kinematic model, with the identified set of parameters, results in a better end-effector accuracy with respect to calibrations by means of other traditional KI methods.

The DC protocol was improved, replacing the independent leg pose selection procedure by a symmetrical pose selection procedure in section 3.2.5.1. The DC protocol is improved with an additional feature:

4. The cost reduction in the design of identification experiments by the use of observability symmetries, *e.g.* the cost is reduced by $1/n_{legs}$ compared with a DC independent leg pose selection .

Section 3.2.3 presents an introduction to symmetry groups theory, required for the symmetrical analysis of end-effector workspace, active-joint workspace and observability of kinematic parameters.

3.2.3 Fundamentals of Symmetry Groups

A group is a set G equipped with an internal binary operation $\odot$ such that the operation is associative, has closure, and have both, a neutral and an inverse element in G [95].

Two instances of groups are used to describe symmetries of the structure, workspace and parameter observability of in parallel mechanisms: The symmetric group Σ, (section 3.2.3.1), and the dihedral group D_{2n}, (section 3.2.3.2).

3.2.3.1 Symmetric group Σ

Let V be a polygon in the plane. The symmetric group $\Sigma(V)$ consists of all the rigid motions λ for which $\lambda(V) = V$. That is, the symmetric group is formed by the operations that allow the polygon to superimpose itself [94].

3.2.3.2 Dihedral group D_{2n}

Let V_n denote a regular polygon with n vertices and center O. The vertices of V_n are denoted by v_i $(i = 1, 2, \ldots, n)$. The symmetric group $\Sigma(V_n)$ is called the dihedral group of V_n with $2n$ elements and denoted by D_{2n}. The elements of the dihedral group depend on the parity of the regular polygon. A complete description of the dihedral group can be found in [94].

As an example, consider the symmetries of the equilateral triangle shown in Fig. 3.12. These symmetries can be expressed by the dihedral group D_6 whose elements are permutations of the set of vertices $V = \{v_1, v_2, v_3\}$. In consequence, the symmetric group is defined by:

$$D_6 = \{\lambda_1, \lambda_2, \lambda_3, \lambda_4, \lambda_5, \lambda_6\}, \tag{3.31}$$

where $\lambda_1 = (1)$ denoting a 0-rotation about point O, $\lambda_2 = (123)$ denoting a $2\pi/3$-rotation about point O, $\lambda_3 = (132)$ denoting a $4\pi/3$-rotation about point O, $\lambda_4 = (23)$ denoting a reflection about the line Ov_1, $\lambda_5 = (13)$ denoting a reflection about the line Ov_2, and $\lambda_6 = (12)$ denoting a reflection about the line Ov_3 (see [102]).

Symmetric group theory is used by [94] to prove the symmetrical theorem of workspace for

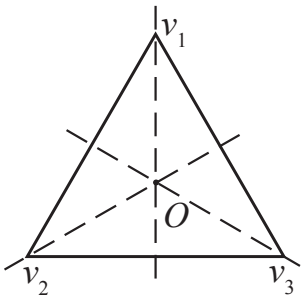

Figure 3.12: Reflection lines of an equilateral triangle [102]

symmetrical parallel mechanisms. The theorem is summarized in section 3.2.4.1.

3.2.4 Symmetrical Active-joint Workspace of Symmetrical Parallel Mechanisms

The workspace of a parallel mechanism is defined as the total volume swept out by the end-effector as the mechanism executes all its possible motions [106]. A symmetry theorem for the workspace of symmetrical parallel mechanisms was proposed by [94] as follows:

3.2.4.1 Theorem. Symmetrical workspace of symmetrical parallel mechanisms

If the symmetric group of the workspace of a mechanism is denoted by G_W and the symmetric group of the kinematic chain structure with the end-effector in a particular configuration is denoted by G_M, then G_M must be a subgroup of G_W. Namely, the following relation always holds:

$$G_M \subseteq G_W. \tag{3.32}$$

Thus, if the kinematic structure of a mechanism has an associated symmetric group G_M, then the end-effector workspace G_W remains unaltered under the symmetry operations λ that are the elements of G_M. Proof of the workspace symmetry theorem is provided in [94] using symmetry group theory.

Workspace symmetry is a necessary condition to declare symmetrically observable sets of leg parameters, section 3.2.5. If a linear model with gain and offset is assumed for the active joints, then a symmetrical active-joint workspace is required too, section 3.2.5.

In section 3.2.4.2 the workspace symmetries are extended to the active-joint workspace of symmetrical parallel mechanisms.

3.2.4.2 Conjecture. Symmetrical active-joint workspace of symmetrical parallel mechanisms

In practice, most parallel mechanisms have a symmetrical structure and a corresponding symmetrical end-effector workspace [94, 101]. However, a symmetrical workspace is not a sufficient condition to obtain a corresponding symmetrical active-joint workspace. Therefore, we propose a symmetrical conjecture for the active-joint workspace of symmetrical parallel mechanisms as follows:

> If a symmetrical parallel mechanism has a symmetrical end-effector workspace characterized by a symmetric group G_W, then it is possible to define a reference system for the active-joint variables that produces a symmetrical active-joint workspace characterized by symmetric group G_Q.

The conditions to configure a symmetrical parallel mechanism with symmetrical workspace are summarized below:

1. The number of legs is equal to the number of degrees of freedom of the mechanism.
2. All the legs have an identical structure. That is, each leg has the same number of active and passive joints and the joints are arranged in an identical pattern.
3. The constraint kinematic equation of each leg of the mechanism, F_κ, can be expressed in its implicit form:

$$F_\kappa = g_\kappa(\varphi_\kappa, \mathbf{r}, \rho) - q_\kappa = 0 \quad (\kappa = 1, 2, \cdots, n_{legs}), \tag{3.33}$$

where κ denotes the κth leg, g_κ is an inverse kinematic function, φ_κ is the set of kinematic parameters, $\mathbf{r}$ is the position vector of the end-effector, ρ is a parametric representation of

the platform orientation (*e.g.* a set of Euler angles), and q_κ is the active-joint variable. The set of constraint equations for the complete mechanism is defined in the following manner:

$$F(\mathbf{q}) = \begin{bmatrix} F_1(q_1) \\ F_2(q_2) \\ \vdots \\ F_{n_{legs}}(q_{n_{legs}}) \end{bmatrix} = \begin{bmatrix} g_1(\varphi_1, \mathbf{r}, \rho) - q_1 \\ g_2(\varphi_2, \mathbf{r}, \rho) - q_2 \\ \vdots \\ g_{n_{legs}}(\varphi_{n_{legs}}, \mathbf{r}, \rho) - q_{n_{legs}} \end{bmatrix}, \tag{3.34}$$

where $\mathbf{q} = [q_1 \; q_2 \; \cdots q_{n_{legs}}]^T$ is the vector of active joint variables.

4. The kinematic structure of the mechanism has an associated symmetric group G_M for a particular configuration of the end-effector.

In addition to the conditions on the symmetrical mechanism and its symmetrical workspace, the following condition to set a symmetrical active-joint workspace is assumed:

5. The active-joints reference system is defined such that in the particular configuration that defines the symmetry group of the mechanism structure G_M, the active-joint variables are symmetrical too. The symmetric group of the active-joint variables is denoted as G_Q.

If the active-joint workspace is symmetrical the following relation holds:

$$F(\lambda_i(\mathbf{q}) = \lambda_i(F(\mathbf{q})) \qquad (i = 1, 2, \cdots, n_{legs}), \tag{3.35}$$

where F is the set of constraint kinematic equations of the mechanisms, Eq. (3.34) and $\lambda_i \in G_Q$ is a symmetrical operation of the active-joint workspace symmetric group.

The proof of Eq. (3.35) is analogous to the forward kinematics problem of parallel mechanisms: it requires the solution of the constraint kinematic equations given the vector of joint variables. In general, it is not possible to express the forward kinematics of parallel mechanisms in an analytical form [7]. Therefore, proof of the symmetry conjecture on the active-joint workspace is not straightforward. An analytical proof of the conjecture is not provided here. However, in section 3.2.6 the conjecture is validated through a numerical analysis of the workspace and active-joint workspace of a three-degree-of-freedom parallel mechanism whit rotational joints only.

In section 3.2.5 the workspace and active joint symmetries are used in the definition of symmetrical sets of leg parameters with an application in kinematic identification of symmetrical parallel mechanisms.

3.2.5 Symmetrical Observability of Kinematic Parameters

If a parallel mechanism meets the conditions of the workspace symmetry theorem (see section 3.2.4.2 and references [94, 101]), then it is possible to define its set of kinematic parameters so as to obtain a symmetrical observability of its legs. In consequence, the planning of the kinematic identification (KI) experiments can be reduced according to the observability-symmetric group.

In order to formulate symmetrically observable sets of leg parameters the following conditions are assumed:

1. The symmetries of the mechanism structure are described by the symmetric group G_M.
2. The mechanism has a symmetrical workspace characterized by a symmetric group G_W. The workspace theorem for spatial parallel mechanisms is proposed in [94,101] and summarized in section 3.2.4.1.
3. A geometric method is adopted for the kinematic modeling of the mechanism. An independent vector-loop constraint kinematic equation is written for each leg in the form of Eq. (3.33). Consistent with this, the following hypotheses are assumed as valid:
   (a) each U-joint forming a leg is modeled as perfect,
   (b) each spherical joint forming a leg is modeled as perfect,
   (c) each prismatic joint is modeled as perfectly assembled with respect to its neighbor joints (U-joints, spherical joints, rotational joints, etc.),
   (d) the axis of each rotational joint is modeled as perfectly orientated,
   (e) if the mechanism is planar, then all the links are modeled as constrained in the mechanism plane.

   The hypotheses (3a) to (3e) are consequent with realistic operation conditions in which the influences of defects in the joints have a minor effect on pose accuracy compared with errors in the location of the joints [97].
4. The position of each base fixed point A_κ (U-joint, spherical joint, etc.) is defined by three parameters, Fig. 3.13:
   (a) the magnitude of the $\overline{OA_\kappa}$ segment ($\kappa = 1, 2, \ldots, n_{legs}$),

(b) the angle α_κ of the $\overline{OA_\kappa}$ segment with respect to the Z axis of the base reference system, $\kappa = 1, 2, \ldots, n_{legs}$,

(c) the angle β_κ of the projection of the segment $\overline{OA_\kappa}$ on plane XY with respect to the X axis of the base reference system ($\kappa = 1, 2, \ldots, n_{legs}$).

5. The position of each platform point b_κ (U-joint, spherical joint, etc.) is described by three parameters, defined analogously to the base fixed points, Fig. 3.13. The $ouvw$ reference system is analogous to the $OXYZ$. The three parameters are denoted as $\overline{ob_\kappa}$, α_{b_κ} and β_{b_κ} ($\kappa = 1, 2, \cdots, n_{legs}$).

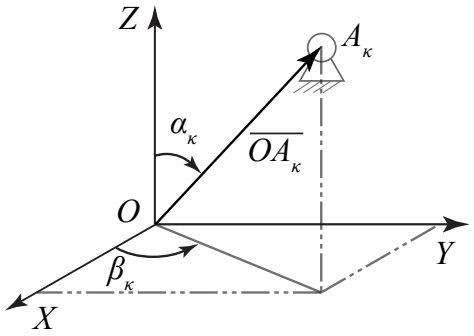

Figure 3.13: Position of fixed point A_κ

A linear model is used for the active joints of the mechanism (Eq. (3.36)). As a result, two additional parameters must be estimated for each leg: the joint gain k, and the joint offset γ. Therefore, additional symmetry conditions are required to allow a symmetrical observability:

6. Each active joint has the same nominal gain k_κ ($\kappa = 1, 2, \ldots, n_{legs}$).

7. The mechanism has configured a symmetrical active-joint workspace characterized by symmetric group G_Q. The conditions to set a symmetrical active-joint workspace are proposed in section 3.2.4, conditions (1) to (5).

The linear active-joint model is defined in the following manner:

$$\theta_\kappa = k_\kappa \psi_\kappa + \gamma_\kappa \qquad (\kappa = 1, 2, \cdots, n_{legs}), \tag{3.36}$$

where θ is the active joint angle, ψ is the sensor reading, k is the gain in the active-joint, and γ is the offset of the sensor.

Symmetrical observability implies that the observability of the ith kinematic parameter of the κth leg in the jth configuration must be the same as the observability of the corresponding parameter of a reference leg in its corresponding symmetrical pose. The symmetric group of observability, G_C, is defined by the symmetry operations that allow the superimposition of the reference leg with the κth leg. Therefore, symmetric group G_C can be derived from the symmetric group of the mechanism G_M: $G_C \subseteq G_M$, where

$$G_C = \left\{\lambda_1, \lambda_2, \ldots, \lambda_{n_{legs}}\right\}. \tag{3.37}$$

When λ_κ is operated onto a point of the end-effector workspace, the transformed point remains the same observability characteristics with respect to the κth leg that the original point has with respect to the reference leg. The observability Jacobian matrix of each leg κ is calculated independently to compute the observability. That is:

$$\begin{aligned} \mathbf{C}_\kappa^T &= \begin{bmatrix} (\mathbf{C}_\kappa^1)^T & (\mathbf{C}_\kappa^2)^T & \cdots & (\mathbf{C}_\kappa^N)^T \end{bmatrix} \quad (\kappa = 1, 2, \ldots, n_{legs}), \\ \mathbf{C}_\kappa^j(\varphi_\kappa, \mathbf{r}^j, \rho^j) &= \frac{\partial F_\kappa(\varphi_\kappa, \mathbf{r}^j, \rho^j)}{\partial \varphi_\kappa^T} \quad (j = 1, 2, \ldots, N), \end{aligned} \tag{3.38}$$

where the F_κ function is the κth constraint kinematic equation of the set of Eqs. (3.34), $\mathbf{r}$ is the end-effector position, and ρ is a parametric represention of the end-effector orientation (*e.g.* a set of Euler angles). Each row of the Jacobian matrix $\mathbf{C}_\kappa$ corresponds to an identification configuration of the mechanism. To evaluate the observability of the parameters, the QR decomposition of the observability Jacobian matrix (Eq.(3.38)) presented in [6] is adopted :

$$\underline{\mathbf{Q}}^T \mathbf{C}_\kappa = \begin{bmatrix} \underline{\mathbf{R}} \\ \mathbf{0} \end{bmatrix}, \tag{3.39}$$

where $\underline{\mathbf{Q}}$ is a $N \times N$ orthogonal matrix, $\underline{\mathbf{R}}$ is a $n_\varphi \times n_\varphi$ upper triangular matrix, $\mathbf{0}$ is a $(N - n_\varphi) \times n_\varphi$ zero matrix, and n_φ is the cardinality of φ_κ. The observability of the ith parameter is estimated by the value of its corresponding element on the diagonal of the $\underline{\mathbf{R}}$ matrix. Therefore, the symmetrical observability for a set of N end-effector poses $\{\mathbf{R}, \mathbf{P}\}$ is stated as:

$$\begin{aligned} |\underline{\mathbf{R}}_{ii}^\kappa\left(\mathbf{C}_\kappa(\varphi_\kappa, \mathbf{R}, \mathbf{P})\right)| = \left|\underline{\mathbf{R}}_{ii}^1\left(\mathbf{C}_1\left(\varphi_1, \lambda_\kappa(\mathbf{R}), \mathbf{P}\right)\right)\right| \\ (i = 1, 2, \ldots, n_\varphi) \quad (\kappa = 1, 2, \ldots, n_{legs}), \end{aligned} \tag{3.40}$$

where, without loss of generality, the first leg is assumed as the reference, $\mathbf{R}$ and $\mathbf{P}$ are column matrices of N position vectors and parametric representations of the orientation of the end-effector

respectively, and λ_κ is the κth symmetry operation of G_C that is applied individually over each end-effector position in $\mathbf{R}$. The parameters with magnitude close to zero are less observable, and the non-observable parameters are those for which $\underline{\mathbf{R}}_{ii} = 0$.

The natural use of the symmetrical observability is in KI. In section 3.2.5.1, a procedure is proposed to symmetrically design the KI poses of parallel mechanisms taking advantage of the symmetrical observability.

3.2.5.1 Symmetrical pose selection for kinematic identification

By the symmetrical planning of the KI of parallel mechanisms it is possible to reduce the optimal posture selection to $1/n_{legs}$ of the original search. The pose selection procedure is proposed in the following manner, Fig. 3.14:

PS1. Calculation of the observability Jacobian matrix. Given the nominal parameters of a reference leg, φ_1, the correspondent constraint kinematic function, F_1, and a representative set of postures of a workspace without singularities, $\{\mathbf{R}, \mathbf{P}\}$, to calculate the observability Jacobian matrix, $\mathbf{C}_1^{\mathbf{R}}$:

$$\mathbf{C}_1^{\mathbf{R}}(\varphi_1, \mathbf{R}, \mathbf{P}) = \frac{\partial F_1(\varphi_1, \mathbf{R}, \mathbf{P})}{\partial \varphi_1^T}. \tag{3.41}$$

here, the calculation of the Jacobian matrix can be performed analytically or numerically. For parallel mechanisms the constraint kinematic function F is usually available for the analytical (symbolic) calculation of the Jacobian matrix. A procedure for the numerical calculation of the Jacobian matrix is proposed in [104].

PS2. Given the observability Jacobian matrix calculated in step (PS1) to select an optimal set of postures $\{\mathbf{R}_1, \mathbf{P}_1\}$, for the KI of the reference leg. To select the poses, an active calibration algorithm developed by [96] is adopted. The optimized identification set of postures is then defined in the following manner:

$$\begin{gathered} \max_{\{\mathbf{R_1}, \mathbf{P_1}\}} O_1, \\ \text{subject to} : \mathbf{R}_1 \subset \mathbf{R}, \mathbf{P}_1 \subset \mathbf{P}, \end{gathered} \tag{3.42}$$

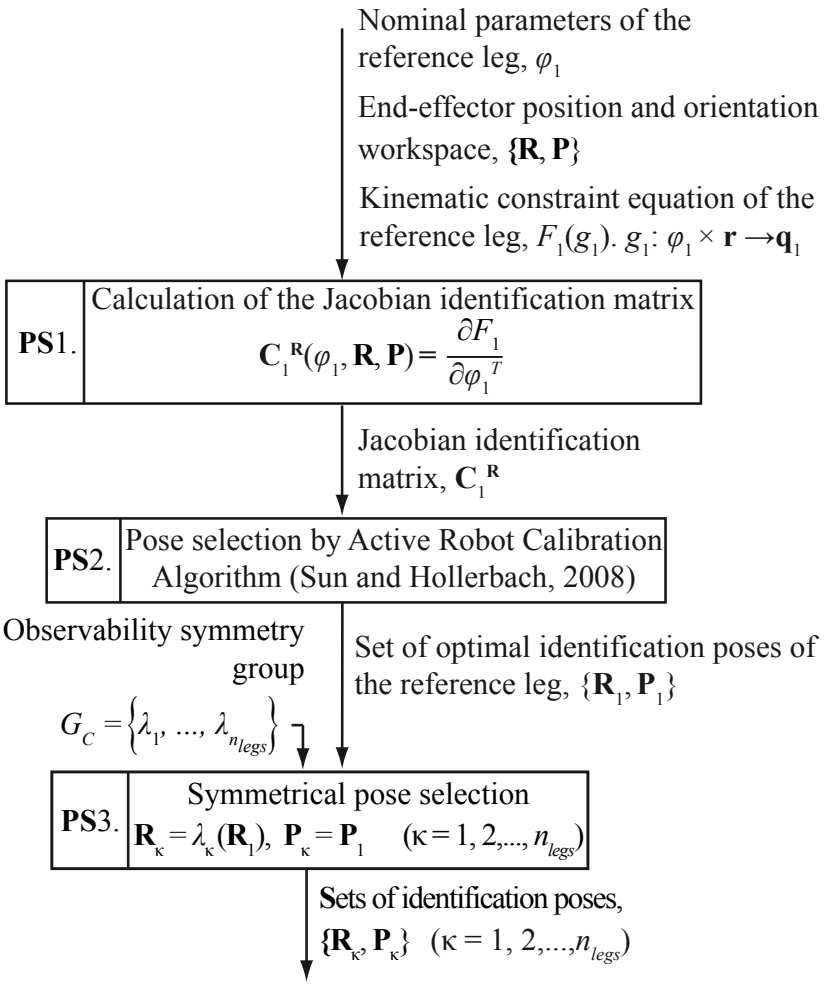

Figure 3.14: Symmetrical pose selection for kinematic identification

where O_1 is an observability index of the Jacobian matrix defined in the following manner,

$$O_1(\mathbf{C}_1(\varphi_1, \mathbf{R}_1, \mathbf{P}_1)) = \frac{(s_1\ s_2 \cdots s_{n_1})^{1/n_\varphi}}{n_\varphi}, \tag{3.43}$$

n_φ is the number of parameters to be estimated, and s_i $(i = 1, 2, \ldots n_\varphi)$ are the singular values of the Jacobian matrix. As rule of thumb, the number of identification poses should be two or three times larger than the number of parameters to be estimated [105].

PS3. Given the selected set of identification poses of the reference leg, $\{\mathbf{R1}, \mathbf{P1}\}$, calculated in step (PS2) and the observability symmetric group, G_C, to find the sets of identification poses

of the remaining $(n_{legs}-1)$ legs:

$$\begin{aligned} \mathbf{R}_\kappa &= \lambda_\kappa(\mathbf{R_1}) \qquad (\kappa = 2,\ldots,n_{legs}), \\ \mathbf{P}_\kappa &= \mathbf{P_1} \qquad (\kappa = 2,\ldots,n_{legs}). \end{aligned} \tag{3.44}$$

where the symmetry operation λ operates onto the end-effector workspace. Here the end-effector workspace is defined as the volume within which the end-effector point (i.e. the geometry center of the moving stage) can be reached [94]. The symmetry operation does not operate onto the orientation of the end-effector.

In section 3.2.5.2, the DC identification protocol by [10] is equipped with the symmetrical pose selection procedure.

3.2.5.2 Divide-and-conquer identification protocol

The protocol has three main steps that are summarized in the following manner, Fig. 3.15:

DC1. Symmetrical pose selection. Given the sets of nominal parameters, φ_κ, the inverse kinematic functions, g_κ, and a representative set of postures of a workspace without singularities, $\{\mathbf{R},\mathbf{P}\}$, to find the independent sets of identification postures, $\{\mathbf{R}_\kappa,\mathbf{P}_\kappa\}$ that maximizes the observability of φ_κ $(\kappa = 1,2,\ldots,n_{legs})$. Compared to [10], a pose selection that takes advantage of the observability symmetries is proposed: the identification poses are optimized for a reference leg and the remaining $n_{legs}-1$ sets are calculated by symmetry operations. The pose selection procedure is detailed in section 3.2.5.1.

DC2. Kinematic parameters identification. Given the optimized set, $\mathbf{R}_\kappa,\mathbf{P}_\kappa$, of identification poses obtained in (DC1), the correspondent sets of active-joint measurements, $\hat{\mathbf{Q}}_\kappa = \left[\hat{q}_\kappa^1 \ \cdots \ \hat{q}_\kappa^N\right]^T$, and end-effector measurements, $\{\hat{\mathbf{R}}_\kappa,\hat{\mathbf{P}}_\kappa\}$, to solve the optimization problem defined in Eq. (3.45) for the estimation of the sets of kinematic parameters φ_κ $(\kappa = 1,2,\ldots,n_{legs})$. The optimization problem is defined in the following manner:

$$\begin{aligned} &\min_{\varphi_\kappa} \sum_{j=1}^{N} \left(g_\kappa^j(\varphi_\kappa,\hat{\mathbf{r}}^j,\hat{\rho}^j) - \hat{q}_\kappa^j\right)^2 \quad (\kappa = 1,2,\ldots,n_{legs}), \\ &\qquad \text{subject to}: \mathbf{r}^j \in \mathbf{R}_\kappa, \rho^j \in \mathbf{P}_\kappa \quad (j = 1,2,\ldots,N), \end{aligned} \tag{3.45}$$

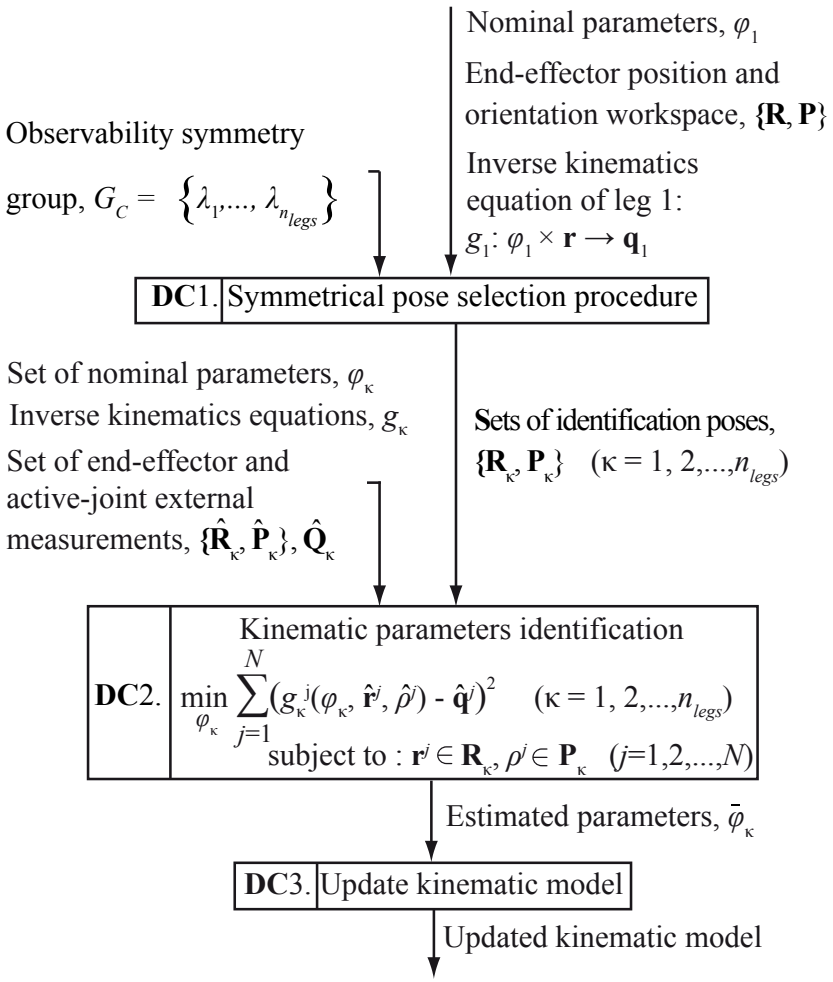

Figure 3.15: Divide-and-conquer kinematic identification of parallel mechanisms protocol with symmetrical pose selection

where $\{\mathbf{R}_\kappa \subset \mathbf{R}, \mathbf{P}_\kappa \subset \mathbf{P}\}$. $\{\mathbf{R}, \mathbf{P}\}$ is a workspace without singularities constraining the optimization problem.

DC3. Update of kinematic model. Given the identified sets of parameters obtained in (DC2) to update the kinematic model of the parallel mechanism.

Section 3.2.6 presents the study of workspace, active-joint workspace and observability symmetries applied in the KI of a $3\underline{R}RR$ symmetrical parallel mechanism.

3.2.6 Results

The application of symmetries in the kinematic identification of symmetrical parallel mechanisms is presented through a $3\underline{R}RR$ parallel robot manipulator case study. The mechanism has three degrees of freedom and is illustrated in Fig. 3.16. It consists of an equilateral moving platform, $b_1b_2b_3$, that is connected by three identical rotational - rotational - rotational ($\underline{R}RR$) kinematic chains (dyads), $A_\kappa C_\kappa b_\kappa$ ($\kappa = 1, 2, 3$), to an equilateral fixed base, $A_1A_2A_3$, Fig. 3.16. Each kinematic chain is actuated from an active-joint that is located on the fixed base. The following nominal-parameters set is assumed:

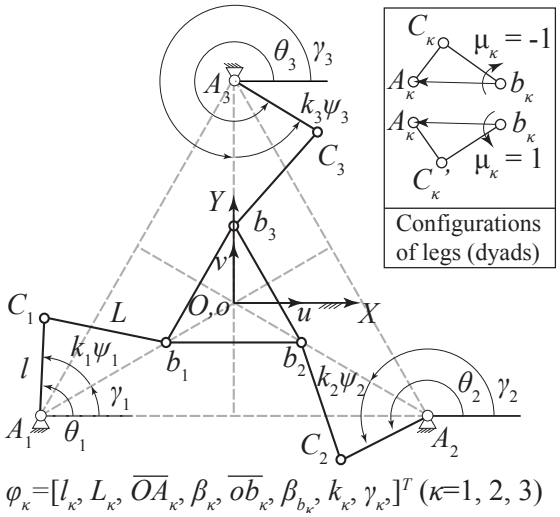

Figure 3.16: $3\underline{R}RR$ symmetrical parallel mechanism. Symmetrical configuration and kinematic parameters

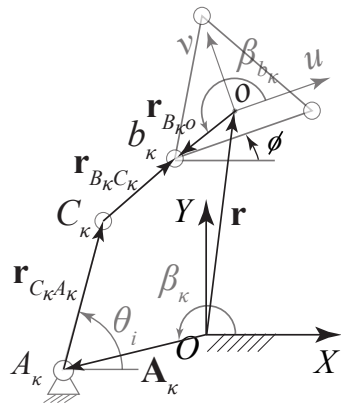

Figure 3.17: $3\underline{R}RR$ symmetrical parallel mechanism. Constraint loop

1. Dimensions of the links: $A_1A_2 = A_2A_3 = A_1A_3 = 6.00$ m, $b_1b_2 = b_2b_3 = b_1b_3 = 1.50$ m, $l = L = 1.50$ m.

2. Configuration of the legs (dyads): $[-1\ -1-1]$. Each leg is to be considered as a dyad that can be configured $+1$ or -1 according to the convention described in Fig. 3.16.

3. Nominal gain in the active-joint sensors: $k_1 = k_2 = k_3 = 1$.

For the kinematic modeling, symmetry analysis and kinematic identification (KI), the origin of the fixed coordinate frame is located at the geometric center of the fixed base $A_1A_2A_3$. The X-axis points along the direction of A_1A_2 and the Y-axis is perpendicular to A_1A_2, Fig. 3.16. A moving frame is attached to the geometric center of the platform. The u-axis of the platform frame points along the line b_1b_2, and the v-axis is perpendicular to b_1b_2, Fig. 3.16. The location of the moving platform is specified by the coordinates of the platform center and the orientation angle of the moving frame with respect to the fixed frame in the following manner:

$$\begin{aligned} \mathbf{r} &= [x\ \ y\ \ 0]^T, \\ \rho &= \phi. \end{aligned} \tag{3.46}$$

3.2.6.1 Workspace symmetry

The $3\underline{R}RR$ symmetrical parallel mechanism satisfies the workspace symmetry conditions (1) to (4), section 3.2.4:

1. The mechanism has three legs and three correspondent degrees-of-freedom.

2. Each leg of the mechanism has an identical $\underline{R}RR$ kinematic structure.

3. The constraint kinematic equation of each leg is expressed by a closed loop in the following manner, Fig. 3.17 :

$$\|\mathbf{r} - \mathbf{A}_\kappa\| - \|\mathbf{r}_{C_\kappa A_\kappa} + \mathbf{r}_{BC_\kappa} - \mathbf{r}_{B_\kappa o}\| = 0 \quad (\kappa = 1, 2, 3). \tag{3.47}$$

4. The mechanism structure symmetric group, G_M, is stated by inspection, Fig. 3.16. The symmetric group G_M is defined in the following manner:

$$G_M = \{\lambda_1, \lambda_2, \lambda_3, \lambda_4, \lambda_5, \lambda_6\}, \tag{3.48}$$

where the first three elements of G_M represent rotations about the Z-axis: 0 rad, $2\pi/3$ rad, and $4\pi/3$ rad, and the last three elements of G_M denote reflections about OA_1, OA_2, and OA_3 respectively.

The actuation of the symmetrical group G_M on the end-effector workspace will make the workspace superimpose itself. The symmetrical workspace theorem for this mechanism is proved in references [94, 101].

3.2.6.2 Active-joint workspace symmetry

For the $3\underline{R}RR$ symmetrical parallel mechanism a linear active joints model (Eq. (3.36)) with $n_{legs} = 3$ is considered. In consequence, to design a symmetrical KI it is also necessary to satisfy the condition (5) of active-joint workspace symmetry, section 3.2.4. Figure 3.16 presents the symmetrical configuration of the $3\underline{R}RR$ mechanism that determines the symmetry of the active-joint workspace, with the active-joint variables vector defined as $\mathbf{q} = [\psi_1\ \psi_2\ \psi_3]^T$. The mechanism is configured symmetrically positioning the active-joint measuring system in the following manner, Fig. 3.16:

$$\gamma_1 = \pi/6 \text{ rad},\ \gamma_2 = 5\pi/6 \text{ rad},\ \gamma_3 = -\pi/2 \text{ rad}. \tag{3.49}$$

A numerical calculation of the active-joint workspace is performed to validate the symmetrical conjecture, Fig. 3.18a. Additionally, three constant orientation workspaces are evaluated: $\phi = 0$ rad, $\phi = 0.4$ rad, $\phi = 0.6$ rad. The results are shown on Figs. 3.18b to 3.18d. The symmetric group of the active-joint workspace corresponds to rotations of 0 rad, $2\pi/3$ rad, and $4\pi/3$ rad around the axis $\psi_1 = \psi_2 = \psi_3$, Fig. 3.18a

3.2.6.3 Formulation of symmetrically observable sets of leg parameters

Nominally, the set of kinematic parameters is defined by the position of base fixed points, $\mathbf{A}_\kappa$, the position of platform points, $\mathbf{b}_\kappa$, the leg lengths, l_κ and L_κ, and the joint gain and offset, k_κ and ψ_κ ($\kappa = 1, 2, 3$). Consequently with the conditions (1)–(7) of symmetrical observability, section 3.2.5, this set of parameters are expressed to be symmetrically observable: The base and platform

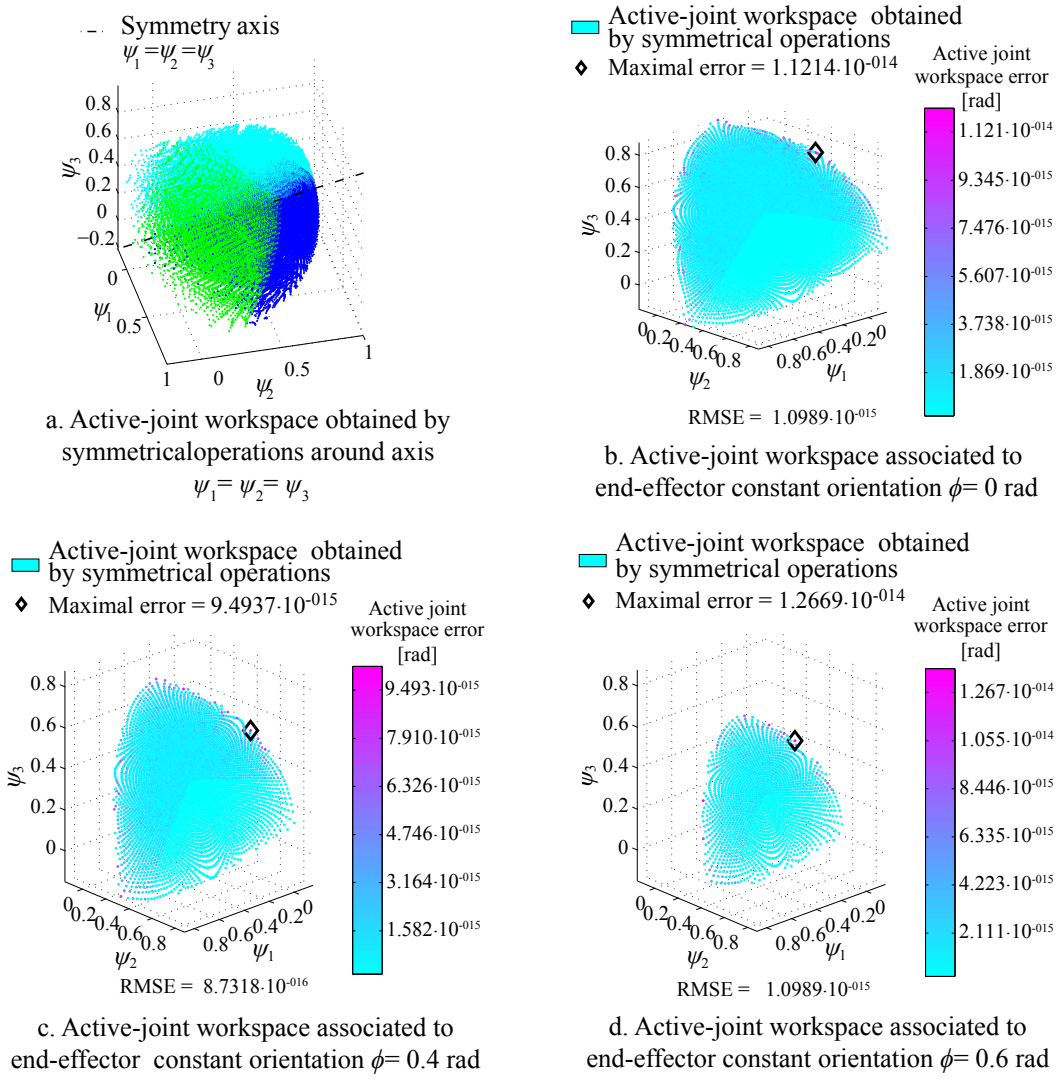

a. Active-joint workspace obtained by symmetricaloperations around axis $\psi_1 = \psi_2 = \psi_3$

b. Active-joint workspace associated to end-effector constant orientation $\phi = 0$ rad

c. Active-joint workspace associated to end-effector constant orientation $\phi = 0.4$ rad

d. Active-joint workspace associated to end-effector constant orientation $\phi = 0.6$ rad

Kinematic parameters: $\overline{A_1A_2} = \overline{A_2A_3} = \overline{A_1A_3} = 6.00$ m, $\overline{b_1b_2} = \overline{b_2b_3} = \overline{b_1b_3} = 1.50$ m
$l = L = 1.50$ m, $k_1 = k_2 = k_3 = 1.00$ m. Dyads configuration = [-1 -1 -1]

Figure 3.18: *3RRR* symmetrical parallel mechanism. Active-joint workspace obtained by symmetrical operations

points are modeled as constrained on the mechanism plane, the fixed base and platform points are defined by the magnitude of the $\overline{OA_\kappa}$ and $\overline{ob_\kappa}$ segments, and the angles β_κ and β_{b_κ} respectively, Fig. 3.17. A linear model is assumed for the active joints (Eq. (3.36)). Consequently, the set of parameters to be identified is defined in the following manner, Fig. 3.16:

$$\varphi_\kappa = \left[l_\kappa, L_\kappa, \overline{OA_\kappa}, \beta_\kappa, \overline{ob_\kappa}, \beta_{b_\kappa}, k_\kappa, \gamma_\kappa\right]^T \quad (\kappa = 1, 2, 3). \tag{3.50}$$

The observability-symmetric group, $G_C \subseteq G_M$, corresponds to the symmetry operations that allows the leg 1 to superimpose the κth leg ($\kappa = 1, 2, 3$):

$$G_C = \{\lambda_1, \lambda_2, \lambda_3\} \qquad (G_C \subseteq G_M), \tag{3.51}$$

where G_M is the symmetric group of the mechanism (Eq. (3.48)).

3.2.6.4 Symmetrical pose selection for kinematic identification

The mechanisms meets the required symmetry conditions:

1. The mechanism is symmetrical as is probed in sections 3.2.6.1 and 3.2.6.2.
2. The sets of leg parameters are declared in order to obtain a symmetrical observability and the corresponding observability-symmetric group is defined (Eqs. (3.50)– (3.51)), section 3.2.6.3.

Prior to perform the KI, the symmetrical pose selection procedure (section 3.2.5.1) is applied:

PS1. Calculation of the identification matrix, $\mathbf{C}_1^{\mathbf{R}}(\varphi_1, \mathbf{R}, \mathbf{P})$ (Eq. (3.41)). The nominal set of parameters, φ_1, is given by the set of conditions (1) – (3), section 3.2.6, the inverse kinematic function, g_1, is given by the Eq. (3.47) with $\kappa = 1$, and the useful workspace, $\{\mathbf{R}, \mathbf{P}\}$, is given by a set of 30 000 singularity-free poses of the mechanism.

PS2. Selection of optimal identification poses. A set of 24 optimal identification poses, $\{\mathbf{R}_1, \mathbf{P}_1\}(\mathbf{C}_1^{\mathbf{R}})$ is selected using a robot calibration algorithm by [96]. The optimized identification poses are registered in Fig. 3.19.

PS3. Symmetrical pose selection. The optimal sets of identification poses for the second and third legs are obtained by symmetry operations over the set $\{\mathbf{R}_1, \mathbf{P}_1\}$:

$$\begin{aligned} \mathbf{R}_\kappa &= \lambda_\kappa(\mathbf{R}_1) \qquad (\kappa = 2, 3), \\ \mathbf{P}_\kappa &= \mathbf{P}_1 \qquad (\kappa = 2, 3), \end{aligned} \tag{3.52}$$

where the symmetry operations, λ_κ are defined by the Eq. (3.51). In Fig. 3.20 the symmetrical observability of the legs is verified by the calculation of the observability index (Eq. (3.40)), for the sets of optimal poses.

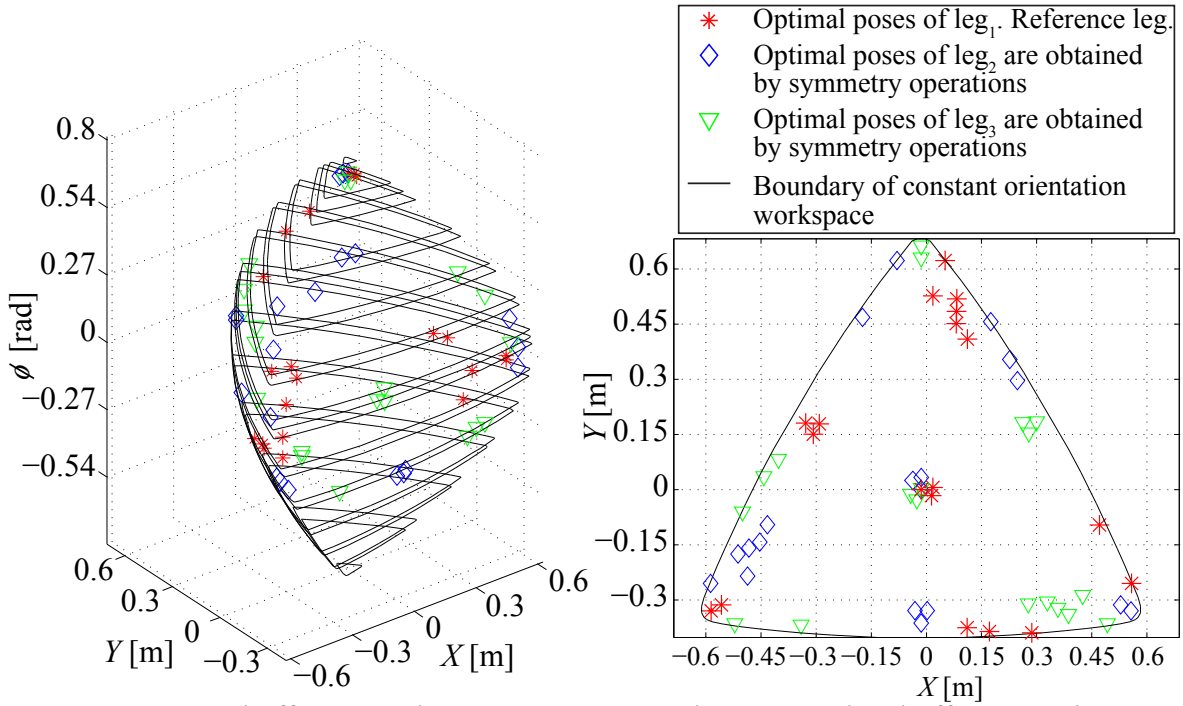

a. End-effector workspace. b. Proyected end-effector workspace.

Kinematic parameters: $\overline{A_1A_2} = \overline{A_2A_3} = \overline{A_1A_3} = 6.00$ m, $\overline{b_1b_2} = \overline{b_2b_3} = \overline{b_1b_3} = 1.50$ m
$l = L = 1.50$ m, $k_1 = k_2 = k_3 = 1.00$ m. Dyads configuration = [-1 -1 -1]

Figure 3.19: 3*RRR* symmetrical parallel mechanism. Selected poses for kinematic identification

Kinematic parameters: $\overline{A_1A_2} = \overline{A_2A_3} = \overline{A_1A_3} = 6.00$ m, $\overline{b_1b_2} = \overline{b_2b_3} = \overline{b_1b_3} = 1.50$ m
$l = L = 1.50$ m, $k_1 = k_2 = k_3 = 1.00$ m. Dyads configuration = [-1 -1 -1]

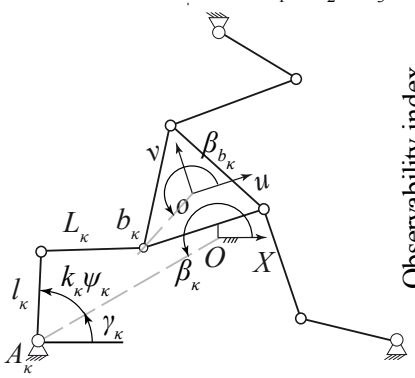

3*RRR* symmetrical parallel mechanism. κ = 1, 2, 3.

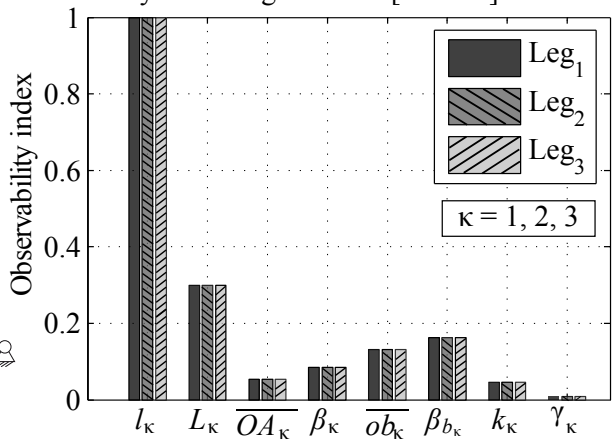

Figure 3.20: 3*RRR* symmetrical parallel mechanism. Observability of kinematic parameters

Once the identification poses are selected, the kinematic identification is carried out.

3.2.6.5 Kinematic identification

The KI is simulated to evaluate the performance of the improved DC identification protocol. The nominal kinematic parameters of the mechanism are disturbed by adding random errors with normal distribution and standard deviation σ in order to simulate the kinematic errors to be identified. The end-effector measurements, $\hat{\mathbf{R}}_\kappa$, are simulated from its corresponding active-joint measurements, $\hat{\mathbf{Q}}_\kappa$, through a forward kinematics model added with normally distributed random disturbances. For the simulations the standard deviations of the measurements were defined in the following manner:

$$\begin{aligned} \sigma_r &= 1.00 \cdot 10^{-4}\ \mathrm{m}, \\ \sigma_\rho &= 1.00 \cdot 10^{-4}\ \mathrm{rad}, \end{aligned} \tag{3.53}$$

where σ_r and σ_ρ are the standard deviations in length and orientation measurements respectively. The identification procedure is as summarized:

DC1. Symmetrical pose selection. The symmetrical pose selection is detailed in section 3.2.6.4.

DC2. Kinematic parameters identification. A linearization of the inverse kinematics is used for solve the non-linear optimization problem of each leg (Eq. (3.45)). The linearization is defined in the following manner:

$$\Delta\mathbf{Q}_\kappa = \mathbf{C}_\kappa(\varphi_\kappa, \mathbf{R}_\kappa, \mathbf{P}_\kappa)\Delta\varphi_\kappa \qquad (\kappa = 1, 2, 3), \tag{3.54}$$

where $\Delta\mathbf{Q}_\kappa = \mathbf{Q}_\kappa(\varphi_\kappa, \hat{\mathbf{R}}_\kappa, \hat{\mathbf{P}}_\kappa) - \hat{\mathbf{Q}}_\kappa$ is the error in the active joint variables and $\Delta\varphi_\kappa$ is the set of parameters to be estimated. The estimation is achieved using a iterative linear least-squares solution of Eq. (3.54):

$$\Delta\varphi_\kappa = (\mathbf{C}_\kappa^T\mathbf{C}_\kappa)^{-1}\mathbf{C}_\kappa^T\Delta\mathbf{Q}_\kappa \qquad (\kappa = 1, 2, 3). \tag{3.55}$$

DC3. Update the kinematic model with the set of estimated parameters $\overline{\varphi} = \{\overline{\varphi}_1, \overline{\varphi}_2, \overline{\varphi}_3\}$ where

$$\overline{\varphi}_\kappa = \varphi_\kappa + \Delta\varphi_\kappa \qquad (\kappa = 1, 2, 3). \tag{3.56}$$

The performance of the identification is evaluated after the kinematic calibration by means the calculation of the root mean square (RMSE) of the difference between the commanded end-effector pose, $\{\mathbf{R}, \mathbf{P}\}$, and a correspondent set of simulated measurements, $\{\hat{\mathbf{R}}, \hat{\mathbf{P}}\}$. The set of measured

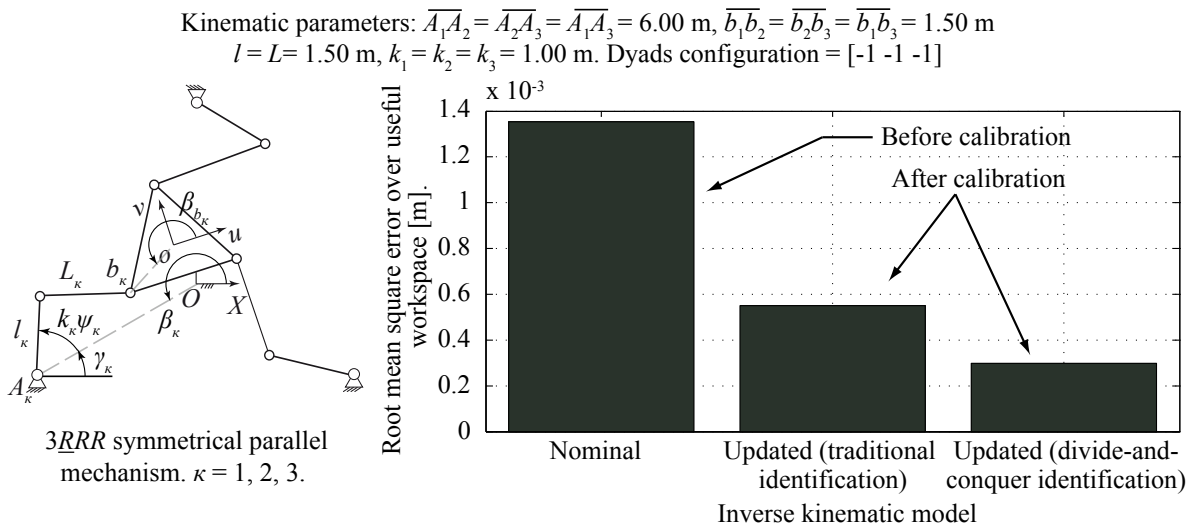

Figure 3.21: 3*RRR* symmetrical parallel mechanism. Estimated end-effector pose root-mean-square error for a singularity-free workspace

poses corresponds to the set of 30 000 poses used to design the identification experiments. An alternative traditional inverse kinematic calibration is performed using 24 poses optimized for the identification of the complete set of parameters of the mechanism. The set of optimal poses is selected using the same active robot calibration algorithm, as in the case of the DC identification. The results are registered in Fig. 3.21 for RMSE of the end-effector pose estimated for the workspace without singularities before and after calibration, and Fig. 3.22 for local end-effector position errors calculated for constant orientation workspaces ($\phi = 0.0$ rad, $\phi = 0.4$ rad, $\phi = 0.6$ rad).

Concluding remarks of the use of observability symmetries in kinematic identification of parallel mechanisms are presented in section 3.2.7.

3.2.7 Conclusions

This article addresses the problem of declaring sets of leg parameters with symmetrical observability for parallel symmetrical mechanisms. The necessary conditions for symmetrical observability are proposed in section 3.2.5 and summarized in the following manner:

1. The mechanism has a symmetric structure and symmetrical workspace characterized by the symmetric groups G_M and G_W respectively, conditions (1) – (2), section 3.2.5.

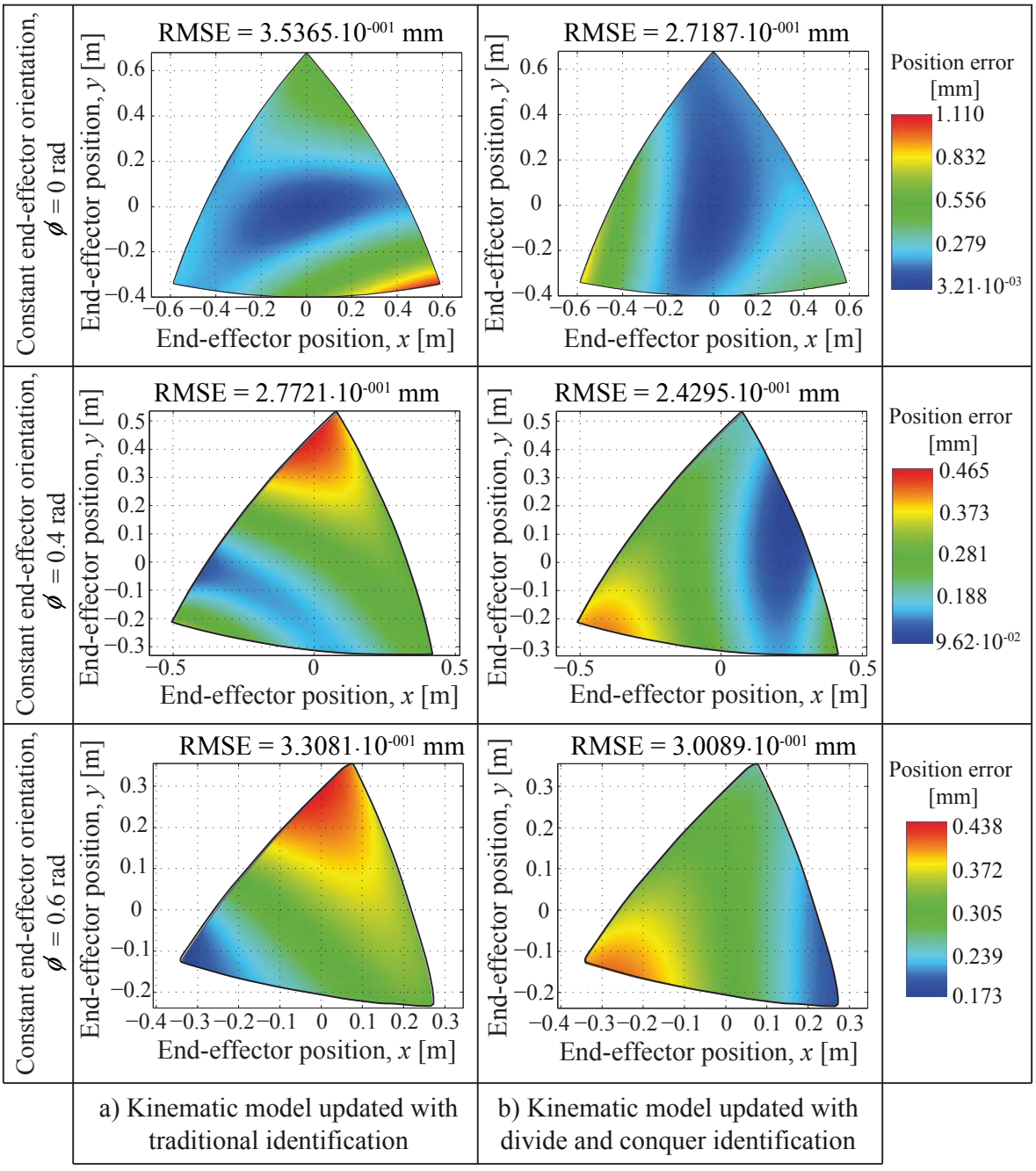

Kinematic parameters: $\overline{A_1A_2} = \overline{A_2A_3} = \overline{A_1A_3} = 6.00$ m, $\overline{b_1b_2} = \overline{b_2b_3} = \overline{b_1b_3} = 1.50$ m
$l = L = 1.50$ m, $k_1 = k_2 = k_3 = 1.00$ m. Dyads configuration = [-1 -1 -1]

Figure 3.22: 3*RRR* symmetrical parallel mechanism. Estimated end-effector position error on constant orientation workspaces

2. The kinematic joints are modeled as perfectly assembled and in the case of planar mechanisms the links are assumed to be constrained in the mechanism plane, condition (3), section 3.2.5.

3. The base and platform joint parameters of each leg are defined in order to obtain a symmetrical observability with respect to the workspace, conditions (4) – (5), section 3.2.5.

4. If a linear model (Eq. (3.36)), is assumed for the active joints, then additional conditions are required: each active-joint has the same nominal gain and the mechanism has configured a symmetrical active-joint workspace G_Q, conditions (6) – (7), section 3.2.5.

To prove the active-joint workspace symmetry results in a problem analogous to the forward kinematics of parallel mechanisms: it requires the solution of the constraint kinematic equations given the vector of input joint variables (Eq. (3.35)). In general, it is not possible to formulate an analytical solution of the forward kinematics of parallel mechanisms [7]. Consequently, the mapping of the structure symmetry to the active-joint workspace symmetry of parallel symmetrical mechanisms is established as a conjecture, section 3.2.4.1.

A natural use for the symmetrical observability would be divide-and-conquer (DC) kinematic identification in which the experiments are designed for a reference leg only and extended to the remaining legs by symmetrical operations. The DC protocol by [10] is equipped with a new symmetrical pose selection procedure based on the formulation of symmetrically observable sets of leg parameters. Compared with [10], the symmetrical pose selection allows for reduction of design of the experiment cost to $1/n_{legs}$. The procedure is developed in section 3.2.5.1 and summarized in the following manner:

PS1. Calculation of an observability Jacobian matrix of a singularity-free workspace.

PS2. Selection of set a of optimal identification poses of a reference leg. The pose selection is calculated using an active robot calibration algorithm by [96] over the observability Jacobian matrix.

PS3. Determination of the optimal poses for the remaining $n_{legs} - 1$ by the symmetrical observability operations over the reference set.

The updated DC kinematic identification protocol is presented in section 3.2.5.2. Compared to traditional identification methods the improved protocol has the following advantages:

1. The cost reduction in the design of identification experiments, by the use of observability symmetries

2. The improvement of the numerical efficiency of the procedure for the selection of optimal identification poses, by the adoption an active robot calibration algorithm by [96].

3. The reduction of kinematic identification computational cost, by the identification of reduced sets of parameters (the sets correspondent with each leg).

As a consequence of (1) – (3), the kinematic identification results are improved.

Chapter 4

General Conclusion

This investigation has undertaken the problem of the accurate kinematic modeling of compliant and parallel mechanisms. The impact of such accurate modeling is significant in both academic and industrial contexts, in which precise motion is mandatory (e.g. micro mechanisms, medical instruments and high precision machine tools).

Position and force analyses in compliant mechanisms are not independent, resulting in a *force–displacement model* concept rather than a kinematic model. This dissertation has tackled the problem of force–displacement modeling of compliant mechanisms and two main contributions have been presented:

1. A force-displacement model of flexure-based compliant mechanisms where the kinematic and force analyses are solved through the decomposition of a rigid-equivalent mechanism into Assur groups (chapter 1, article 1.1) is proposed. The model is based on a structural decomposition routine (see section 1.1.4.1) and a convention for the equivalent joints location is presented (see section 1.1.4.2). This allows an extended analysis capability in which the force-displacement model of a wide variety of mechanisms can be assessed depending on the amount of Assur groups available in a kinematic and force analysis solution library. The large deflection analysis is solved using a non-linear Euler-Bernoulli beam model that uses the kinematics and force analyses of the Assur groups as inputs, and updates the elastic (deflected) configuration of the mechanism with an iterative strategy (see algorithm 1, page 14). The model was implemented in the workspace analysis of a 3-DOF flexure-based compliant mechanism (section 1.1.5), and compared with FEA obtaining a good match (see figures 1.13 and 1.14).

2. A force-displacement model of compliant mechanisms based on Design of Computer Experiments (see chapter 2). The model is aimed at obtaining an Input / Output transfer function useful for developing real-time control. Although Design of Computer Experiments is not intended to replace real-experiment-based Design of Experiments, it can be implemented to

forecast / ignore possible interactions, and to fine-tune ranges; therefore reducing costs of experimentation and model / product development. Unlike the contribution in 1, "Design of Computer Experiments" can be applied to a wide variety of compliant mechanisms, e.g. mechanisms with distributed flexibility, spatial movement, and complex geometry. A scaled mechanism does not have the scaled transfer function of the original mechanism, due to the non-linear relationship between the stiffness of the mechanism and its dimensions.

In the case study (the HexFlex 6 DOFs mechanism, section 2.1.5) a linear model was obtained, adding to the applicability of the model. The resulting objective function is a polynomial fitting around the operation point, guarantying the non-singularity of the model even though the obtained model was not linear.

During the design of the kinematic and force models for the Assur groups implemented in the force-displacement model of compliant mechanisms (see contribution 1), the following contribution was developed:

3. A solution for the kinetostatics of Assur groups dealing with the non-linear behavior of the friction force acting on the kinematic pairs (chapter 1, article 1.2). The proposed methodology is as versatile as a MBS program (generally used in commercial software, e.g. Working Model ®and Symmechanics ®). However, our frictional force estimation stands for a more accurate result, since in MBS the frictional force estimation typically corresponds to the one calculated on the first iteration of our contribution. The analysis method is restricted to cases in which the mechanism is near to self-locking, in such configurations the influence of frictional forces is important and an approximated estimation leads to big calculation errors.

Chapter 3 presents a new Divide and Conquer protocol for the kinematic identification of parallel mechanisms with the following contributions when contrasted with traditional identification methods:

4. A cost reduction in the design of identification experiments by the use of observability symmetries. The pose selection is carried out only for a reference leg, and symmetry operations are performed in order to calculate the identification poses of the remaining $(n_{legs} - 1)$ legs.

5. The improvement of the numerical efficiency of the protocol for the selection of optimal identification poses, by the adoption of the active robot calibration algorithm [96].

4.1 Recommendations for Future Research

Future work can be conducted in the field of accurate kinematic models concerning compliant and parallel mechanisms by researching the following topics:

1. A more general force-displacement model based on Assur groups disaggregation in which compliant mechanisms with distributed compliance can be analyzed. This could be accomplished by the implementation of an incremental solution of large deflection analysis.

2. An extension of the force-displacement model of compliant mechanisms in which inertial effects are accounted for.

3. The implementation of graph theory into the analysis and synthesis of compliant mechanisms. Graph theory has been traditionally applied to the rigid-body mechanisms science. Therefore, it could be extended to the compliant mechanisms field.

4. The implementation of the Divide and Conquer identification protocol in the case of spherical and spatial parallel mechanisms. Although the Divide and Conquer protocol was tested in the identification of a complex planar parallel mechanism, the spherical and spatial cases could provide new challenges and conclusions.

5. The use of symmetric groups theory for the dynamic parameters identification of parallel mechanisms.

6. The development of modules for the analysis of high-class Assur groups (third-class and over), and the inclusion of more refined models (e.g. a Dahl friction model) for the frictional forces acting on the kinematic pairs.

The main difficulties that arose during the research are summarized as follows:

1. Evaluation of the forward kinematics of parallel mechanisms. It is not generally possible to express the forward kinematics of parallel mechanisms in an analytical way [7]. This kinematical problem has multiple solutions, i.e. a parallel mechanism can be assembled in several ways given the actuated joint coordinates. We used numerical methods in which allowable information of a former pose was used to properly select the forward kinematics solution.

2. Identification of active-joint parameters. Active-joint parameters have the lowest observability among all parameters e.g. k and γ in Fig. 2. A solution to this problem was developed carrying out a two 'step' identification. A set without active joint parameters was identified and used to update the kinematic model on the first step, and the active-joint parameters were identified using a set of poses designed to improve their observability on the second step (see figure 4.1). The two step identification was not not implemented on the Divide and Conquer protocol, because even though an improvement of the observability of the active-joint parameters was achieved, the global performance of the kinematic calibration (the end-effector accuracy) did not reflect an improvement.

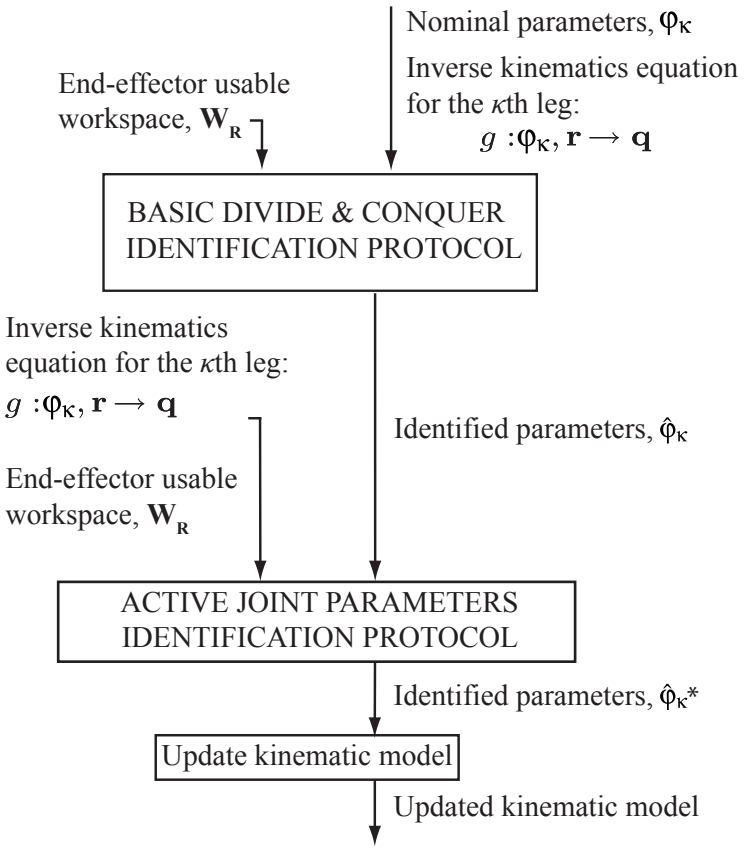

Figure 4.1: Two step identification protocol

References

[1] L.L. Howell and A. Midha. A loop-closure theory for the analysis and synthesis of compliant mechanisms. *Journal of Mechanical Design*, 118:121, 1996.

[2] S. Durango, G. Calle, and O. Ruiz. Analytical method for the kinetostatic analysis of the second–class RRR Assur group allowing for friction in the kinematic pairs. *Journal of the Brazilian Society of Mechanical Sciences and Engineering*, 32(3):200–207, 2010.

[3] H. Chanal, E. Duc, P. Ray, and J.Y. Hascoët. A new approach for the geometrical calibration of parallel kinematics machines tools based on the machining of a dedicated part. *International Journal of Machine Tools and Manufacture*, 47(7-8):1151–1163, 2007.

[4] H. Zhuang, J. Yan, and O. Masory. Calibration of Stewart Platforms and Other Parallel Manipulators by Minimizing Inverse Kinematic Residuals. *Journal of Robotic Systems*, 15(7), 1998.

[5] G. Pritschow, C. Eppler, and T. Garber. Influence of the dynamic stiffness on the accuracy of pkm. In *Third Chemnitz Parallel Kinematic Seminar*, 2002.

[6] S. Besnard and W. Khalil. Identifiable Parameters for Parallel Robots Kinematic Calibration. In *IEEE International Conference on Robotics and Automation*, volume 3, 2001.

[7] P. Renaud, A. Vivas, N. Andreff, P. Poignet, P. Martinet, F. Pierrot, and O. Company. Kinematic and Dynamic Identification of Parallel Mechanisms. *Control Engineering Practice*, 14(9):1099–1109, 2006.

[8] D. Restrepo, D. Acosta, S. Durango, and O. Ruiz. Design of computer experiments applied to modeling compliant mechanisms. In *Tools and Methods of Competitive Engineering*, volume 2, pages 775–788, 2010.

[9] S. Venanzi, P. Giesen, and V. Parenti-Castelli. Erratum to "A novel technique for position analysis of planar compliant mechanisms" [Mech. Machine Theory 40 (2005)1224-1239]. *Mechanism and Machine Theory*, 45(5):811 – 811, 2010.

[10] S. Durango, D. Restrepo, O. Ruiz, J. Restrepo-Giraldo, and S. Achiche. Kinematic identification of parallel mechanisms by a divide and conquer strategy. In *International Conference on Informatics in Control, Automation and Robotics*, volume 2, pages 167–173, 2010.

[11] S. Venanzi, P. Giesen, and V. Parenti-Castelli. A novel technique for position analysis of planar compliant mechanisms. *Mechanism and Machine Theory*, 40:1224–1239, 2005.

[12] L.L. Howell. *Compliant mechanisms*. Wiley-Interscience, 2001.

[13] N. Lobontiu. *Compliant mechanisms: design of flexure hinges*. CRC, 2003.

[14] Y. Tian, B. Shirinzadeh, and D. Zhang. A flexure-based five-bar mechanism for micro/nano manipulation. *Sensors and Acuators A: Physical*, 153:96–104, 2009.

[15] Y. Tian, B. Shirinzadeh, and D. Zhang. Design and dynamics of a 3-DOF flexure-based parallel mechanism for micro/nano manipulation. *Microelectronic Engineering*, 87:230–241, 2010.

[16] Y.K. Yong and T.F. Lu. Kinetostatic modeling of 3-RRR compliant micro-motion stages with flexure hinges. *Mechanism and Machine Theory*, 44(6):1156–1175, 2009.

[17] Y. Li and Q. Xu. Modeling and performance evaluation of a flexure-based XY parallel micro manipulatior. *Mechanism and Machine Theory*, 44:2127–2152, 2009.

[18] A. Saxena and S.N. Kramer. A simple and accurate method for determining large deflections in compliant mechanisms subjected to end forces and moments. *Journal of Mechanical Design*, 120:392, 1998.

[19] C. Kimball and L.W. Tsai. Modeling of flexural beams subjected to arbitrary end loads. *Journal of Mechanical Design*, 124:223, 2002.

[20] N.T. Pavlovic and N.D. Pavlovic. Compliant mechanism design for realizing of axial link translation. *Mechanism and Machine Theory*, 44(5):1082 – 1091, 2009.

[21] N.T. Pavlović and N.D. Pavlović. Mobility of the compliant joints and compliant mechanisms. *Theoretical and Applied Mechanics*, 32(4):341–357, 2005.

[22] M. Callegari, A. Cammarata, A. Gabrielli, M. Ruggiu, and R. Sinatra. Analysis and Design of a Spherical Micromechanism With Flexure Hinges. *Journal of Mechanical Design*, 131:051003, 2009.

[23] J. Buśkiewicz. A method of optimization of solving a kinematic problem with the use of structural analysis algorithm (sam). *Mechanism and Machine Theory*, 41:823–837, 2006.

[24] M.R. Hansen. A general method for analysis of planar mechanisms using a modular approach. *Mechanism and Machine Theory*, 31:1155–1166, 1996.

[25] Q. Zhang, H.J. Zou, and W.Z. Guo. Position analysis of higher-class assur groups by virtual variable searching and its application in a multifunction domestic sewing machine. *The International Journal of Advanced Manufacturing Technology*, 28(5):602–609, 2006.

[26] G.G. Baranov. *Curso de la Teoría de Mecanismos y máquinas. 2 ed.* MIR, Moscú, 1979. 524 p.

[27] I.I. Artobolevski. *Theory of mechanisms and machines*. Nauka, Moscu, 1988. 640 p. (In Russian).

[28] L.V. Assur. Investigation of plane hinged mechanisms with lower pairs from the point of view of their structure and classification (in russian): Part i, ii. *Bull. Petrograd Polytech. Inst.*, 23, 1916.

[29] P. E. Nikravesh. *Computer aided analysis of mechanical systems*. Prentice Hall, New Jersey, 1988.

[30] W. Schiehlen. Multibody system dynamics: Roots and perspectives. *Multibody System Dynamics*, 1:149 – 188, 1997.

[31] P. Eberhard and W. Schiehlen. Hierarchical modeling in multibody dynamics. *Archive of Applied Mechanics*, 68:237 – 246, 1998.

[32] R. Kubler and W. Schiehlen. Modular simulation in multibody system dynamics. *Multibody System Dynamics*, 4:107 – 127, 2000.

[33] E. Pennestri, P.P. Valenti, and L. Vita. Multibody dynamics simulation of planar linkages with dahl friction. *Multibody System Dynamics*, 17:321 – 347, 2007.

[34] E.D. Stoenescu and D.B. Marghitu. Dynamic analysis of a planar rigid-link mechanism with rotating slider joint and clearance. *Journal of Sound and Vibration*, 266(2):394 – 404, 2003.

[35] E.D. Stoenescu and D.B. Marghitu. Effect of prismatic joint inertia on dynamics of kinematic chains. *Mechanism and Machine Theory*, 39(4):431 – 443, 2004.

[36] P. Larochelle and J.M. McCarthy. Static analysis of spherical nr chains with joint friction. In *Flexible Mechanisms, Dynamics and Analysis*, volume DE-47, pages 173–177. ASME, September 1992.

[37] M. Cavic, M. Kostic, and M. Zlokolica. Position analysis of the high class kinematic group mechanisms. In *12 IFToMM World Congress*, Besaçon, FR, 2007. IFToMM.

[38] K. D. Bouzakis S. Mitsi and G. Mansour. Position analysis in polynomial form of planar mechanism with an assur group of class 4 including one prismatic joint. *Mechanism and Machine Theory*, 39:237–245, 2004.

[39] G. Mansour S. Mitsi, K. D. Bouzakis and I. Popescu. Position analysis in polynomial form of planar mechanisms with assur groups of class 3 including revolute and prismatic joints. *Mechanism and Machine Theory*, 38:1325–1344, 2003.

[40] S. Mitsi. Position analysis in polynomial form of planar mechanisms with a closed chain of the assur group of class 4. *Mechanism and Machine Theory*, 34:1195–1209, 1999.

[41] G. Calle, H.F. Quintero, and A. Díaz. Análisis cinemático de mecanismos planos a partir del análisis estructural según assur. In *V Congreso Iberoamericano de Ingeniería Mecánica, CIBIM V*, Mérida, VEN, 2001.

[42] C. Liang L. Han, Q. Liao. Closed-form displacement analysis for a nine-link barranov truss or a eight-link assur group. *Mechanism and Machine Theory*, 35:379–390, 2000.

[43] S. Durango. Dynamics of second-class planar mechanisms by means of a computer aided modular approach. In Hrishi Vera, editor, *23rd International Conference on CAD/CAM Robotics and Factories of the Future, CARS and FOF 07*, volume 1, pages 421–428, Bogota, August 2007. ISPE.

[44] D.B. Marghitu and M.J. Crocker. *Analytical elements of mechanisms*. Cambridge University Press, Cambridge, 2001.

[45] S. Molian. Software for mechanism design. In *Proceedings of Mechanisms Conference*, volume 2, Granfield, 1984.

[46] V. Bràt and P. Lederer. Kidyan: Computer-aided kinematic and dynamic analysis of planar mechanisms. *Mechanism and Machine Theory*, 8:457–467, 1973.

[47] H. Wang, Z-Q. Lin, and X-M. Lai. Composite modeling method in dynamics of planar mechanical system. *Science in China Series E: Technological Sciences*, 51(45):576 – 590, 2008.

[48] G. Calle, H.F. Quintero, and A. Díaz. Propuesta de enseñanza de la cinemática de mecanismos planos con la ayuda de programas cad paramétricos. In *Innovación docente, CREA'02 (2002*, La Habana, CUBA, 2002.

[49] C. Gosselin and J. Angeles. Singularity analysis of closed-loop kinematic chains. *IEEE Transactions on Robotics and Automation*, 6(3):281–290, 1990.

[50] Z. Luo, L. Tong, M.Y. Wang, and S. Wang. Shape and topology optimization of compliant mechanisms using a parameterization level set method. *Journal of Computational Physics*, 227(1):680–705, 2007.

[51] B.D. Jensen and L.L. Howell. The modeling of cross-axis flexural pivots. *Mechanism and Machine Theory*, 37(5):461–476, 2002.

[52] Z. Liu and J.G. Korvink. Using artificial reaction force to design compliant mechanism with multiple equality displacement constrains. *Finite Element in Analysis and Design*, 45:555–568, 2009.

[53] K-J. Lu and S. Kota. Parameterization strategy for optimization of shape morphing compliant mechanisms using load path representation. In *Proceedings of DETC03*. ASME, 2003.

[54] G-W. Jang, K.J. Kim, and Y.Y. Kim. Integrated topology and shape optimization software for compliant mems mechanism design. *Advances In Engineering Software*, 39:1–14, 2008.

[55] P. Bernardoni, P. Bidaud, C. Bidard, and F. Gosselin. A new compliant mechanism design methodology based on flexible building blocks. *Smart Material and Structures, USA*, 5383:244–254, 2004.

[56] G.K. Ananthasureh and S. Kota. Designing compliant mechanisms. *Mechanical Engineering*, 117(11):93–96, 1995.

[57] M.H.F. Dado. Limit position synthesis and analysis of compliant 4-bar mechanisms with specified energy levels using variable parametric pseudo-rigid-body model. *Mechanism and Machine Theory*, 40:977–992, 2005.

[58] T.W. Simpson, J.D. Peplinski, P.N. Koch, and J.K. Allen. Metamodels for computer-based engineering desing: survey and recommendations. *Engineering with Computers*, 17:129–150, 2001.

[59] S.B. Crary. Design of computer experiments for metamodel generation. *Analog Integrated Circuits and Signal Processing*, 32:7–16, 2002.

[60] M.L. Culpepper, G. Anderson, and P. Petri. Hexflex: A planar mechanism for six-axis manipulation and aligment. In *ASPE Annual Meeting*. ASPE, 2002.

[61] M.L. Culpepper. Multiple degree of freedom compliant mechanism. United States Patent, Number: US007270319B, September 2007.

[62] T.E. Bruns and D.A. Tortorelli. Topology optimization of non-linear elastic structures and compliant mechanisms. *Computer Methods in Applied Mechanics and Engineering*, 190(26-27):3443–3459, 2001.

[63] A. Saxena. A material-mask overlay strategy for continuum topology optimization of compliant mechanisms using honeycomb discretization. *Journal of Mechanical Design*, 130(06):2304–1–9, 2008.

[64] M.P. Bendsøe and O. Sigmund. Material interpolation schemes in topology optimization. *Archive of Applied Mechanics (Ingenieur Archiv)*, 69(9):635–654, 1999.

[65] M.P. Bendøse and O. Sigmund. *Topology Optimization: Theory, Methods and Applications*. ISBN: 3-540-42992-1. Springer, 2003, 2003.

[66] C.B.W. Pedersen, N.A. Fleck, and G.K. Ananthasuresh. Design of a Compliant Mechanism to Modify an Actuator Characteristic to Deliver a Constant Output Force. *Journal of Mechanical Design*, 128:1101, 2006.

[67] I. Her and J.C. Chang. A linear scheme for the displacement analysis of micropositioning stages with flexure hinges. *Journal of Mechanical Design*, 116:770, 1994.

[68] B.P. Trease, Y.M. Moon, and S. Kota. Design of large-displacement compliant joints. *Journal of Mechanical Design*, 127:788, 2005.

[69] C.M. Dibiaso. Comparison of molecular simulation and pseudo-rigid-body model predictions for a carbon nanotube based compliant parallel-guiding mechanism. *Journal of Mechanical Design*, 130(04):2302–1–8, 2008.

[70] W.K. Kim, D.G. Kim, and B.J. Yi. Analysis of a planar 3 degree-of-freedom adjustable compliance mechanism. *Journal of Mechanical Science and Technology*, 10(3):286–295, 1996.

[71] P.G. Opdahl, B.D. Jensen, and L.L. Howell. An investigation into compliant bistable mechanisms. In *Proc. 1998 ASME Design Engineering Technical Conf*, 1998.

[72] S.L. Chang, J.J. Lee, and H.C. Yen. Kinematic and compliance analysis for tendon-driven robotic mechanisms with flexible tendons. *Mechanism and Machine Theory*, 40(6):728–739, 2005.

[73] N. Lobontiu, J.S.N. Paine, E. Garcia, and M. Goldfarb. Design of symmetric conic-section flexure hinges based on closed-form compliance equations. *Mechanism and Machine Theory*, 37(5):477–498, 2002.

[74] R.W. Brockett and A. Stokes. On the synthesis of compliant mechanisms. In *1991 IEEE International Conference on Robotics and Automation, 1991. Proceedings.*, pages 2168–2173, 1991.

[75] N. Lobontiu, J.S.N. Paine, E. Garcia, and M. Goldfarb. Corner-filleted flexure hinges. *Journal of Mechanical Design*, 123:346, 2001.

[76] S.R. Park and S.H. Yang. A mathematical approach for analyzing ultra precision positioning system with compliant mechanism. *Journal of Materials Processing Technology*, 164:1584–1589, 2005.

[77] A. Banerjee, B. Bhattacharya, and A.K. Mallik. Forward and inverse analyses of smart compliant mechanisms for path generation. *Mechanism and Machine Theory*, 44(2):369–381, 2009.

[78] C. Boyle, L.L. Howell, S.P. Magleby, and M.S. Evans. Dynamic modeling of compliant constant-force compression mechanisms. *Mechanism and Machine Theory*, 38(12):1469–1487, 2003.

[79] B. Zettl, W. Szyszkowski, and W.J. Zhang. Accurate low dof modeling of a planar compliant mechanism with flexure hinges: the equivalent beam methodology. *Precision Engineering*, 29(2):237 – 245, 2005.

[80] F. De Bona and M.G. Munteanu. Optimized Flexural Hinges for Compliant Micromechanisms. *Analog Integrated Circuits and Signal Processing*, 44(2):163–174, 2005.

[81] A. Saxena and G.K. Ananthasuresh. Topology synthesis of compliant mechanisms for nonlinear force-deflection and curved path specifications. *Journal of Mechanical Design*, 123:33, 2001.

[82] S. Zhang and E.D. Fasse. A finite-element-based method to determine the spatial stiffness properties of a notch hinge. *Journal of Mechanical Design*, 123:141, 2001.

[83] H. Zhou and K.L. Ting. Geometric Optimization of Spatial Compliant Mechanisms Using Three-Dimensional Wide Curves. *Journal of Mechanical Design*, 131:051002, 2009.

[84] K.T. Fang and R. Li. Uniform design for computer experiments and its optimal properties. *International Journal of Materials and Product Technology*, 25:2058–2080, 2006.

[85] M.L. Culpepper and G. Anderson. Desing of a low-cost nano-manipulator wich utilizes a monolithic, spatial compliant mechanism. *Precision Engineering*, 28:469–482, 2004.

[86] R.P. Paul. *Robot manipulators: mathematics, programming, and control*. MIT Press Cambridge, MA, USA, 1982.

[87] G.E.P. Box, W.G. Hunter, and J.S. Hunter. *Use of Data Sampling, Surrogate Models, and Numerical Optimization in Engineering Design*. Jhon Wiley and Sons, New York, 1978.

[88] NIST. Engineering statistics handbook.nist/sematech e-handbook of statistical methods, November 2008.

[89] R.V. Lenth. Quick and easy analysis of unreplicated factorials. *Technometrics*, 31(4):469–473, 1989.

[90] K.T. Fang, D.K.J Lin, P. Winker, and Y. Zhang. Uniform design: theory and application. *Technometrics*, 42(3):237–248, 2000.

[91] T.W. Simpson, J.D. Peplinski, P.N. Koch, and J.K.Allen. On the use of statistics in design and the implications for deterministic computer experiments. In *1997 ASME Design Engineering Technical Conferences*, 1997.

[92] D.M. Bates and S. DebRoy. Linear mixed models and penalized least squares. *Journal of Multivariate Analysis*, 91(1):1–17, 2004.

[93] D. Ruppert and M.P. Wand. Multivariate locally weighted least squares regression. *The annals of statistics*, pages 1346–1370, 1994.

[94] J-S. Zhao, F. Chu, and Z-J. Feng. Symmetrical characteristics of the workspace for spatial parallel mechanisms with symmetric structure. *Mechanism and Machine Theory*, 43(4):427 – 444, 2008.

[95] O. Ruiz and C. Cadavid. *Geometrics Functions in Computer Aided Geometric Design*. Fondo Editorial Universidad EAFIT, first edition, 2008.

[96] Y. Sun and J.M. Hollerbach. Active robot calibration algorithm. In *IEEE International Conference on Robotics and Automation*, pages 1276–1281, May 2008.

[97] D. Daney. Kinematic calibration of the gough platform. *Robotica*, 21(06):677–690, 2003.

[98] O. Masory, J. Wang, and H. Zhuang. Kinematic modeling and calibration of a Stewart platform. *Advanced Robotics*, 11(5):519–539, 1997.

[99] D. Daney and I.Z. Emiris. Robust parallel robot calibration with partial information. In *IEEE International Conference on Robotics and Automation*, volume 4, pages 3262–3267, 2001.

[100] C.C. Iuraşcu and F.C.P. Park. Geometric algorithms for kinematic calibration of robots containing closed loops. *Journal of Mechanical Design*, 125:23, 2003.

[101] J-S. Zhao, M. Chen, K. Zhou, J-X. Dong, and Z-J. Feng. Workspace of parallel manipulators with symmetric identical kinematic chains. *Mechanism and Machine Theory*, 41(6):632 – 645, 2006.

[102] J.-S. Zhao, F. Chu, and Z.-J. Feng. Singularities within the workspace of spatial parallel mechanisms with symmetric structures. *Proceedings of the Institution of Mechanical Engineers, Part C: Journal of Mechanical Engineering Science*, 224(2):459–472, 2010.

[103] I.A. Bonev and C.M. Gosselin. Analytical determination of the workspace of symmetrical spherical parallel mechanisms. *IEEE Transactions on Robotics*, 22(5):1011 –1017, oct. 2006.

[104] H. Zhuang and Z. Roth. *Camera-Aided Robot Calibration*. CRC press, Boca Raton, 1996.

[105] J.H. Jang, S.H. Kim, and Y.K. Kwak. Calibration of geometric and non-geometric errors of an industrial robot. *Robotica*, 19(03):311–321, 2001.

[106] B. Siciliano and O. Khatib, editors. *Springer Handbook of Robotics*. Springer, Berlin, 2008.

Vita

Doctoral Student M.Sc. Eng. Sebastián Durango

Sebastián Durango (Manizales, Colombia, 1977) obtained the Diploma in Mechanical Engineering (2000) at Universidad Autónoma, Manizales, Colombia, and a M.Sc. degree with emphasis in Automatic Systems of Production (2006) at Universidad Tecnológica, Pereira, Colombia. Since 2002 Sebastián is a staff-docent with the Mechanical Engineering Department at Universidad Autónoma de Manizales, Colombia. In 2007 Sebastián joined the CAD CAM CAE Laboratory as doctoral student under the supervision of Prof. Oscar Ruiz. Sebastián was a Research Intern at the Technical University of Denmark in 2009. His academic interests are Mechanism and Machine Science and Robotics.

Prof. Dr. Eng. Oscar E. Ruiz, Doctoral Supervisor

Associate Professor Oscar Ruiz (Tunja, Colombia 1961) obtained B.Sc. degrees in Mechanical Engineering (1983) and Computer Science (1987) at Los Andes University, Bogot, Colombia, a M.Sc. degree with emphasis in CAM (1991) and a Ph.D. with emphasis in CAD (1995) from University of Illinois at Urbana–Champaign, USA. Prof. Ruiz has been Visiting Researcher at Ford Motor Co. (USA. 1993, 1995), Fraunhofer Institute for Computer Graphics (Germany 1999, 2001), University of Vigo (Spain 1999, 2002), Max Planck Institute for Informatik (Germany 2004) and Purdue University (USA 2009). In 1996 Prof. Ruiz was appointed as Faculty of the Mechanical Eng. and Computer Science Depts. and as coordinator of the CAD CAM CAE Laboratory at EAFIT University, Medellin, Colombia. His academic interests are Computer Aided Geometric Design, Geometric Reasoning and Applied Computational Geometry.

FINAL EXAM OF DISSERTATION
DOCTORAL PROGRAM IN ENGINEERING
EAFIT UNIVERSITY

Doctoral Student:	**Sebastian Durango Idárraga**
Thesis Supervisor:	**Prof. Dr. Ing. Oscar Ruiz**
Topic of Examination:	**ASSESSMENT OF INTENDED DEFORMATIONS AND KINEMATIC IDENTIFICATION OF PARALLEL MECHANISMS UNDER QUASI-STATIC CONDITIONS**
Room:	**38 – 125. Humanities & Sciences Bldg. Medellin Campus**
Date:	**December 16, 2010**
Time:	**10:30h**
Jury:	**Dr. Ing. Rodrigo Marin** **Schlumberger Riboud Product Center** **Clamart, France.**
	Prof. Dr. Ing. Gabriel Calle **Universidad Tecnológica de Pereira, Colombia**
	Prof. Dr. Diego Acosta **Universidad EAFIT, Colombia**

The Jury considers that the Doctoral Student has **APPROVED** (APPROVED / FAILED) this Final Examination, faced by the Doctoral Student in the mentioned place and date.

Juror Dr. Ing. Rodrigo Marin

Juror Prof. Dr. Ing. Gabriel Calle

Juror Prof. Dr. Ing. Diego Acosta

witnesses:

Thesis Supervisor
Prof. Dr. Ing. Oscar Ruiz

President of the Doctoral Board
Dean Alberto Rodriguez